



## UvA-DARE (Digital Academic Repository)

### Adaptive radiotherapy for preoperative gastric cancer

Bleeker, M.

**Publication date**

2024

**Document Version**

Final published version

[Link to publication](#)

**Citation for published version (APA):**

Bleeker, M. (2024). *Adaptive radiotherapy for preoperative gastric cancer*. [Thesis, fully internal, Universiteit van Amsterdam].

**General rights**

It is not permitted to download or to forward/distribute the text or part of it without the consent of the author(s) and/or copyright holder(s), other than for strictly personal, individual use, unless the work is under an open content license (like Creative Commons).

**Disclaimer/Complaints regulations**

If you believe that digital publication of certain material infringes any of your rights or (privacy) interests, please let the Library know, stating your reasons. In case of a legitimate complaint, the Library will make the material inaccessible and/or remove it from the website. Please Ask the Library: <https://uba.uva.nl/en/contact>, or a letter to: Library of the University of Amsterdam, Secretariat, Singel 425, 1012 WP Amsterdam, The Netherlands. You will be contacted as soon as possible.

# ADAPTIVE RADIOTHERAPY FOR PREOPERATIVE GASTRIC CANCER



MARGOT BLEEKER



# Adaptive radiotherapy for preoperative gastric cancer

Margot Bleeker

© Margot Bleeker, 2024

**Cover design** Margot Bleeker  
**Lay out design** Margot Bleeker  
**Printed by** ProefschriftMaken  
**ISBN** 978-94-6469-784-1

The research presented in this thesis was financially supported by the Dutch Cancer Society (KWF Kankerbestrijding) under grant number KWF 10882.

Financial support for printing of this thesis was kindly provided and supported by Cancer Center Amsterdam and Amsterdam UMC.

# Adaptive radiotherapy for preoperative gastric cancer

ACADEMISCH PROEFSCHRIFT

ter verkrijging van de graad van doctor  
aan de Universiteit van Amsterdam  
op gezag van de Rector Magnificus  
prof. dr. ir. P.P.C.C. Verbeek

ten overstaan van een door het College voor Promoties ingestelde commissie,  
in het openbaar te verdedigen in de Agnietenkapel  
op maandag 22 april 2024, te 14.00 uur

door Margot Bleeker  
geboren te Heemskerk

## Promotiecommissie

<i>Promotores:</i>	prof. dr. ir. J.J. Sonke	AMC-UvA
	prof. dr. A. Bel	AMC-UvA
<i>Copromotores:</i>	dr. ing. A. van der Horst	NKI-AvL
	dr. M.C.C.M. Hulshof	AMC-UvA
<i>Overige leden:</i>	prof. dr. H.A. Marquering	AMC-UvA
	dr. E. Versteijne	AMC-UvA
	dr. O.J. Gurney-Champion	AMC-UvA
	prof. dr. M.B. van Herk	University of Manchester
	prof. dr. M. Verheij	Radboud Universiteit
	prof. dr. M.S. Hoogeman	Erasmus Universiteit Rotterdam

Faculteit der Geneeskunde







## Table of contents

<b>Chapter 1</b>	General Introduction	9
<b>Chapter 2</b>	Endoscopically placed fiducial markers for image-guided radiotherapy in preoperative gastric cancer: Technical feasibility and potential benefit	23
<b>Chapter 3</b>	Stomach motion and deformation: implications for preoperative gastric cancer radiotherapy	37
<b>Chapter 4</b>	Feasibility of cone beam CT-guided library of plans strategy in preoperative gastric cancer radiotherapy	55
<b>Chapter 5</b>	Gastric deformation models for adaptive radiotherapy: Personalized vs population-based strategy	69
<b>Chapter 6</b>	Dosimetric benefit of a library of plans versus single-plan strategy for preoperative gastric cancer radiotherapy	85
<b>Chapter 7</b>	General Discussion	99
<b>Appendices</b>	Bibliography	114
	Summary	122
	Samenvatting	126
	Supplemental Materials	130
	PhD Portfolio	160
	Author Contributions	162
	Dankwoord	166
	Curriculum Vitae	169



## **General Introduction**

---

# 1

The stomach, located in the upper abdomen, is a vital part of the human digestive system. This muscular, distensible, and hollow organ is connected to the esophagus on one side and the duodenum on the other. The stomach allows for the temporary storage and partial digestion of food that enters from the esophagus<sup>1</sup>. Once the food is partially digested, it is gradually passed on to the duodenum. This process triggers a range of stomach motions and shape changes. Due to its location in the upper abdomen, the stomach is closely surrounded by various other organs, including the liver, pancreas, kidneys, spleen, and bowels (Figure 1.1). Unfortunately, various pathological conditions can develop in the stomach, including cancer.

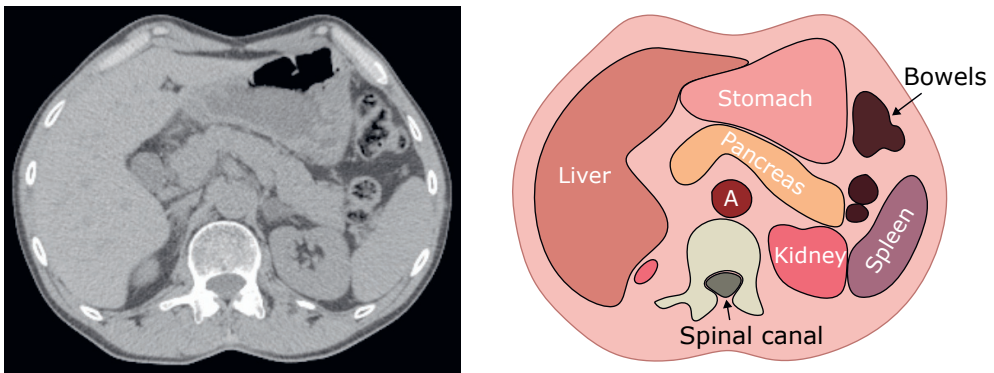


Figure 1.1: Axial slice of computed tomography (CT) scan with accompanying schematic representation of several organs as seen on the CT. The structure 'A' represents the aorta.

## 1.1 Gastric cancer

### 1.1.1 Epidemiology

Gastric cancer is a major public health concern worldwide, ranking the fifth most common cancer and the fourth leading cause of cancer-related deaths<sup>2</sup>. The risk factors for developing gastric cancer include alcohol consumption, smoking, a high-salt diet, and infection with *Helicobacter pylori*<sup>3,4</sup>. There are substantial differences in the incidence and mortality rates between genders, as rates for men are approximately twice as high as those for women. Furthermore, the incidence rates vary widely across regions, with Eastern Asia and Eastern Europe exhibiting the highest rates. In the Netherlands, gastric cancer was responsible for 2099 new cancer cases (1.6% of all sites) and 1240 cancer-related deaths in 2020 (2.5%)<sup>2</sup>. Despite declining gastric cancer incidence rates in the Netherlands over the past few decades, the poor three-year overall survival rate of 25% has unfortunately remained relatively stable<sup>5,6</sup>. As such, improving gastric cancer treatment remains a priority for healthcare professionals.

## 1.1.2 Treatment

Surgery is the primary treatment for gastric cancer, often combined with perioperative chemotherapy or postoperative chemoradiotherapy for better outcomes<sup>7,8</sup>. However, despite the demonstrated benefits of postoperative treatments, they often suffer from poor patient compliance, with 40–60% of patients being unable to complete the treatment<sup>8–10</sup>. The poor patient compliance, combined with uncertainties in the target definition for postoperative radiotherapy due to the prior (partial) stomach removal, has prompted investigations into preoperative regimens<sup>11,12</sup>, as seen in the CRITICS-II trial<sup>10</sup>. The CRITICS-II trial aims to identify the most effective preoperative treatment by comparing (1) preoperative chemotherapy, (2) preoperative chemotherapy and chemoradiotherapy, and (3) preoperative chemoradiotherapy, followed by surgery. Preoperative radiotherapy for gastric cancer is a relatively recent development, thereby making it essential to evaluate and, when necessary, optimize the treatment protocols. Hence, this thesis focuses specifically on the topic of preoperative gastric cancer radiotherapy.

## 1.2 Preoperative gastric cancer radiotherapy

For gastric cancer, *external beam radiotherapy* (EBRT) is applied. EBRT employs ionizing radiation produced by a linear accelerator to irradiate malignant cells. The primary objective is to target the affected area with minimal harm to the healthy surrounding tissue.

### 1.2.1 Treatment planning

The target (i.e., *clinical target volume*; CTV) for preoperative gastric cancer radiotherapy within the CRITICS-II trial consists of a large volume, including not only the tumor but also the entire stomach and the first draining lymph node stations to address potential microscopic tumor spread that is not visible on the acquired imaging. The first lymph node stations are located along the outer wall of the stomach, in the peri-cardial, peri-esophageal, para-aortic, and peri-pancreatic areas, and at the hila of the liver and spleen. Radiotherapy comprises a 5-week course in which 45 Gy is delivered to the target in 25 daily fractions of 1.8 Gy. To design the treatment plan, a single *computed tomography* (CT) scan is made prior to treatment. The CTV and surrounding *organs at risk* (OARs) are delineated on this planning CT. Typical OARs during gastric cancer radiotherapy are the kidneys, liver, spleen, heart, and spinal canal. The goal is to deliver a homogenous dose to the CTV; for this, a *planning target volume* (PTV) is created by adding a typically isotropic CTV-to-PTV safety margin to the CTV to account for geometrical uncertainties during treatment. The treatment plan, based on the planning CT, the PTV and the OAR delineations, is designed to deliver a homogenous dose to the PTV while minimizing radiation exposure to the OARs.

While safety margins are in place to ensure target coverage during treatment in the presence of uncertainties, they should be as small as possible to limit the dose received by the surrounding OARs. Various sources of uncertainties during treatment planning and delivery should be accounted for by the safety margins<sup>13</sup>. These uncertainties can be classified into two categories: systematic errors, which occur consistently throughout the treatment and include those that originate during treatment planning, and random errors, which vary from day-to-day. The planning CT provides a snapshot of the patient's anatomy at an arbitrary moment in time. Hence, anatomical variations that are random in nature but 'frozen' in the planning CT have a systematic effect throughout treatment. Systematic errors also originate from the target delineations made on planning CT as these errors are transferred throughout treatment. Random errors can, for instance, be the daily variations in patient positioning, organ shape, and respiratory motion. Random errors cause blurring of the dose distributions, resulting in a slight decrease in dose at the edge of the high-dose region. In contrast, systematic errors can have more severe effects as they lead to shifts in the dose distribution, which could potentially shift part of the CTV out of the high-dose region. Therefore, systematic errors have the greatest impact on the safety margins<sup>13</sup>.

### **1.2.2 Image-guided radiotherapy**

Prior to each radiotherapy session, a patient is positioned on the treatment couch in a similar position as on their planning CT. The initial positioning of the patient on the linear accelerator is established by aligning in-room lasers with skin marks (e.g., tattoos); however, variations in internal anatomy relative to the skin will limit radiation accuracy and precision. *Image-guided radiotherapy* (IGRT) is often used to further guide radiation delivery to the predefined target using imaging techniques, thereby reducing the necessary safety margins. Various image-guidance modalities can be used, including planar kilovoltage and megavoltage imaging (i.e., two-dimensional), *cone-beam CT* (CBCT), and *magnetic resonance imaging* (MRI). CBCT and MRI can capture *three-dimensional* (3D) and *four-dimensional* (4D) images with different levels of soft-tissue contrast depending on the modality used. For daily IGRT, these images are acquired on the treatment couch directly before each fraction to visualize the patient's internal anatomy. Subsequently, these images are compared with the original planning CT and, when necessary, the treatment couch or treatment plan is shifted (and for some linear accelerators, slightly rotated) to reduce the patient setup error and thereby ensure that the radiation is delivered to the target in the most precise and accurate manner possible.

### **1.2.3 Radiation toxicity**

Although radiotherapy has proven to be an effective strategy to control malignancies, it can severely affect the surrounding healthy tissue. For preoperative gastric cancer radiotherapy,

where the target constitutes a large volume and radiosensitive organs surround the target, it is essential to be aware of acute and late radiation-induced toxicities, as they can negatively impact treatment compliance, a patient's quality of life, or even survival<sup>14</sup>. Common acute side effects associated with (upper) gastrointestinal tract irradiation include fatigue, diarrhea, nausea, and anorexia<sup>15</sup>. Additionally, exposure to too high a dose of radiation can cause acute and/or late (chronic) side effects on organs such as the spleen, kidneys and heart<sup>16–18</sup>. To limit radiation-induced toxicities, OAR-specific constraints on the dose and the volume that receives a specific dose are set during treatment planning. However, as the treatment plan is typically based on the observed anatomy on planning CT, internal anatomical variations during radiotherapy may cause the actual delivered dose to the OARs to differ from the planned dose and potentially exceed these constraints.

### 1.3 Challenges in gastric radiotherapy

The stomach presents several challenges for radiotherapy. The aforementioned large target volume for preoperative gastric cancer radiotherapy and the stomach's central position in the upper abdominal cavity make it challenging to minimize exposure of the OARs during treatment. Additionally, the stomach's highly mobile and deformable nature further complicates precise radiotherapy.

#### 1.3.1 Stomach motion and deformation

The stomach's role in the temporary storage and partial digestion of food causes anatomical changes on various time scales (Figure 1.2). Day-to-day (interfractional) variations in stomach appearance pose the biggest challenge to accurate radiotherapy delivery because changes in food intake can substantially alter the stomach's volume and shape, making it difficult to deliver radiation precisely to the intended target<sup>19</sup>. Although food intake may be restricted, this approach may be not only undesirable for patients undergoing this highly toxic treatment but also not necessarily effective in controlling stomach volume. Despite dietary restrictions, the stomach may display substantial changes in volume and position. To illustrate, one study reported a patient's stomach volume varying between 279–989 mL during a 5-week treatment course despite a three-hour fast<sup>19</sup>; another reported stomach wall displacements of >50 mm with an overnight fast<sup>20</sup>. Besides these unavoidable interfractional stomach filling changes, day-to-day changes in lung volume or bowel filling (i.e., content or changing gas volumes) may also alter the stomach's position or shape.

Apart from interfractional changes, the stomach also experiences anatomical variations during irradiation (i.e., intrafractional changes), specifically caused by peristalsis and respiration. Peristaltic waves are the rhythmic contraction and relaxation of muscles that propagate through



the stomach towards the pylorus, causing temporary periodic anatomical deformations<sup>21–24</sup>. Such peristaltic waves can result in stomach displacements larger than 10 mm<sup>21</sup>. Furthermore, common to other organs in the upper abdomen, the stomach experiences respiratory motion, with reported average or median amplitudes between 1.7–14.0 mm<sup>20,25,26</sup>, and respiratory-induced deformations<sup>27</sup>.

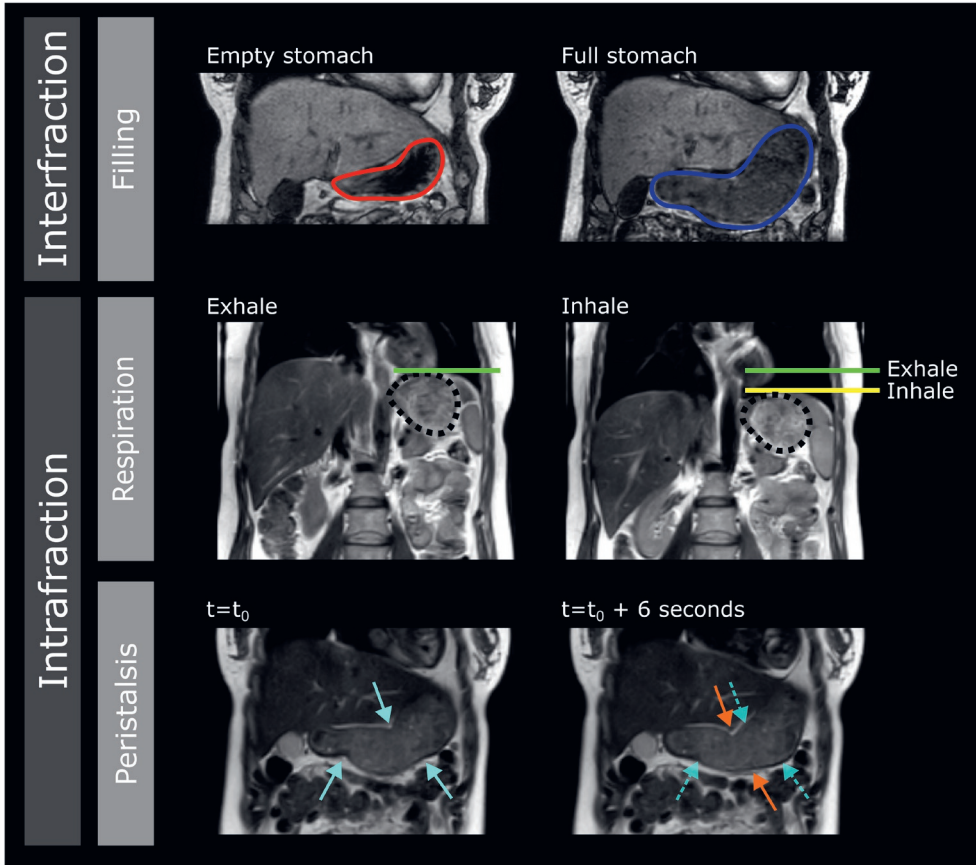


Figure 1.2: Coronal slices of magnetic resonance imaging (MRI) with examples of the stomach's interfractional and intrafractional changes in one healthy volunteer. Interfractional changes can be caused by stomach filling (red is an empty stomach, and blue is a full stomach). Intrafractional changes can be caused by various factors, including respiration or peristalsis. Respiratory motion is depicted by the change in the left diaphragm dome position on exhale (green line) and inhale (yellow line) phase images from a 4D scan, with the stomach indicated by the black dashed line. Peristalsis is demonstrated by the change in stomach wall contractions over time with the location of peristaltic contractions at  $t=0$  (light blue arrows) and 6 seconds later (orange arrows).

When radiotherapy consists of a single treatment plan based on the planning CT, these aforementioned sources of stomach motion and deformation put adequate radiotherapy at risk. As the exact motions and deformations of the stomach are still unclear, there is a need to identify and quantify them. Such quantifications are essential as each type of organ motion and deformation can impose different levels of uncertainty during radiotherapy. With such knowledge, appropriate strategies can be selected to mitigate motion and minimize uncertainties during radiotherapy delivery. Imaging can enable such motion and deformation quantifications. For instance, respiratory motion is typically evaluated using 4D imaging, which consists of numerous (e.g., 10) 3D images that each represent a different respiratory phase. However, for all imaging modalities (e.g., CBCT and MRI), the quality suffers from (intrafractional) anatomical variations during acquisition, as this leads to image artifacts and/or blurring<sup>28-30</sup>. As image acquisition typically takes between tens of seconds and several minutes, such anatomical variations inevitably occur during image acquisition.

### 1.3.2 Image-guidance modalities

Currently, IGRT is most commonly performed using CBCT imaging, as it generally provides sufficient anatomical information and is widely available in clinics. However, soft-tissue contrast is typically low and can vary per patient and treatment day (Figure 1.3A and 1.3B). Specifically for the stomach, its high mobility during image acquisition and the presence of (moving) gas in the gastrointestinal tract can severely impact image quality. Alternatively, MR-guidance, a promising, relatively new development, can be used, as it generally provides superior soft-tissue contrast compared to CBCT<sup>31</sup>. However, as MRI also suffers from motion during image acquisition<sup>29</sup>, adequate daily target visualization of the stomach may not be evident with MR-guidance. Moreover, practical limitations such as its high costs, long treatment durations, and the limited availability<sup>32</sup> may restrict its application for most gastric cancer patients. As CBCT-guided radiotherapy remains the conventional method for treating gastric cancer patients, exploring strategies to optimize CBCT-guided gastric cancer radiotherapy will benefit most patients. To enable target localization during CBCT-guided radiotherapy despite poor image quality, fiducial markers implanted in the stomach wall may be advantageous.

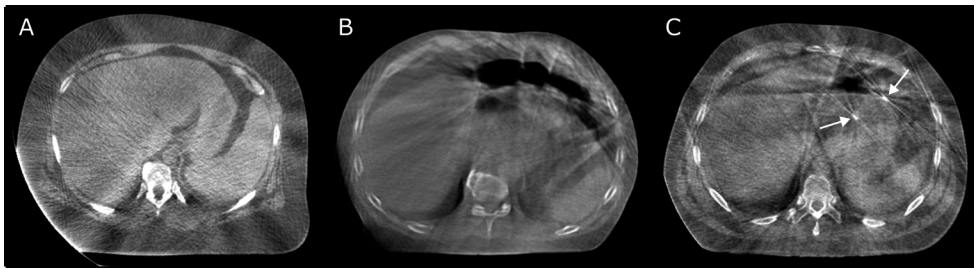


Figure 1.3: Axial slices of cone-beam computed tomography (CBCT) images of three different patients indicating various image qualities (A and B) and the visibility of gold spiral fiducial markers implanted in the stomach wall (C; fiducial markers indicated by arrows).

### 1.3.3 Fiducial markers

Fiducial markers are designed to enhance the target's visibility on imaging. When placed near or in the target volume for radiotherapy, they can serve as a surrogate for the actual target (Figure 1.3C). Fiducial markers can assist in target delineations on planning CT<sup>33,34</sup> as well as target localization and positioning on daily imaging during IGRT<sup>35–37</sup>. Various types of fiducial markers are available, such as the gold spiral marker or a liquid marker, each offering its own benefits. Fiducial markers implantations were proven safe and feasible in various other targets, including hollow and deformable organs like the bladder<sup>38</sup> and esophagus<sup>39,40</sup>, and have been shown to provide added value during IGRT. Besides potentially improving target visualization, fiducial markers may provide a landmark for motion and deformation assessments when found to be positionally stable<sup>37,41</sup>. However, due to limited research on this topic, it remains unclear whether fiducial markers implantations in the stomach are feasible and whether the markers remain visible on imaging given the stomach's mobility.

## 1.4 Adaptive radiotherapy

Although IGRT is widely adopted in clinical practice, daily positioning does not correct for interfractional size and shape changes of the target, which is especially relevant for the stomach. Therefore, despite the use of IGRT, ensuring target coverage for single-plan gastric radiotherapy most likely requires large safety margins, which causes considerable risk to the sparing of surrounding OARs. Due to the stomach's highly mobile and deformable nature, *adaptive radiotherapy* (ART) may be a suitable alternative, as it allows adjustments to the treatment plan to (better) match the daily anatomy.

With ART, multiple treatment plans are used to adapt treatment to the anatomical changes observed on imaging. There are two types of ART: offline and online ART. In offline ART, the treatment plan for subsequent fractions is adapted based on previously acquired imaging,

thereby aiming to minimize systematic errors. Since with offline ART the treatment plan is adapted to observed changes in previous fractions, it is most suitable for targets that exhibit large systematic errors (e.g., slow interfractional anatomical changes). On the other hand, with online ART, the daily treatment plan is adapted based on in-room imaging directly before irradiation, which minimizes both systematic and random errors. While online ART requires more resources than offline ART (such as increased workload and treatment time), it can yield the largest benefit for targets with potentially large and frequent anatomical variations, such as the stomach.

The ideal online ART strategy would be daily generation of a new treatment plan based on the observed anatomy on CBCT or MRI. However, this approach presents several challenges, such as the need for excellent image quality, high-quality automated segmentations of the target and OARs, and increased treatment duration. Therefore, a more simple yet effective online ART approach may be the *library of plans* (LoP).

### 1.4.1 Library of plans

A LoP is a collection of treatment plans covering various anatomical scenarios and is primarily applicable for targets demonstrating predictable (potentially) large changes. As such, it has been clinically implemented for targets like the bladder<sup>42,43</sup>, cervix<sup>44,45</sup>, and rectum<sup>46</sup>. Prior to daily radiotherapy delivery, the best-fitting treatment plan can be selected (Figure 1.4), leading to more accurate target irradiation and reduced safety margins. However, for daily plan selection, the target should be sufficiently visible on acquired imaging to be identified by physicians and radiation therapists, which can be challenging for the stomach because of the aforementioned imaging challenges. Currently, a LoP for preoperative gastric cancer does not yet exist, and the development of a LoP for this target would require a thorough investigation of the daily anatomical variations and the creation of high-quality treatment plans that can accommodate these daily changes.

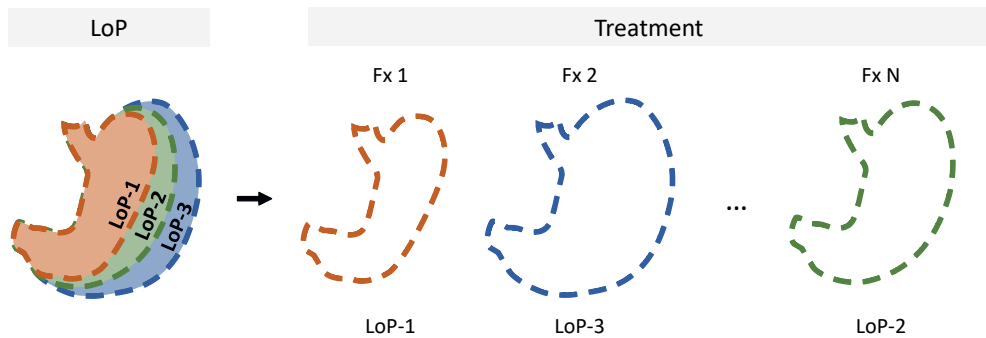


Figure 1.4: Schematic illustration of a library of plans (LoP) approach. The three plans in the library (LoP-1, LoP-2, LoP-3) represent various anatomical scenarios. Each treatment day (i.e., fraction (Fx)), the best-fitting plan can be selected.

To create treatment plans that fit the anatomical variations well, accurate prediction of these variations is crucial. A simple method to create multiple treatment plans is to create a LoP based on the observed anatomical variations in the first week of radiotherapy<sup>47</sup>. However, this approach may not capture the full range of anatomical variations, and the time required to create the LoP may limit its availability to the last 3–4 weeks of treatment. Alternatively, a LoP may be created before radiotherapy delivery using deformation models and the anatomy observed on planning CT, which has been successfully demonstrated for cervical<sup>48,49</sup> and rectal cancer<sup>50</sup>. However, such anatomical deformation models have not yet been developed for the stomach. Regardless of the strategy used, residual anatomical variations between the daily anatomy and the selected plan are inevitable. The extent of this variation is influenced by the number of plans available in the library and how accurately the plans conform to the patient's daily anatomy, and dictate the necessary safety margins. Since each adaptive strategy requires additional resources, evaluating the potential clinical benefits is crucial before the clinical implementation of any strategy aimed at improving radiotherapy accuracy.

## 1.5 Objective and outline of this thesis

Preoperative gastric cancer radiotherapy is a relatively recent treatment approach and still faces several uncertainties. The stomach's highly mobile and deformable nature implies a need for appropriate management of these uncertainties to ensure adequate radiotherapy. Therefore, the primary objective of this thesis is to explore a CBCT-guided adaptive strategy for preoperative gastric cancer radiotherapy. To achieve this, we pursue the following objectives: 1) explore the need for an adaptive strategy by quantifying stomach motions and deformations using fiducial markers, 2) assess the feasibility of a LoP strategy, and 3) develop and evaluate a LoP to determine its potential benefit. Hereby, we aim to improve the accuracy and precision of preoperative gastric cancer radiotherapy.

### ***The need for an adaptive strategy: quantification of motion and deformation***

Fiducial markers have demonstrated their value in radiotherapy for various organs, aiding in target delineation and daily target localization and positioning; however, fiducial markers in the stomach are relatively new. In **Chapter 2**, we assess the technical feasibility of fiducial marker implantations in the stomach wall in gastric cancer patients and assess their visibility on CT and CBCT imaging.

In **Chapter 3**, we utilize these implanted fiducial markers in the stomach and 4D imaging to identify and quantify the various sources of interfractional and intrafractional stomach motion and deformation. These motion and deformation quantifications allow identification of the most appropriate mitigation strategies to manage these uncertainties.

### ***Feasibility of a library of plans***

The substantial interfractional anatomical variations presented in Chapter 3 underscore the need for an adaptive strategy. Whether a gastric LoP is feasible greatly depends upon the target's visibility on daily imaging. Therefore, in **Chapter 4**, we assess whether the target for preoperative gastric cancer radiotherapy is sufficiently visible on the acquired CBCTs to enable consistent daily plan selections. Additionally, we investigate the (variety of) selected plans per patient to gain insight into the need and potential benefit of a LoP for this patient group.

### ***Development and evaluation of a library of plans***

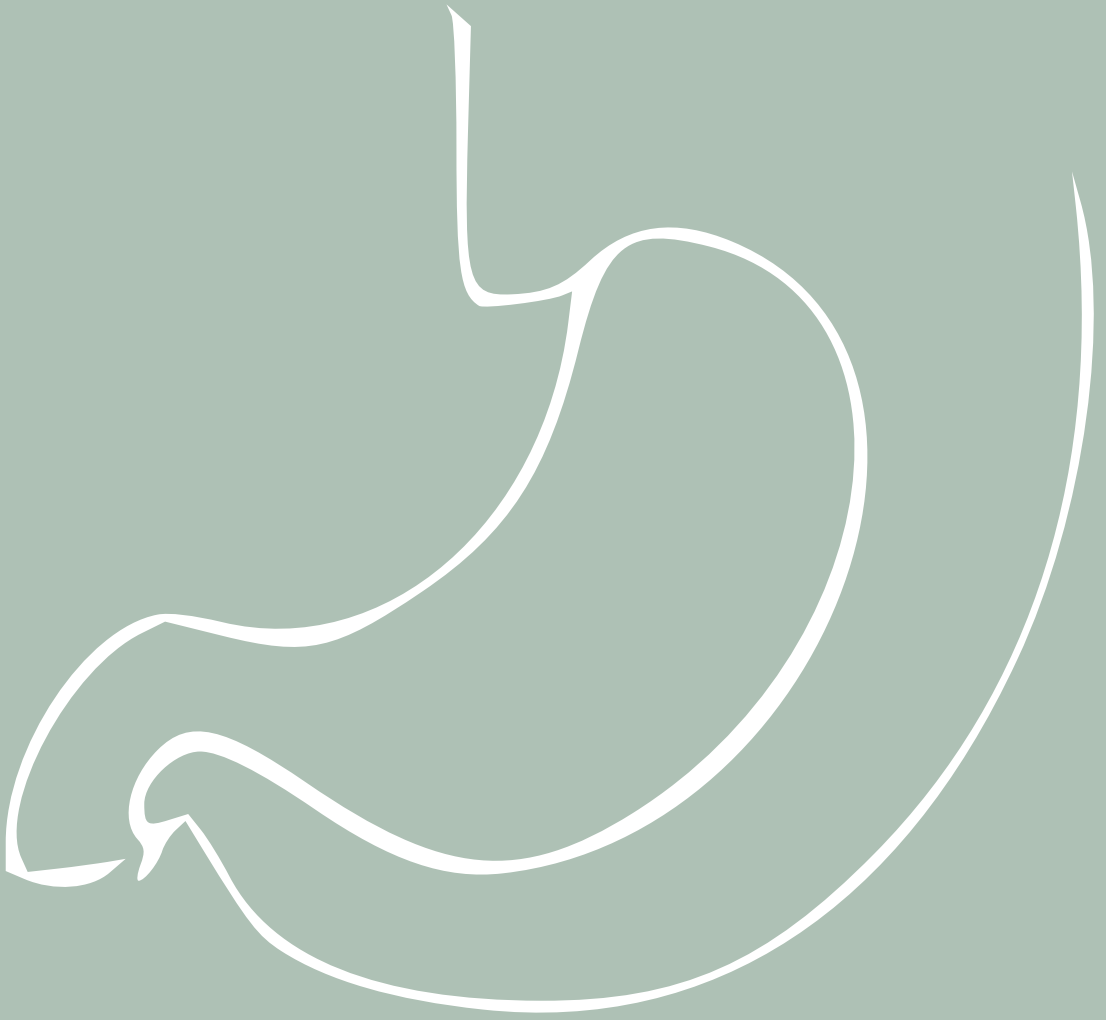
Since the performance of a gastric LoP relies upon the quality of stomach shape predictions for various stomach volumes, **Chapter 5** evaluates the ability of a personalized and a population-based gastric deformation model to predict stomach shape using data from healthy volunteers and patients. The personalized approach yields multiple stomach shapes based on observed anatomical deformation within a subject, whereas the population-based approach utilizes anatomical deformations in a group of subjects to predict shape changes.

Using the best-performing deformation model in Chapter 5, in **Chapter 6**, we present a strategy to create a model-based gastric LoP and perform a dosimetric comparison between the created LoP and the traditional single-plan strategy. We ensure sufficient target coverage by calculating appropriate safety margins, allowing for a comparison in dose to the OARs between the LoP and the single-plan strategy.

Finally, in **Chapter 7**, we discuss the overall findings and put them into a broader context. In addition, recommendations and future perspectives on preoperative gastric cancer adaptive radiotherapy are discussed.







**Endoscopically placed fiducial markers  
for image-guided radiotherapy in  
preoperative gastric cancer: Technical  
feasibility and potential benefit**

2

Margot Bleeker  
Astrid van der Horst  
Arjan Bel  
Jan-Jakob Sonke  
Jeanin E. van Hooft  
Roos E. Pouw  
Maarten C.C.M. Hulshof

Modified from:  
Endoscopy International Open, 2023, 11, E866–E872.  
DOI: 10.1055/a-2129-2840

## Abstract

*Purpose:* Fiducial markers have demonstrated clinical value in radiotherapy in several organs, but little is known about markers in the stomach. Here, we assess the technical feasibility of endoscopic placement of markers in gastric cancer patients and their potential benefit for image-guided radiotherapy (IGRT).

*Materials and methods:* In this prospective feasibility study, 14 gastric cancer patients underwent endoscopy-guided gold (all patients) and liquid (7 patients) marker placements distributed throughout the stomach. Technical feasibility, procedure duration, and potential complications were evaluated. Assessed benefit for IGRT comprised marker visibility on acquired imaging (3–4 CTs and 19–25 cone-beam CTs (CBCTs) per patient) and lack of migration. Marker visibility was compared per marker type and location (gastroesophageal junction (i.e., junction/cardia), corpus (corpus/antrum/fundus), and pylorus).

*Results:* Of the 93 marker implantation attempts, 59 were successful, i.e., marker in stomach wall and present during entire 5-week radiotherapy course (2–6 successfully placed markers per patient), with no significant difference (Fisher's exact test;  $p > 0.05$ ) in success rate between gold (39/66=59%) and liquid (20/27=74%). Average procedure duration was 24.4 min (range 16–38 min). No procedure-related complications were reported. All successfully placed markers were visible on all CTs, with 81% visible on  $\geq 95\%$  of CBCTs. Five markers were poorly visible (on  $< 75\%$  of CBCTs), possibly due to small marker volume and peristaltic motion since all five were liquid markers located in the corpus. No migration was observed.

*Conclusions:* Endoscopic placement of fiducial markers in the stomach is technically feasible and safe. Being well visible and positionally stable, markers provide a potential benefit for IGRT.

## 2.1 Introduction

Curative treatment of gastric cancer generally includes surgical resection combined with perioperative chemotherapy or postoperative chemoradiotherapy<sup>7,8</sup>. However, due to poor patient compliance during postoperative treatment regimens and uncertainties in target definition, research interest has recently shifted towards preoperative (chemo)radiotherapy<sup>10,51</sup>. For accurate image-guided radiotherapy (IGRT), localization of the target volume on pre-treatment CT imaging and daily in-room cone-beam CT (CBCT) imaging is essential. However, for the stomach, target localization can be challenging because of (organ) motion and low soft-tissue contrast. The use of fiducial markers potentially enhances target visualization during IGRT, which can aid target delineations<sup>33,34</sup>, and daily target localization and positioning<sup>35-37</sup>.

The feasibility and safety of fiducial marker placement have been demonstrated for various organs/cancers, including (upper) gastrointestinal sites<sup>34,52,53</sup>. Markers may improve IGRT accuracy as demonstrated for, e.g., pancreas<sup>54,55</sup>, rectum<sup>56,57</sup>, and esophagus<sup>56,58</sup>. For the stomach, however, marker implantation has only been investigated in a few small (case) studies<sup>59-61</sup>, with none covering visibility during IGRT courses. The stomach has distinct anatomical characteristics (i.e., hollow, deformable and experiencing peristaltic motion), which can affect implantation feasibility as well as marker visibility and stability on imaging. Therefore, more research regarding gastric fiducial markers is needed.

This prospective feasibility study aims to assess the technical feasibility and safety of endoscopic placement of (gold and liquid) fiducial markers in gastric cancer patients and their potential benefit during a 5-week IGRT course.

## 2.2 Materials and methods

### 2.2.1 Patient population

From October 2018 to January 2022, gastric cancer patients were enrolled in this prospective, non-randomized, single arm, feasibility study. Patient inclusion criteria were: histologically proven, stage IB-IIIc (TNM 8th edition), primary gastric adenocarcinoma, and referral for preoperative radiotherapy at our center. All eligible patients who were randomized to preoperative chemoradiotherapy within the CRITICS-II trial (NCT02931890) at our center were asked to participate in this fiducial study<sup>10</sup>. The ethics committee of the Amsterdam University Medical Center approved the protocol (study registration number NTR7241). Seventeen patients were eligible, 14 of whom gave written informed consent and were included. Included patients received fiducial marker placement in the stomach wall (not tumor) and additional imaging (CTs and CBCTs) during IGRT.

### 2.2.2 Fiducial marker placement

All patients underwent an endoscopy under conscious sedation with midazolam and fentanyl or under deep sedation with propofol. The procedures were performed by one of four experienced gastroenterologists. Intended marker locations were determined prior to implantation, at 4–6 stomach sites, taking distribution throughout the stomach and tumor location into consideration. Two different markers were used: the flexible 10-mm-long coil-shaped gold Visicoil marker (Visicoil, Core Oncology, CA, USA; outer  $\varnothing=0.35$  mm); and the liquid BioXmark marker (Nanovi A/S, Lyngby, Denmark). The liquid marker solidifies as a three-dimensional structure after implantation, thereby preventing diffusion. Gold markers were placed in all 14 patients; liquid markers were placed in the final seven patients once CE mark approval was obtained.

Gold markers were individually back-loaded into a 22-gauge FNA needle, with the stylet pulled back about 2 cm; the needle tip was sealed with sterile bone wax to prevent accidental marker loss prior to implantation. For each gold marker, the loaded needle was placed in the gastroscope (GIF-HQ190; Olympus, Tokyo, Japan) for implantation. Following needle placement in the gastric wall, the marker was pushed out of the needle by pushing the stylet into the needle. For each marker, the needle was reloaded; sometimes, two needles were used to limit procedure time.

For the liquid marker, a 23- or 25-gauge injection needle was primed prior to the injection procedure with 1 mL of liquid marker followed by saline solution until the injection system was fully filled. Next, multiple consecutive markers were placed into the gastric wall, using a unit dose syringe (Luer Lock, Vlow medical, Eindhoven, The Netherlands) for controlled dosage of injected volume. For fiducial markers in the esophagus, a volume of  $>0.05$  mL proved sufficiently visible on CT and CBCT<sup>58</sup>; however, as the stomach possibly experiences more movement during imaging, we aimed for approximately 0.1 mL of injected volume per marker. The needle was maintained in the tissue for about 5 seconds because of slow release of the viscous liquid marker. Fluoroscopy was sometimes used to check marker placement.

### 2.2.3 Image-guided radiotherapy

The target for IGRT was the entire stomach and regional lymph nodes. IGRT (45 Gy in 25 fractions) treatment planning was based on a reference CT scan. For all patients except one, this reference scan was acquired after implantation (0–5 days, median 1 day). During the IGRT course, daily CBCTs and three repeat CTs were acquired. Median time between implantation and the first and last CBCT scan was 13 days (5–28) and 46 days (range 37–60), respectively. For details on chemoradiotherapy, see Supplemental Materials S2A.

## 2.2.4 Outcome measures

### **Technical feasibility**

Following each marker implantation, the gastroenterologist assessed expected success of placement. A marker was successfully placed when placed in the stomach wall and present for the entire course of IGRT (i.e., at time of the reference scan, and the first and last CBCT scan). Successful placement was assessed for all markers, per marker type and for three sites: gastroesophageal junction (i.e., gastroesophageal junction/cardia), corpus (i.e., corpus/antrum/fundus), and pylorus. Also, the technical difficulty of implantation (i.e., easy, reasonable, or difficult) was scored. Finally, the duration of the entire procedure (from first loaded needle entering the gastroscope to final marker placed) and average time per attempted marker implantation were assessed.

### **Adverse events**

For each marker, the gastroenterologist scored whether bleeding occurred at the implantation location. Potential adverse events occurring in the first 24–48 hours following implantation were registered. The following adverse events were potentially procedure-related: bleeding, infection/fever, and pain.

### **Potential benefit**

The potential benefit of markers for target delineation and position verification during IGRT depends upon their visibility on (CB)CT scans and positional stability throughout radiotherapy. For each successfully placed marker, visibility was separately assessed for each available CT and CBCT scan. Marker visibility was defined as good (marker visible on  $\geq 95\%$  of scans), moderate (on  $\geq 75\%$ ), or poor ( $< 75\%$ ). Marker visibility was assessed for the three sites: gastroesophageal junction, corpus, and pylorus. For analyses of marker visibility on respiratory phase images, see Supplemental Materials S2B. Positional stability was defined as lack of observable migration within the tissue.

Technical feasibility and potential benefit were compared between gold and liquid markers.

## 2.2.5 Statistical analyses

Feasibility of marker implantation was assessed using descriptive statistics. Ratios were compared with the two-sided Fisher's exact test ( $\alpha=0.05$ ).

Table 2.1: Patient, tumor, and procedure characteristics, combined with the number of successful implantations.

No.	Age (years)	Sex	Tumor location	No of attempts, type of markers	Successful implantation	Procedure duration (minutes)	Fluoroscopy used
1	62	M	Cardia	7 gold	4 gold	38	Yes
2	38	M	Antrum	5 gold	3 gold	25	Yes
3	48	M	Corpus and pylorus	6 gold	3 gold	16	Yes
4	70	M	Corpus and antrum	5 gold	4 gold	19	Yes
5	65	M	Antrum	7 gold	6 gold	19	Yes
6	71	M	Antrum and pylorus	6 gold	3 gold	21	No
7	58	F	Corpus	6 gold	4 gold	24	No
8	48	M	Cardia	4 gold; 4 liquid	1 gold; 3 liquid	27	No
9	45	M	Cardia	3 gold; 3 liquid	2 gold; 2 liquid	30	No
10	56	F	Antrum	4 gold; 4 liquid	2 gold; 4 liquid	20	No
11	64	M	Cardia and distal esophagus	5 gold; 3 liquid	2 gold; 3 liquid	24	No
12	69	M	Corpus	3 gold; 4 liquid	3 gold; 3 liquid	24	Yes
13	61	M	Cardia	3 gold; 4 liquid	2 liquid	33	No
14	60	M	Antrum and pylorus	2 gold; 5 liquid	2 gold; 3 liquid	21	No
Median (range)						Mean (range)	
Total	61 (38-71)			66 gold; 27 liquid	39 gold; 20 liquid	24.4 (16-38)	

## 2.3 Results

### 2.3.1 Technical feasibility

In the 14 patients, 93 endoscopy-guided markers implantations attempts were performed (66 gold and 27 liquid markers; Table 2.1). For each liquid marker, a volume of 0.08–0.20 mL was injected.

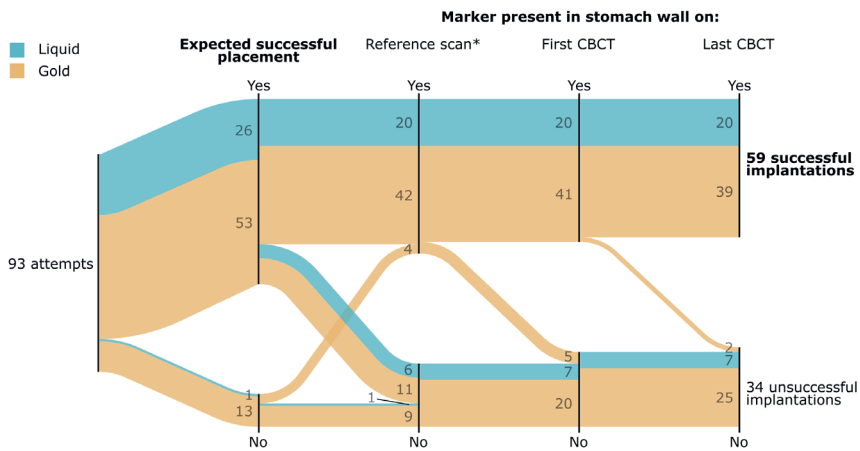


Figure 2.1: Sankey plot showing the number of implantation attempts (N=93), the number of marker implantations expected to be successful (N=79), the number of markers placed in the stomach wall and present on the reference scan (N=66), the first CBCT (N=61), and the last CBCT (N=59). Seventeen markers expected to be successfully placed were either not visible on the reference scan (N=10) or not placed in the stomach wall (N=7). \*For one patient, the reference scan was acquired prior to marker implantation; for this patient, we regarded the first CBCT also as reference scan.

Fifty-nine markers (63%; 2–6 per patient) were successfully placed (Figure 2.1); this was 59% and 74% for gold and liquid markers, respectively. No significant difference between success rates of gold and liquid markers was found ( $p>0.05$ ), also when only comparing in the seven patients with both marker types. Moreover, success rates differed between sites as it was 63% (10 successfully placed out of 16 attempts) for markers in the gastroesophageal junction, 60% (37/62) in the corpus, and 80% (12/15) in the pylorus. Of the unsuccessful implantations, 17 markers that were expected to be successfully placed were either not visible on the reference scan (N=10; lost in the first 0–5 days following implantation) or not placed in the stomach wall (N=7; 5 gold and 2 liquid markers); of these latter seven, three were placed outside the



stomach wall (<1 cm), one in the spleen, one in the diaphragm, and two in surrounding fat. All seven markers placed outside the stomach wall were present for the entire radiotherapy course. In addition, five markers were lost between the reference scan (on days 0–3 following implantation) and the start of IGRT delivery (i.e., first CBCT; on days 9–14 following implantation), and two were lost during IGRT delivery (on day 15 and 22 post-implantation). Of the 93 attempts, 14 were expected not successfully placed during implantation (13 gold and 1 liquid), for instance, because the marker was partially sticking out of the mucosa into the lumen, the marker could not be pushed out of the needle, or liquid marker that leaked intraluminally from the tissue. Of these 14 markers expected not to be successfully placed, four were visible on the reference scan; three of these four were lost prior to the end of IGRT.

The average procedure duration was 24.4 min (range 16–38 min), with time per marker attempt 2.5–5.4 min (average 3.7 min). The technical feasibility was rated easy for 77 markers, reasonable for 9, and difficult for 7. All difficult implantations were unsuccessful. Reasons for difficult marker implantation included challenges with pushing the gold or liquid marker out of the needle; causes included sharp angulation of the gastroscope or changes in bone wax type/brand.

### **2.3.2 Adverse events**

Only mild bleeding occurred (N=15, all gold), indicating that the bleeding stopped immediately. No procedure-related complications were reported afterwards.

### **2.3.3 Potential benefit**

For each patient, 3–4 CTs (total = 53) and 19–25 CBCTs (total = 339) were used to score marker visibility (Figure 2.2). The visibility of all successfully placed markers was good on CT scans (Figure 2.3). On CBCTs, most markers (81%) had good visibility. For only five markers (four patients), visibility was poor on CBCT. All five were liquid markers (significantly more often than gold marker;  $p=0.003$ ) located in the corpus (not significant compared to the other locations); three were visually assessed as small.

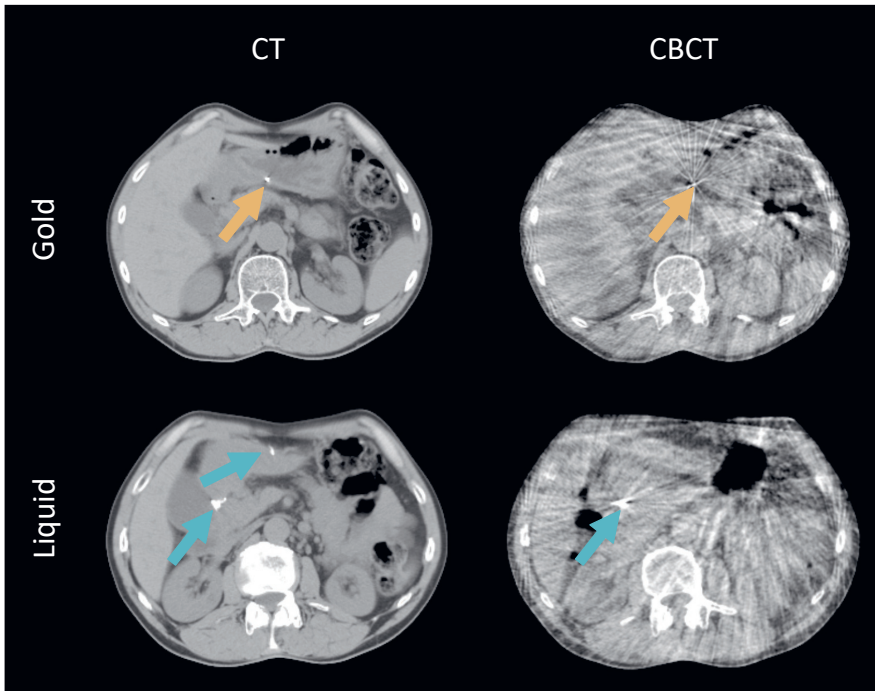


Figure 2.2: Typical example of gold (orange arrows) and liquid (blue arrows) fiducial markers on CT and CBCT. On the CTs, two liquid markers are visible; one of the two was, although present, not visible on the CBCTs.

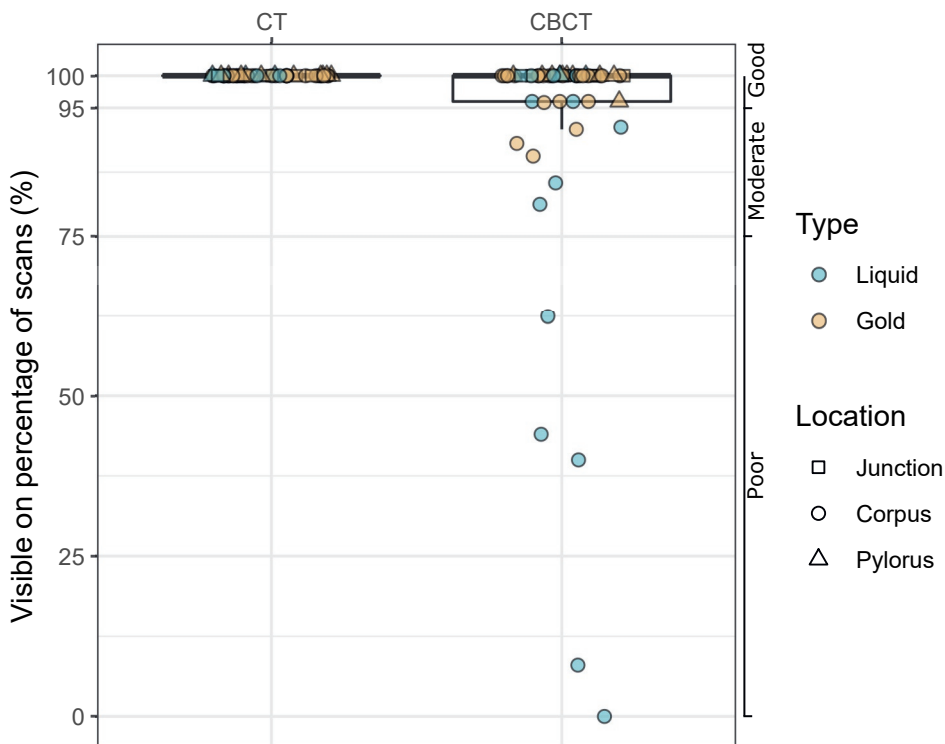


Figure 2.3: Boxplots of the visibility of successfully placed markers (N=59) on CT and CBCT scans for liquid (blue) and gold markers (orange). Symbols indicate marker location: square = gastroesophageal junction (i.e., junction), circle = corpus, triangle = pylorus). Boxplots: box = interquartile range (IQR), whiskers = lowest and highest data point within  $1.5 \times IQR$ .

Besides marker loss between the first and last acquired scan, no apparent migration within the tissue was observed.

## 2.4 Discussion

Currently, there is limited research on fiducial marker implantations in the stomach. Hence, in this prospective feasibility study, we demonstrate that endoscopic fiducial marker placement in the stomach is technically feasible and safe. In addition, the successfully implanted fiducial markers are positionally stable and sufficiently visible on acquired imaging, thereby showing their potential benefit.

Implantations were successful in 63% of implantation attempts, with no significant difference in success rates between gold and liquid markers. Every patient had at least two (range

2–6) markers successfully implanted in the stomach wall remaining present for the entire IGRT course (i.e., 37–60 days post-implantations). In similar studies for gastrointestinal cancers<sup>40,53–55,59,62</sup>, technical success is often measured by the ability to successfully place at least two markers in the target. With this measure, our technical success rate per patient is 100%, which is similar to or higher than previous studies that include gastric cancer<sup>59,62</sup>. The characteristics of the stomach (e.g., hollow and flexible with peristaltic motion) may complicate implantations, as reflected in the success rate of 60% in the corpus. Similarly, implantations in the gastroesophageal junction were occasionally challenging due to the retroflexed position of the gastroscope (success rate 63%). In contrast, implantations in the pylorus, with a success rate of 80%, were generally more straightforward. However, although some implantations were unsuccessful, these were regularly expected to be unsuccessful already during the procedure (N=14; e.g., gold markers partially sticking out of the tissue), and additional markers could still be placed at the same location. Hence, the clinical impact of these unsuccessful implantations on IGRT was minimal.

During this study, the implantation procedures were found to be generally efficacious. A large number of implantation attempts (5–8) and successful implantations (2–6) per patient were performed within a relatively short implantation procedure duration (24.4 minutes). Furthermore, few technical difficulties were encountered and four different gastroenterologists performed the implantations, thereby showing broad applicability. In addition, similarly to other studies where these gold (Visicoil) and/or liquid markers (BioXmark) were implanted, we found no procedure-related complications<sup>53,58,62</sup>. Hence, we demonstrated that fiducial marker implantations in the stomach are technically feasible and safe.

Most successfully placed markers had good visibility on both CT and CBCT imaging. Poor visibility on CBCT was likely primarily caused by marker location (i.e., corpus has largest peristaltic motion) and/or type (i.e., small volume liquid marker). Migration within the tissue was not observed but is also difficult to assess because of the large day-to-day stomach shape changes. In this feasibility study, markers were placed distributed throughout the stomach and frequently also near the tumor borders. Even though in this study the target for IGRT included the entire stomach, these markers can evidently also assist in tumor demarcation when the tumor is the intended target. Hence, with good overall marker visibility and no marker migration, fiducial markers in the stomach show great potential to improve target delineations, and daily target localization and positioning during gastric cancer IGRT. Consequently, by implanting fiducial markers, radiotherapy accuracy may be enhanced, thereby potentially contributing to reduced toxicity and improved treatment outcomes for patients with gastric cancer.

Including patients with both marker types, although only seven, enabled fair comparisons of the implantation procedure, the number of successful implantations, and marker visibility,

unlike other studies with multiple marker types<sup>40,55,62</sup>. For liquid markers, multiple markers could be placed without retraction and reloading of the needle. Therefore, in addition to being user-friendly, liquid markers have the potential to reduce procedure time and the associated costs. Moreover, when multiple markers are required, the cost of liquid marker implantations may be further reduced compared to gold markers as multiple markers can be implanted from a single purchased 1 mL ampoule. Conversely, despite the use of a unit dose syringe to regulate the injected liquid marker volume, various marker volumes were observed (e.g., very large and too small volumes). By comparison, gold markers always contain the same amount of gold and have a higher contrast due to the higher density. Gold markers are thus more consistently visible in imaging and easier to locate. However, the visibility of liquid markers may be enhanced by clinical implementation of advanced CBCT reconstruction methods<sup>63</sup> or by ensuring that an adequate volume of the liquid marker is injected<sup>58</sup>. Hence, each marker has its benefits, and the type of marker should be selected based on the intended use.

Strengths of this study include the clear focus on the stomach, the relatively large number of implanted fiducial markers, and the extensive evaluation of marker visibility on imaging data. As a result, we were able to show the evident clinical applicability of fiducial markers during IGRT, despite the relatively small patient cohort in this feasibility study. As liquid markers were placed only in the final 7 patients due to the absence of CE mark approval at the start of patient inclusion, this study contained unequal samples sizes of gold and liquid markers. Moreover, as each patient had multiple markers, the statistical tests included non-independent observations. Hence, statistical comparisons between marker types and locations should be cautiously interpreted. Furthermore, marker implantations were performed in this study without EUS guidance, unlike similar studies. Limiting factors of EUS guidance can be its technical characteristics (e.g., less flexible scope) and lack of widespread availability<sup>59</sup>. Although implantations outside the stomach wall occurred for only a small number of markers (N=7), EUS guidance may prove beneficial in preventing such unsuccessful implantations. A greater positive impact on the success rate in general may be expected from more clinical experience by the gastroenterologist in both needle loading/sealing and marker injection or consistent use of fluoroscopy.

In conclusion, fiducial marker implantations, both gold (Visicoil) and liquid (BioXmark), were feasible and safe in gastric cancer patients. Furthermore, as they have good overall visibility on the acquired images during 5-week IGRT, gastric fiducial markers have potential benefit for radiotherapy.

***Additional funding***

Study product and financial contribution only for access to study data upon trial completion were provided by Nanovi (Nanovi A/S, Lyngby, Denmark).



**Stomach motion and deformation:  
implications for preoperative gastric  
cancer radiotherapy**

3

Margot Bleeker  
Maarten C.C.M. Hulshof  
Arjan Bel  
Jan-Jakob Sonke  
Astrid van der Horst

Modified from:  
Int J Radiant Oncol Biol Phys, 2023.  
DOI: 10.1016/j.ijrobp.2023.08.049:



## Abstract

*Purpose:* Selection and development of image-guided strategies for preoperative gastric radiotherapy requires quantitative knowledge of the various sources of anatomical changes of the stomach. This study aims to investigate the magnitude of interfractional and intrafractional stomach motion and deformation using fiducial markers and 4D imaging.

*Materials and methods:* Fourteen patients who underwent preoperative gastric cancer radiotherapy received 2–6 fiducial markers distributed throughout the stomach (total of 54 markers) and additional imaging (i.e., one planning 4DCT (pCT), 20–25 pre-treatment 4DCBCTs, 4–5 post-treatment 4DCBCTs). Marker coordinates on all end-exhale (EE) and end-inhale (EI) scans were obtained following a bony anatomy match. Interfractional marker displacements (i.e., between EE pCT and all EE CBCTs) were evaluated for five anatomical regions (i.e., cardia, small curvature, proximal and distal large curvature, and pylorus). Motion was defined as displacement of the center-of-mass of available markers ( $COM_{\text{stomach}}$ ), deformation as the average difference in marker-pair distances. Interfractional (i.e., between EE pCT and all EE CBCTs), respiratory (between EE and EI pCT and CBCTs), and pre-post (pre- and post-treatment EE CBCTs) motion and deformation were quantified.

*Results:* The interfractional marker displacement varied per anatomical region and direction, with systematic and random errors ranging from 1.6–8.8 mm and 2.2–8.2 mm, respectively. Respiratory motion varied per patient (median 3D amplitude 5.2–20.0 mm) and day (interquartile range 0.8–4.2 mm). Regarding  $COM_{\text{stomach}}$  motion, respiratory motion was larger than interfractional motion (median 10.9 vs 8.9 mm;  $p < 0.0001$ ; Wilcoxon rank-sum), which was larger than pre-post motion (3.6 mm;  $p < 0.0001$ ). Interfractional deformations (median 5.8 mm) were significantly larger than pre-post deformations (2.6 mm;  $p < 0.0001$ ), which were larger than respiratory deformation (1.8 mm;  $p < 0.0001$ ).

*Conclusions:* The demonstrated sizable stomach motions and deformations during radiotherapy stress the need for generous non-uniform PTV margins for preoperative gastric cancer radiotherapy. These margins can be decreased by daily image guidance and adaptive radiotherapy.

### 3.1 Introduction

For the treatment of gastric cancer, surgical resection has been the standard of care; however, research focus has recently shifted towards (neo)adjuvant chemoradiotherapy<sup>9,10,64–66</sup>. With organ motion and deformation being an important source of uncertainty during radiotherapy (RT)<sup>13</sup>, accurate radiotherapy for the stomach is challenging. With an increased interest/application of preoperative gastric cancer radiotherapy (e.g., within the CRITICS-II study<sup>10</sup>), it is essential to improve the understanding of the various dynamics of the stomach.

The stomach is a highly mobile and deformable organ, as it experiences interfractional and intrafractional anatomical changes. As previously demonstrated, the stomach has considerable day-to-day changes in shape and size due to gastrointestinal filling differences<sup>67</sup> and, therefore, would benefit from adaptive radiotherapy<sup>68,69</sup>. Besides day-to-day anatomical changes, organ motion and deformation also occur during irradiation, for example, caused by respiration and peristalsis. Respiratory-induced motion amplitudes for stomach have been found to be similar to amplitudes for other upper-abdominal organs<sup>24–26</sup>; however, little focus has been on respiratory-induced deformations. Furthermore, peristaltic motion also causes stomach shape changes<sup>21,22,24,70</sup>; however, in free breathing the effect of peristalsis on treatment accuracy may be limited since for the stomach respiratory displacements are often considerably larger than deformations caused by peristalsis<sup>22</sup>. Additionally, differences in stomach position and shape can occur between the start and end of treatment fractions (i.e., pre-post displacement and deformation) due to prolonged supine positioning (e.g., due to gravitational sagging or patient relaxation), as observed not only for the stomach<sup>71</sup>, but also for the prostate<sup>72,73</sup>, liver<sup>74,75</sup> and lung<sup>76,77</sup>.

These various sources of organ motion and deformation, each with its own time scale and magnitude, impose different levels of uncertainty for radiotherapy and potentially require different managing strategies, such as daily imaging for soft-tissue matching, adaptive radiotherapy and/or increased PTV margins. Stomach motion has been quantified using delineations or visual assessment<sup>20,22,25,26</sup>; however, these strategies do not enable a point-to-point correspondence. Instead, fiducial markers in the stomach do provide such point-wise motion analyses and, combined with 4D imaging, allow for an extensive quantification of stomach motion and deformation, as previously demonstrated for other organs<sup>35,41,78</sup>.

Hence, this study aims to investigate the magnitude of motions and deformations in the stomach using fiducial markers and 4D pre-treatment and post-treatment imaging. Specifically, interfractional and intrafractional (i.e., respiratory-induced and pre-post) motion and deformation are quantified in order to evaluate how these should be accounted for during gastric cancer radiotherapy.

## 3.2 Materials and Methods

From October 2018 to January 2022, 14 patients who received CBCT-guided preoperative gastric cancer radiotherapy (prescription dose: 45 Gy in 25 fractions; supine positioning) within the CRITICS-II study (NCT02931890)<sup>10</sup> were included in this prospective study. The study protocol was approved by the ethics committee of the Amsterdam University Medical Center (study registration number NTR7241), and all included patients gave written informed consent. Patients received fiducial markers at different anatomical regions of the stomach and additional imaging. For patient and marker characteristics, see Supplemental Materials S3A.

### 3.2.1 Fiducial markers

To enable motion and deformation quantification, all patients had 2–6 fiducial markers placed in the stomach. For all but one patient, markers were implanted prior to the planning CT; for the one patient, marker implantation was after planning CT but prior to radiotherapy. All patients received flexible coil-shaped gold Visicoil markers (Visicoil, Core Oncology, CA, USA; outer  $\varnothing=0.35$  mm, length = 10 mm); the final 7 patients also received liquid BioXmark markers (Nanovi A/S, Lyngby, Denmark).

### 3.2.2 Imaging and delineations

The imaging data per patient included: one planning 4DCT (pCT; total 14; voxel pitch  $0.98 \times 0.98 \times 2.5$  mm<sup>3</sup>), 20–25 daily pre-treatment 4D cone-beam CTs (CBCT; total 340;  $1 \times 1 \times 1$  or  $0.91 \times 0.91 \times 1$  mm<sup>3</sup>), and 4–5 post-treatment 4DCBCTs (total 65; one in each week of radiotherapy; acquired for pre-post analyses). For 4DCT and 4DCBCT reconstructions, the respiratory cycle was divided into 10 phase bins. All imaging was typically acquired prior to 1 pm. Patients were instructed to eat only a light breakfast on pCT/treatment days.

For each 4D scan, end-exhale (EE) and end-inhale (EI) phase scans were identified by visual inspection of the diaphragm position. In line with clinical practice in our institute, bony anatomy matches were performed between the pCT EE scan and all other pre- and post-treatment CBCTs EE scans. When visible, each marker was segmented on EE and EI phase scans by applying an automatic threshold over a small region of interest that contained the marker. Subsequently, the marker coordinates, i.e., the center-of-mass coordinates of the marker segmentations with respect to the pCT coordinate system (using the bony anatomy match), were retrieved. For the patient with no markers on pCT, a repeat CT acquired during the first week of radiotherapy was used as a substitute. The marker coordinates on EE scans were used as reference, as several studies have demonstrated that EE scans result in more stable and reproducible organ positions than EI scans<sup>76,79</sup>. In total, 54 markers were visible on at least 8 EE

pre- and post-treatment CBCTs, and therefore included in the subsequent analyses. Of these 54 markers, one marker was visible on fewer than 8 EI pre-treatment CBCTs; therefore, 53 were included in the respiratory analyses.

### 3.2.3 Analyses

This study analyzed interfractional and intrafractional (pre-post and respiratory) motion and deformation (Figure 3.1). For interfractional anatomical variations, occurring between days, the EE pCT and pre-treatment CBCTs scan were used for analyses. Pre-post analyses were based on anatomical changes occurring in the minutes during treatment; for this, the paired pre- and post-treatment CBCTs were used. Finally, for respiratory-induced anatomical changes, which occur over seconds, paired EE and EI CBCTs were used.

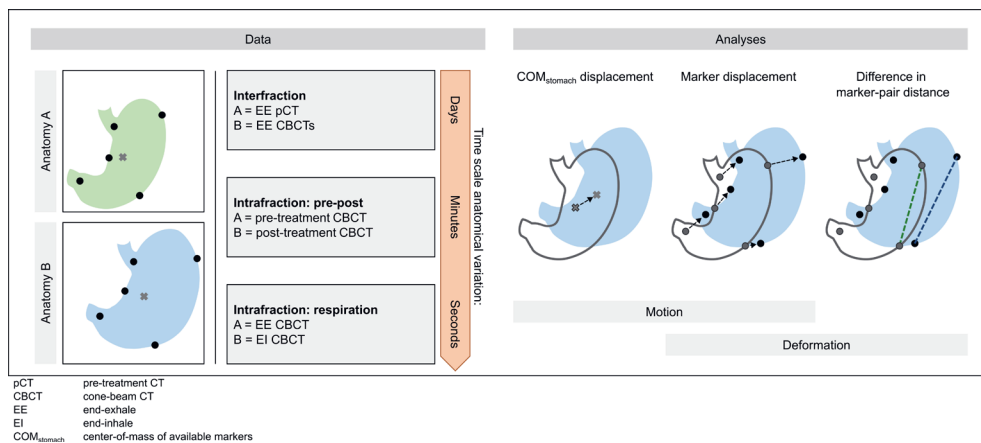


Figure 3.1: Schematic of the data that are used (left) and the most used analyses in this study (right). Every analysis constitutes a comparison between anatomies/stomach A and B with a potential difference in shape and size. Dots indicate markers, the  $COM_{stomach}$  is indicated by the cross. Interfractional motion and deformation occur between days and for this, stomach on EE pCT was compared with stomach on EE CBCTs. Intrafractional pre-post motion and deformation occurs in the minutes during treatment and constitutes a comparison between pre-treatment and post-treatment stomach anatomies. Intrafractional respiratory motion and deformation occur on the scale of seconds and were quantified using EE and EI CBCTs. For analyses,  $COM_{stomach}$  displacements represent stomach motion. Individual marker displacements are influenced by stomach motion as well as deformation, and were used to quantify interfractional and intrafractional respiratory motion and deformation. Finally, differences in marker-pair distances reflect stomach deformations and were measured for both interfractional and intrafractional deformations.

Several common analyses were used to evaluate inter- and intrafractional motion and deformation. Positional changes of markers are due to both stomach motion and deformation; a separate assessment of motion and deformation was therefore not feasible. For this study,

stomach motion between scans was defined as displacement of the center-of-mass of markers available on both scans ( $COM_{\text{stomach}}$ ). Stomach deformations were defined by the average difference in marker-pair distances between scans.

### 3.2.3.1 Interfractional marker displacements

#### Position variation per anatomical region

Stomach delineations on pCT were converted to triangulated meshes and subsequently mapped to one stomach (non-rigid iterative closest point algorithm<sup>80</sup>), with the sole purpose of transferring all markers onto one reference stomach (patient 2; Figure 3.2; similarly done as Bleeker et al. (2022)<sup>67</sup>). This mapping was specifically performed to facilitate the division of the 54 markers available for EE analyses into five anatomical regions based on their position on the reference stomach: cardia (12 markers from 11 patients), small curvature (12 markers from 10 patients), proximal large curvature (9 markers from 6 patients), distal large curvature (12 markers from 8 patients), and pylorus (10 markers from 9 patients).

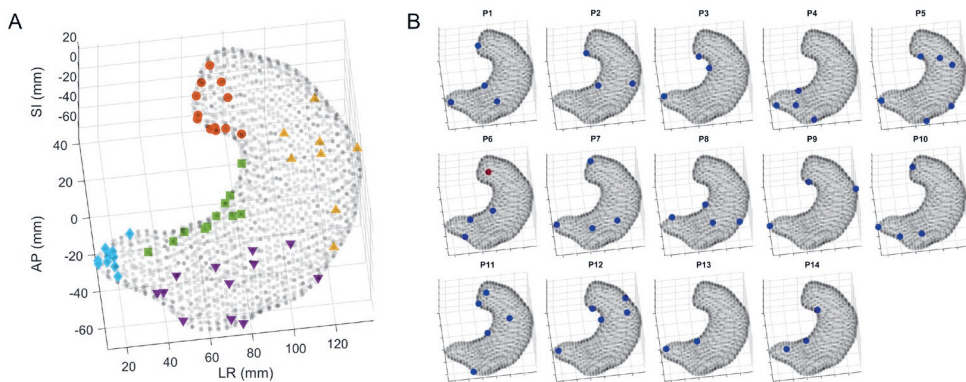


Figure 3.2: A) All 54 markers illustrated on the reference stomach. The different colors and symbols represent the anatomical regions: cardia (dark orange circles), small curvature (green squares), proximal large curvature (yellow up-pointing triangles), distal large curvature (purple down-pointing triangles), and pylorus (blue diamonds). B) The included markers per patient displayed on the reference stomach. One marker in patient 6 (red) was not included in the respiratory analyses. SI = superior-inferior; AP = anterior-posterior; LR = left-right. Positive is S, P, and L.

The interfractional position variation of the individual markers with respect to their position on pCT was evaluated separately for SI, AP and LR directions and for the separate anatomical regions. First, the mean and standard deviation (SD) of individual marker displacements were calculated as they are estimates of the systematic and random errors for individual markers. Next, the overall mean error (GM), systematic error ( $\Sigma$ ; SD of individual systematic error) and

random error ( $\sigma$ ; root mean square of individual random errors) were calculated for each anatomical region. Subsequently, based on these values, simplified margins were calculated according to the van Herk recipe ( $2.5\Sigma+0.7\sigma$ ) assuming that every marker within an anatomical region originated from a different patient<sup>81</sup>.

#### *Marker time trends*

Time trends in marker position with respect to the pCT were evaluated over the course of treatment using linear regression analyses (Bonferroni-Holm correction for multiple testing applied with a significance level  $\alpha=0.05$ ). The time trends were evaluated separately for SI, AP, and LR direction. Also, for every marker-pair, time trends in marker-pair distance throughout treatment were evaluated.

### **3.2.3.2 Intrafractional displacements**

#### *Respiratory-induced displacements*

For pCT and each CBCT, the difference in  $COM_{stomach}$  position between EE and EI phase scans resulted in the  $COM_{stomach}$  respiratory amplitude (peak-to-peak) in SI, AP, LR, and the vector length (3D). For each patient, the  $COM_{stomach}$  3D respiratory amplitude on pCT was compared with the respiratory amplitude distribution acquired from CBCTs. Also, CBCT  $COM_{stomach}$  displacements were averaged per patient to compare respiratory amplitude per direction (paired Wilcoxon signed-rank test;  $\alpha=0.05$ ).

To evaluate whether respiratory amplitude varied over the stomach surface, a linear mixed-effect analysis was used (detailed description in Supplemental Materials S3B). The linear mixed-effect analyses was performed using the marker coordinates on pCT and the 3D marker respiratory amplitudes on CBCTs. The estimated maximum difference in respiratory amplitude over the stomach was calculated for each patient using the fitted model and the vertex coordinates of the triangulated meshes of pCT stomach delineations.

#### *Displacements between pre-treatment and post-treatment CBCTs*

Displacements of the  $COM_{stomach}$  between pre- and post-treatment EE scans were evaluated (i.e., pre-post displacement). Furthermore, differences in  $COM_{stomach}$  3D respiratory amplitude between pre- and post-treatment CBCT were determined. The Pearson correlation ( $\alpha=0.05$ ) was calculated between: 1) treatment duration and  $COM_{stomach}$  3D pre-post displacement, and 2) the  $COM_{stomach}$  3D pre-post displacement and the difference in  $COM_{stomach}$  3D respiratory amplitude between pre- and post-treatment scans.

### 3.2.3.3 Motions and deformations

The 3D  $COM_{stomach}$  displacements were calculated between EE pCT and EECBCTs (interfractional), EE and EI CBCTs (respiratory; previously described above) and EE pre- and post-treatment CBCTs (pre-post; previously described above). Comparisons between the types of deformations were performed on the same scans. Statistical differences between the different sources of motions and different sources of deformations were tested using the Wilcoxon rank-sum test with Bonferroni-Holm correction applied to the significance level  $\alpha=0.05$ .

## 3.3 Results

### 3.3.1 Interfractional marker displacements

Substantial differences in interfractional displacements were observed between individual markers (Figure 3.3) and between the five anatomical regions (Table 3.1 and Figure 3.3). Considering the anatomical regions and directions, substantial variations in the systematic and random errors were observed, ranging from 1.6–8.8 mm and 2.2–8.2 mm, respectively. The cardia displayed the smallest interfractional mean and SD of marker displacement. The largest (variations in) displacements were observed for the distal large curvature.

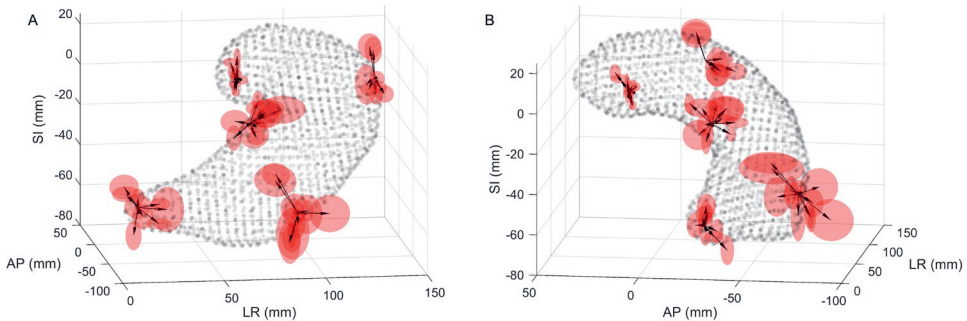


Figure 3.3: Interfractional marker displacements. Illustration of the systematic error (i.e., mean displacement; length and direction of arrows) and random error (i.e., standard deviation; axis of ellipsoids) of interfractional displacements of individual markers with respect to their position on pCT viewed from (A) anterior and (B) right direction. The arrows for each marker originate in one location within the anatomical region they were assigned to. The grey dots represent the vertices of the reference stomach (i.e., stomach on pCT of patient 2). The amplitudes of the errors are scaled to the reference stomach. For resulting systematic and random errors, see Table 3.1. SI = superior-inferior; AP = anterior-posterior; LR = left-right. Positive is S, P, and L.

Table 3.1: For the interfractional displacements, the overall mean error (GM), the systematic error ( $\Sigma$ ), the random error ( $\sigma$ ), and the corresponding simplified margin calculation for the five anatomical regions in superior-inferior (SI), anterior-posterior (AP) and left-right (LR) direction.

		SI (mm)	AP (mm)	LR (mm)
Cardia	GM	0.6	0.3	-0.3
	$\Sigma$	4.8	2.8	1.6
	$\sigma$	2.8	2.4	2.2
	$2.5\Sigma + 0.7\sigma$	14.0	8.8	5.5
Small curvature	GM	1.6	-0.6	3.7
	$\Sigma$	5.3	6.7	6.2
	$\sigma$	5.2	6.0	6.7
	$2.5\Sigma + 0.7\sigma$	16.8	20.9	20.1
Proximal large curvature	GM	0.7	-5.0	-0.7
	$\Sigma$	7.8	6.0	2.5
	$\sigma$	5.7	6.0	4.4
	$2.5\Sigma + 0.7\sigma$	23.6	19.3	9.4
Distal large curvature	GM	-1.3	-0.4	-1.2
	$\Sigma$	8.8	8.8	6.6
	$\sigma$	8.2	8.2	6.6
	$2.5\Sigma + 0.7\sigma$	27.7	27.7	21.0
Pylorus	GM	0.2	-2.0	2.1
	$\Sigma$	6.3	4.4	7.1
	$\sigma$	5.9	3.5	5.8
	$2.5\Sigma + 0.7\sigma$	20.0	13.5	21.7

For nine patients, at least one marker demonstrated a linear time trend with significant slope in interfractional position during treatment in at least one direction (20/54 markers; see Supplemental Materials S3C for a detailed table of all significant time trends). For 12/54 markers (from 5 patients) and 7/54 markers (from 3 patients), the absolute slope was larger than 0.4 and 0.8 mm/fraction, respectively. Such slopes result in position changes of >10 and >20 mm over the course of treatment (i.e., 25 fractions), respectively. The variation of slopes among markers within the same patient, indicate that these slopes were not only caused by stomach motion, but also by deformation. Of the 82 identified marker-pairs, 17 marker-pairs (6 patients) had time trends in their marker-pair distance with significant slopes ranging from -1.4–0.6 mm/fraction (details in Supplemental Materials S3D).



### 3.3.2 Intrafractional displacements

$COM_{\text{stomach}}$  3D respiratory amplitude on CBCTs varied per patient and day (Figure 3.4). Specifically, the median respiratory value per patient ranged from 5.2–20.0 mm (median 10.8 mm) and the interquartile range (IQR) of these respiratory amplitudes ranged from 0.8–4.2 mm (median 1.7 mm). For 28/340 CBCTs, the difference between pCT and CBCT 3D respiratory amplitude was >5 mm. For five patients, pCT respiratory amplitude was not within the 5 and 95 percentiles of CBCT respiratory amplitudes.

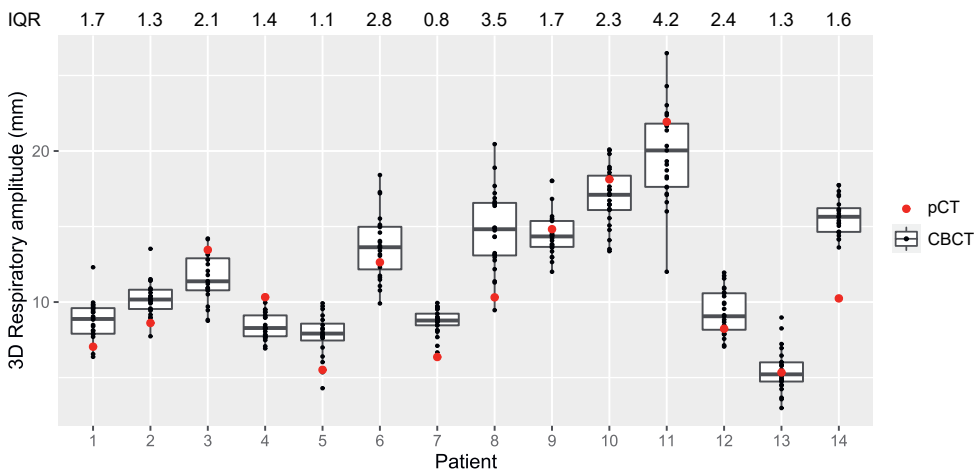


Figure 3.4: 3D respiratory amplitude of marker center-of-mass on CBCT (boxplot) and pCT (red dot) per patient. The interquartile range (IQR) of CBCT respiratory amplitudes per patient is displayed at the top. For patients 2, 4, 7, 8, and 14, respiratory amplitude on pCT was not within 5 and 95 percentiles of CBCT respiratory amplitudes. Boxplots: box = IQR, whiskers = lowest and highest data point within  $1.5 \times \text{IQR}$ .

The  $COM_{\text{stomach}}$  significantly moved 10.3 [4.3–16.6] mm in inferior direction (median [range]), 3.4 [1.7–10.3] mm in anterior direction, and 0.7 [-1.7–5.5] mm to the right upon inhalation. The  $COM_{\text{stomach}}$  respiratory amplitude was significantly larger in SI than AP (paired Wilcoxon signed-rank test;  $p < 0.001$ ), and amplitude in AP was significantly larger than in LR ( $p < 0.001$ ).

The mixed-effect model demonstrated a relation between a marker's respiratory amplitude and its coordinates in SI, AP and LR, with slopes of 0.062, 0.041, and -0.027 mm/mm, respectively. Based on the vertex coordinates of the stomachs of the 14 patients, the model yielded a maximum difference in 3D respiratory amplitude ranging between 3.8–7.4 (median 5.8 mm).

Treatment duration (i.e., time between the acquisition of pre- and post-treatment CBCT) was 13 [10–20] minutes (median [5–95 percentiles]; rounded to the nearest minute). During daily treatment, median  $COM_{\text{stomach}}$  3D pre-post displacement was 3.6 [0.98–8.2] mm. Specifically,  $COM_{\text{stomach}}$  significantly moved 1.4 [-1.9–7.6] mm in superior and 0.9 [-1.4–4.1] mm in posterior direction; no significant movement in LR direction (-0.4 [-4.1–4.1] mm). Also, 3D respiratory amplitude was significantly larger on pre-treatment than post-treatment imaging (median difference 0.77 [-2.2–4.0] mm; paired Wilcoxon signed rank test;  $p < 0.001$ ). Furthermore, a significant but weak correlation was found between treatment duration and 3D pre-post displacement ( $\rho = 0.26$ ,  $p = 0.03$ ; Supplemental Materials S3E). However, no significant correlation was found between 3D pre-post displacement and the difference in respiratory amplitude during treatment ( $\rho = 0.04$ ,  $p = 0.75$ ).

### 3.3.3 Motions and deformations

Interfractional and intrafractional motion and deformation are illustrated in Figure 3.5. Respiratory  $COM_{\text{stomach}}$  motion (median 10.9 mm) was significantly larger than interfractional motion (median 8.9 mm;  $p < 0.0001$ ). Interfractional motion was significantly larger than motion between pre- and post-treatment imaging (median 3.6 mm;  $p < 0.0001$ ). Also, interfractional deformation (median 5.8 mm) was significantly larger than both respiratory (1.8 mm;  $p < 0.0001$ ) and pre-post deformation (2.6 mm;  $p < 0.0001$ ). Moreover, respiratory-induced deformation was significantly smaller than pre-post deformation ( $p < 0.0001$ ).

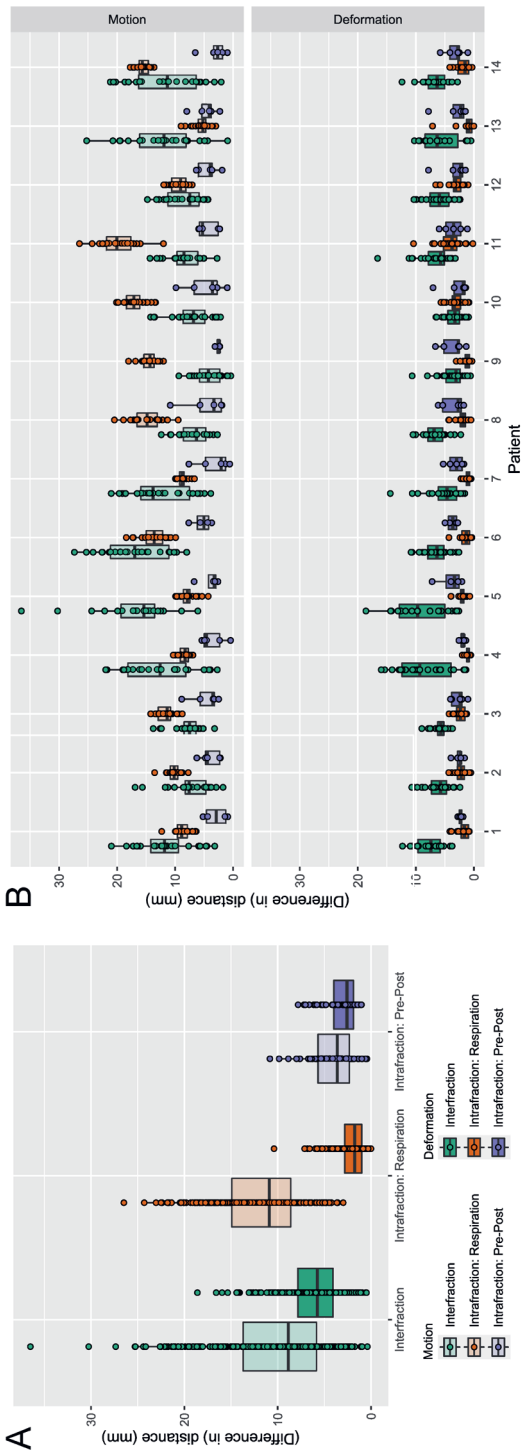


Figure 3.5: A) Interfractional, respiratory and pre-post motion and deformation combined for all patients. Motions were defined as the displacement of the center-of-mass of available markers (i.e.,  $COM_{\text{markers}}$ ) between end-exhale (EE), planning CT (pCT) and CBCT (interfractional; green), EE and end-inhale (EI) CBCTs (respiration; orange), and EE pre- and post-treatment CBCT (Pre-Post; purple). Deformations were defined as the mean difference in marker-pair distance between pCT and CBCTs. B) Motion (top) and deformation (bottom) separately for each patient. Note: The boxplots of deformation between pre-post imaging in panel B only contain 4 data points. Boxplots: box = interquartile range (IQR), whiskers = lowest and highest data point within  $1.5 \times IQR$ .

### 3.4 Discussion

This study investigated the magnitude of various sources of stomach motions and deformations using fiducial markers and 4D imaging. Specifically, interfractional and intrafractional (i.e., respiratory-induced and pre-post) motions and deformations were quantified. Respiratory and interfractional stomach motion were both considerably more prominent than pre-post motion. Furthermore, day-to-day deformations (i.e., interfractional) were more extensive than stomach deformations during treatment (i.e., intrafractional).

The most impactful anatomical variations during gastric cancer radiotherapy are caused by interfractional changes, as these result in systematic errors whereas respiratory motion causes dose blurring. Within this study, substantial day-to-day variations in stomach position with respect to the bony anatomy were observed (i.e.,  $COM_{\text{stomach}}$  interfractional motion and marker position time trends). Potential causes of these day-to-day variations include changes in gastrointestinal filling and/or tumor response. With both positive and negative slopes in marker-pair distances during treatment, the sources for interfractional variations may differ per patient. As such interfractional variations increase the risk for reduced target coverage or reduced sparing of surrounding organs-at-risk, stomach irradiations would benefit from daily image guidance with soft-tissue matching instead of a bony anatomy match. However, CBCT image quality in the upper-abdomen suffers from the stomach's high mobility and (moving) gas pockets in stomach and bowel during the 4-minute image acquisition (Supplemental Materials S3F). As a result, accurate and reliable soft-tissue matching may be challenging, even when assisted by fiducial markers. Although fiducial markers can introduce image artefacts on CBCT, they do serve as anatomical landmarks and thereby potentially aid target localization<sup>82</sup>. When CBCT image quality does allow for soft-tissue matching, the here calculated non-uniform PTV margins will probably be reduced; however, the remaining required margins will likely still be generous, as indicated by the here reported substantial deformations.

Eventhough day-to-day variations in stomach position would be accounted for using daily image guidance, substantial interfractional changes in stomach shape and size (i.e., interfractional deformation and marker displacement per anatomical region) should be managed differently. These interfractional shape and size changes, caused mainly by differences in stomach filling (e.g., food, drink, and gas), differ per anatomical region. Specifically, the cardia, where the stomach is attached to the esophagus and partly fixed by the diaphragm, demonstrated relatively minor systematic and random errors in all three directions compared to the other anatomical regions. As stomach filling is also affected by gas, changes in stomach shape and size are unpredictable and probably unavoidable despite eating instructions and irradiations being scheduled in the morning. As a result, large margins would be needed; for example, margins of >20 mm were suggested previously<sup>25,69</sup>. Although such generous margins could

ensure adequate target coverage, they do cause high dose to the surrounding organs-at-risk.

Alternatively, stomach shape and size changes could be accounted for with an adaptive radiotherapy strategy, as widely reported for other deformable targets such as bladder<sup>42,83</sup>, rectum<sup>84,85</sup>, and cervix<sup>86</sup>. In a recent study, the use of a gastric library of plans shows the potential to reduce necessary PTV margins and dose to organs-at-risk<sup>69</sup>. Application of online adaptive radiotherapy might further improve radiotherapy accuracy; however, whether image quality is sufficient for online adaptive radiotherapy should be investigated. Specifically, the high stomach mobility and the presence of (moving) gas in the stomach can severely affect (CB)CT and magnetic resonance (MR) image quality. Overall, the large interfractional motions and deformations suggest the need for large margins and/or adaptive radiotherapy to ensure adequate target coverage.

Besides interfractional anatomical changes, respiratory motion also causes considerable uncertainty during gastric cancer radiotherapy. Observed respiratory amplitudes were similar to previously measured stomach respiratory amplitudes (10.3, 3.4 and 0.7 mm for SI, AP and LR directions, respectively)<sup>20,24–26</sup>. For free breathing radiotherapy, the respiratory amplitude could be included in a non-uniform PTV margin, for example by including  $0.358 \times$  respiratory amplitude in the random error for each direction separately<sup>87</sup>. However, consistent with observations in other studies<sup>78,88,89</sup>, the respiratory amplitude varied between patients (median 3D amplitude ranged from 5.2–20.0 mm) and treatment days (IQR ranged from 0.8–4.2). Consequently, a margin based on a patient-specific respiratory amplitude instead of a single population-based amplitude may be preferred. Also, appropriate random errors may be applied to account for the day-to-day variations in amplitude. Besides including respiratory amplitudes in the margins, other respiratory motion management strategies may also be applied to minimize respiratory motion uncertainty, including breath-holding, regularized breathing, respiratory-gating, or respiratory-tracking<sup>90,91</sup>. Even with the implementation of such strategies, some level of residual respiratory motion uncertainty will persist. To illustrate, in the case of respiratory gating, the width of the gating window will determine the residual respiratory motion a target can experience. Overall, the selected respiratory motion management strategy will dictate the amount of residual respiratory uncertainties that must be included in margins.

As the stomach is not a rigid organ, not every part of the stomach experiences the same respiratory amplitudes, as demonstrated by the respiratory deformations and the mixed-effect model. Similar characteristics were previously displayed presented in the esophagus<sup>41,92,93</sup>. With potential amplitude differences as substantial as 7.4 mm over the stomach surface of these 14 patients, a single (patient-specific) respiratory amplitude incorporated as random error in margin calculations as proposed by van Herk et al. (i.e.,  $0.358 \times$  respiratory amplitude)<sup>87</sup>, may result in local over- and underestimations of respiratory amplitudes. Alternatively,

target delineation on every respiratory phase within 4D imaging may be used to determine inhomogeneous margins that account for the respiratory deformations.

Also, anatomical changes were detected between the start and end of radiotherapy delivery (i.e., pre-post motion and deformation). Intrafraction superior and posterior drifts or displacements may be explained by gravitational sagging, patient relaxation and/or changes in breathing, as also observed for the liver and lung<sup>75,76</sup>. However, no correlations were found between pre-post displacement and respiratory amplitude differences between pre- and post-treatment imaging. In our study, the measured pre-post motion (median 3.6 mm in median treatment duration of 13 minutes) was slightly smaller than that reported by Liu et al. (2021), who observed absolute stomach displacements ranging from 0.7 mm/min to 1.4 mm/min during a single 20-minute MRI examination<sup>16</sup>. This difference may be attributed to variations in patient relaxation or the employed imaging protocols; unlike the study of Liu et al., the patients in our study received repeated daily image acquisitions, which may have influenced patient relaxations and subsequently affected the measured pre-post motion. Even though each source of anatomical variation might affect radiotherapy accuracy, pre-post motion (median 3.6 mm) and deformation (2.6 mm) were relatively small and inclusion in PTV margins would likely have a limited impact on the margin. However, because of the large target volume in preoperative gastric radiotherapy and the radiosensitivity of direct surrounding organs-at-risk (e.g., bowels and kidneys), even a small margin reduction might affect toxicity. Accordingly, as treatment duration significantly correlated with pre-post displacement, treatment duration should be as short as possible to limit pre-post motion.

It is important to consider the potential significance of these smaller uncertainties, such as pre-post motion and deformation, but also peristalsis, within the context of ongoing efforts to reduce uncertainties and margins in radiotherapy for all targets. In this particular study, peristaltic motion was not taken into consideration, as it cannot be quantified using the available 4DCBCT scans. While peristaltic contractions can lead to displacements up to 1 cm<sup>24</sup>, these random uncertainties have a relatively small impact on radiotherapy accuracy, also due to the typical motion characteristics of gastric peristalsis, when compared to the measured interfractional displacements. However, despite being relatively small, these uncertainties may become increasingly important after other major uncertainties are addressed. Once mitigation strategies for the large interfractional motion and deformation and respiratory motion have been implemented for preoperative gastric cancer radiotherapy, further investigation is warranted to explore the impact of these smaller uncertainties. Here, pre- and post-treatment imaging was used as a substitute for anatomical variations during radiotherapy delivery. Radiotherapy delivery with an MR-linac might prove useful as it may provide further insights into intrafractional stomach motions and deformations as it allows simultaneous imaging and irradiation.

All motions and deformations were measured using a limited number of fiducial markers implanted in the stomach, thereby inducing some limitations and uncertainties. First, preferably, these markers would be evenly distributed over the stomach surface; however, this appeared to be challenging. The varying number of markers (2–6), with no homogenous distribution over the stomach surface, can affect motion and deformation quantifications. In addition, motion and deformation quantifications might be affected by the presence of a tumor, as a tumor may limit the local mobility of the stomach. Second, as measured with these markers, motion and deformation are not purely separated. Motion (i.e.,  $COM_{\text{stomach}}$  displacement) was also affected by stomach deformations and therefore likely did not equal true stomach motion. Ideally, stomach motion would be quantified using the COM of the stomach rather than the available markers. However, due to poor CBCT image quality (Supplemental Materials S3F), this was not feasible. On the other hand, the reported deformations (i.e., differences in marker-pair distance) were underestimations since the markers were not evenly distributed. Consequently, a comparison between the magnitudes of motion vs deformation includes large uncertainties; however, comparing the different types of deformations or motions (i.e., interfractional and both intrafractional) was feasible, as mostly the same set of markers was used. Third, all measurements were based on the segmentation of each marker on CT and CBCT phase images; hence, the accuracy of measurements was limited by image resolution and potentially image quality. However, uncertainty in the center-of-mass of marker segmentations is relatively small compared to measured motions and deformations and can therefore probably be neglected. Moreover, migration of the markers within the tissue was not observed and was not considered likely<sup>39,40,52</sup>. Fourth, although margins were calculated in this study, they should be interpreted cautiously. These margins only include uncertainty due to interfractional displacements with respect to a bony anatomy match and originate from simplified calculations with a limited number of non-independent measurements per anatomical region. Hence, margins were reported to provide insight into the position variation per anatomical region, and these calculations were not the focus of the study. Finally, all motions and deformations are calculated for the stomach specifically, while the target for preoperative gastric cancer radiotherapy often also includes regional lymph nodes. Although anatomical variations of these regional lymph nodes was not covered here, this study provides an understanding of the complex mobility of the stomach, which is an essential step toward accurate radiotherapy for gastric cancer patients. For accurate radiotherapy with the target being both stomach and regional lymph nodes, further research is necessary on the mobility of these regional lymph nodes.

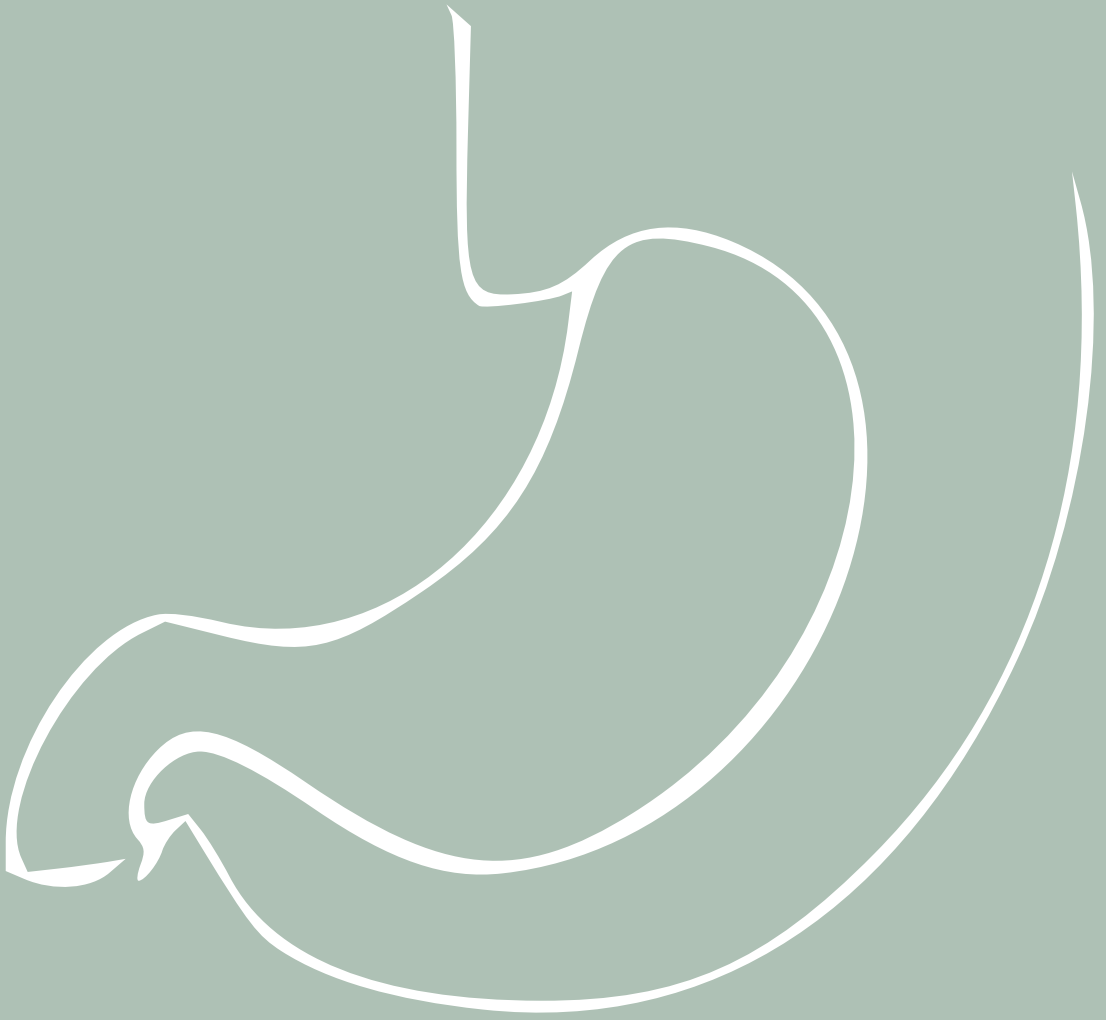
With preoperative gastric cancer radiotherapy being a relatively novel treatment approach, accurate identification of the uncertainties associated with this highly mobile and deformable target is essential. Hence, the goal of this paper was to provide an overview and initial insight into the magnitudes of anatomical changes during radiotherapy, enabling prioritization and

selection of the best mitigation strategies. The current work demonstrates that the largest uncertainties during radiotherapy are caused by the substantial interfractional changes the stomach experiences, which require generous non-uniform margins. While position changes may, when feasible, be mitigated by soft-tissue guidance, adaptive radiotherapy is the preferred approach for managing the sizable daily shape and size variations. One simple yet effective strategy for adaptive radiotherapy that can relatively easily be implemented is a library of plans<sup>69,94</sup>. A library of plans has been demonstrated to be a viable adaptive strategy for preoperative gastric cancer as visibility on CBCT was sufficient to perform plan selections<sup>68</sup>. Daily online segmentation and replanning may not be feasible yet as it requires high quality daily imaging. Another major uncertainty during radiotherapy is introduced by respiratory motion. Various respiratory motion management strategies could reduce the extent of this uncertainty, such as breath-holding and respiratory gating or tracking. Overall, mitigating these major uncertainties is expected to have the greatest impact on radiotherapy accuracy. Regardless of the chosen mitigation strategy or combination of strategies, the residual motion and deformation should still be quantified and the necessary margins should be determined for that specific workflow. Given the highly deformable nature of the stomach, margin calculations are preferably based on assessments of the local variation of the stomach with respect to the treatment plan.

### 3.5 Conclusion

The stomach is a challenging target for radiotherapy due to its complex and highly mobile and deformable nature. The wide variety of observed sources and magnitudes of stomach motion and deformation during radiotherapy stress the need for generous anisotropic PTV margins; these required margins can be reduced when using daily image guidance and adaptive radiotherapy. The comprehensive quantifications in this study enable selection of the most effective mitigation strategies to counteract these uncertainties, thereby optimizing gastric cancer radiotherapy.





**Feasibility of cone beam CT-guided library  
of plans strategy in preoperative gastric  
cancer radiotherapy**

4

Margot Bleeker  
Karin Goudschaal  
Arjan Bel  
Jan-Jakob Sonke  
Maarten C.C.M. Hulshof  
Astrid van der Horst

Modified from:  
Radiotherapy and Oncology, 2020, 149, 49–54.  
DOI: [10.1016/j.radonc.2020.04.057](https://doi.org/10.1016/j.radonc.2020.04.057)

## **Abstract**

*Purpose:* The stomach displays large anatomical changes in size, shape and position, which implies the need for plan adaptation for gastric cancer patients who receive preoperative radiotherapy. We evaluated the feasibility and necessity of a CBCT-guided library of plans (LoP) strategy in gastric cancer radiotherapy.

*Materials and methods:* Eight gastric cancer patients treated with 24–25 fractions of single-plan radiotherapy with daily CBCT imaging were included. The target was delineated on the pre-treatment CT and first 5 CBCTs to create a patient-specific LoP. Plan selections were performed by 12 observers in a training stage (2–3 CBCTs per patient) and an assessment stage (17 CBCTs per patient). The observers were asked to select the smallest plan that encompassed the target on the CBCT. A total of 136 plan selections were evaluated in the assessment stage.

*Results:* Delineations on CBCTs showed that in 90% of the 40 delineated fractions part of the CTV was outside the PTV based on the pre-treatment CT. At least two-thirds of the observers agreed on the selected plan in 65.2% and 70% of the fractions in the training stage and the assessment stage, respectively. For each patient, at least two different plans from the LoP were the most selected plan.

*Conclusion:* A CBCT-guided patient-specific LoP strategy is feasible for gastric cancer patients, yielding good agreement in plan selections. Unless generous margins are used to avoid frequent geometric misses, it is likely that part of the target will be missed with single-plan radiotherapy.

## 4.1 Introduction

For gastric cancer, surgical resection currently forms the basis for curative treatment. Adjuvant chemoradiotherapy has shown to improve outcome<sup>95</sup>. Recently, the CRITICS-II trial (NCT02931890) started, in which the effect of preoperative chemoradiotherapy is evaluated<sup>10</sup>. Within this trial, two of the three treatment arms include radiotherapy. The entire stomach and certain regional lymph nodes (determined by tumor location) are the clinical target volume (CTV) for radiotherapy, which currently consists of a single plan delivered in 25 daily fractions. The stomach, however, is a very deformable and mobile organ due to gastrointestinal filling, peristalsis, and breathing<sup>20</sup>. As a result, a single treatment plan is suboptimal, as it introduces the risk of partially missing the target and/or unnecessary delivery of high doses to surrounding organs.

The development of adaptive radiotherapy (ART) for gastric cancer may ensure adequate irradiation with acceptable PTV margins of the target by adapting the treatment plan to daily anatomical changes. ART for complete gastric irradiation was only applied in one case report<sup>96</sup>, in which MR-guidance was used. Our institutes currently use daily CBCT imaging during radiotherapy of gastric cancer within the CRITICS-II trial. ART based on CBCT imaging can be applied using a library of plans (LoP) strategy. With such a strategy, multiple treatment plans are created prior to or during the first part of treatment and the best fitting plan is selected based on daily CBCT imaging. LoP strategies have been successfully applied clinically in radiotherapy of bladder<sup>43,97,98</sup>, cervical<sup>44,45,99</sup> and rectal cancer<sup>100,101</sup> to increase target coverage and/or normal tissue sparing. However, this approach has not yet been applied for gastric cancer. Although a LoP has the potential to improve radiation accuracy, it may be challenging to identify stomach boundaries, due to poor soft tissue contrast and image artefacts on CBCT.

To assess feasibility of CBCT-guided LoP strategies, inter-observer studies have previously been performed for bladder<sup>102</sup> and rectal cancer<sup>100,101</sup>. In such an inter-observer study, multiple observers perform plan selections on a set of CBCT images to assess variability and consistency in plan selection. Overall, these studies found good concordance between observers; however, less agreement was observed for CBCTs with substantial image artefacts<sup>102</sup> or when instructions were inadequate<sup>101</sup>.

The aim of this study was to assess the feasibility of CBCT-guided gastric cancer ART. In this study, a LoP was created based on the observed anatomy on pre-treatment CT (pCT) and daily CBCTs in the first week of treatment. The visibility of the target on CBCT for delineations and plan selection was evaluated, as well as the necessity and challenges of a LoP strategy for this patient group.

## 4.2 Materials and methods

### 4.2.1 Patient population

Retrospectively, we included the first 8 patients who received single-plan preoperative radiotherapy within the CRITICS-II trial with daily CBCT-guidance in our two institutes<sup>10</sup>. Patients were treated with the volumetric modulated arc therapy (VMAT) delivery technique and received 45 Gy in 25 fractions; patient 6 received only 24 fractions due to radiation toxicity (Table 4.1). Patients 5 and 6 had gold fiducial markers in the stomach to increase visibility on CBCT. To obtain homogeneous patient data, these markers were retrospectively removed on pCT and CBCT using in-house developed software. On CBCT, markers were smoothed on 2D projection images prior to reconstruction.

### 4.2.2 Imaging

Patients were instructed to eat a light breakfast on the days of pCT and treatment. Generally, the pCT and all fractions were scheduled prior to 1 pm. The CRITICS-II protocol<sup>10</sup> defines the CTV as the gross tumor volume, the entire stomach and regional lymph nodes. The planning target volume (PTV) margin was 10 mm in all directions. Daily CBCTs were acquired with the Elekta XVI system (Elekta AB, Stockholm, Sweden) prior to each fraction for setup verification and evaluation of target coverage.

Retrospectively, all acquired CBCTs were rigidly re-registered to the pCT based on bony anatomy and corrected in longitudinal direction for left diaphragm position, which was regarded as a substitute for the coronal border of the stomach (Velocity 4.0, Varian).

### 4.2.3 Library of plans

We used the anatomical variation observed on the CBCT scans in the first week of treatment to create a LoP (Figure 4.1)<sup>47</sup>. Hence, the CTV was delineated on the pCT and the first 5 CBCTs by an expert radiation oncologist. For delineation on CBCT, the CTV of the pCT was copied and subsequently adjusted. The resulting 6 CTVs were used to create the LoP. The study consisted of a training stage and an assessment stage; the strategy used to create the LoP differed between these two stages (Figure 4.1; steps 3B1 and 3B2). As the goal for this study was to assess feasibility of CBCT-guided gastric ART rather than what strategy to use for the LoP, a straightforward strategy to create the LoP was used.

Table 4.1: Patient and imaging characteristics.

Patient	Age	Sex	Treated at <sup>a</sup>	# fractions <sup>b</sup>	Markers	CT scanner	LINAC <sup>e</sup>	CBCT settings: Field of view (mm <sup>3</sup> ); kV; mAs
1	69	Male	AMC	25	No	GE Lightspeed RT 16 <sup>c</sup>	Elekta Synergy	410×410×264; 120; 1056 <sup>f</sup>
2	61	Male	AMC	25	No	GE Lightspeed RT 16 <sup>c</sup>	Elekta Infinity	410×410×264; 120; 845
3	70	Female	AMC	25	No	GE Lightspeed RT 16 <sup>c</sup>	Elekta Infinity	410×410×264; 120; 1056
4	82	Male	AMC	25	No	GE Lightspeed RT 16 <sup>c</sup>	Elekta Infinity	410×410×264; 120; 1056
5	62	Male	AMC	25	Yes	GE Lightspeed RT 16 <sup>c</sup>	Elekta Infinity	410×410×264; 120; 1056
6	38	Male	AMC	24	Yes	GE Lightspeed RT 16 <sup>c</sup>	Elekta Infinity	410×410×264; 120; 1056 <sup>g</sup>
7	65	Male	NKI	25	No	Siemens Sensation Open <sup>d</sup>	Elekta Synergy	300×300×256; 120; 525
8	60	Male	NKI	25	No	Siemens Sensation Open <sup>d</sup>	Elekta Synergy	300×300×256; 120; 525

<sup>a</sup>AMC: Amsterdam UMC, location AMC; NKI: The Netherlands Cancer Institute<sup>b</sup>One fraction = 1.8 Gy<sup>c</sup>General Electric, Fairfield, CT, USA<sup>d</sup>Siemens, Erlangen, Germany<sup>e</sup>Elekta AB, Stockholm, Sweden<sup>f</sup>One fraction 845 mAs<sup>g</sup>Two fractions 845 mAs

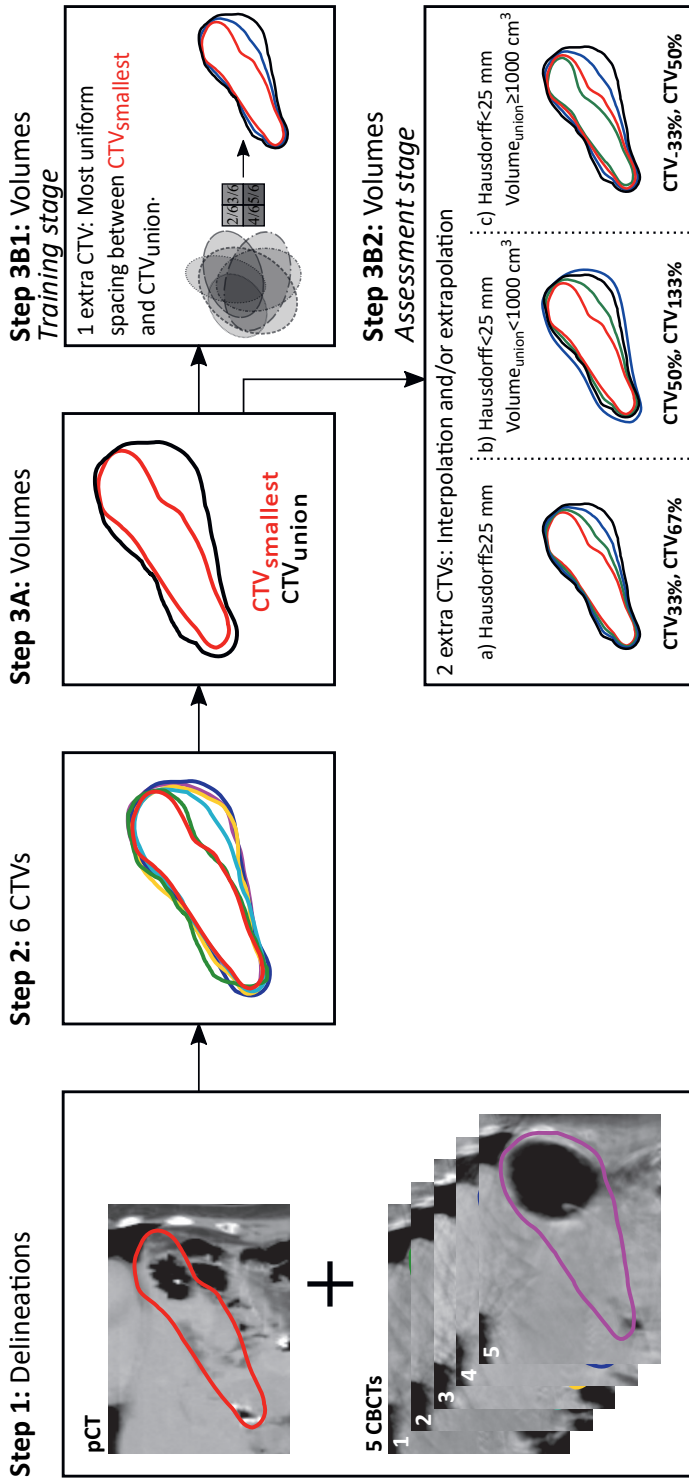


Figure 4.1: Schematic representation of LoP creation. CTV delineated on pCT and first 5 CBCTs (step 1), yielding 6 CTVs contours (step 2), from which the smallest delineated CTV ( $CTV_{smallest}$ ) and union of all delineations ( $CTV_{union}$ ) are created (step 3A). Training stage (step 3B1): one additional CTV created based on the volume contained in at least 2,3,4 or 5 CTV delineations; the contour was selected that showed the most uniform spacing between  $CTV_{smallest}$  and  $CTV_{union}$ . Assessment stage (step 3B2): two additional CTVs created by interpolation and/or extrapolation between  $CTV_{smallest}$  and  $CTV_{union}$  depending on the Hausdorff distance between  $CTV_{smallest}$  and  $CTV_{union}$  and on the volume of  $CTV_{union}$ .

Three contours were created for the training stage, while four were created for the assessment stage. For both stages, one of these contours was the smallest ( $CTV_{\text{smallest}}$ ) and one was the union ( $CTV_{\text{union}}$ ) of the six delineated CTVs. For the training stage, a single intermediate contour was used. For this, first we created 4 intermediate contours, namely the volumes that were occupied in at least 2, 3, 4, or 5 out of 6 CTV delineations (with 1 out of 6 delineations being the union and 6 out of 6 delineations being the intersection; see Figure 4.1 step 3B1). We visually inspected these 4 contours and selected the contour with the most uniform spacing between  $CTV_{\text{smallest}}$  and  $CTV_{\text{union}}$  as the additional contour. For the assessment stage, two additional contours were created by interpolation and/or extrapolation between  $CTV_{\text{smallest}}$  and  $CTV_{\text{union}}$  using a structure-based deformable image registration algorithm (RayStation 9, RaySearch Laboratories). When the Hausdorff distance between the two existing contours ( $CTV_{\text{smallest}}$  (0%) and  $CTV_{\text{union}}$  (100%)) was  $\geq 25$  mm, two contours were created in between the existing contours (at 33% and 66%). When the Hausdorff distance was  $< 25$  mm, one contour was created in between (at 50%); the other contour was created larger than  $CTV_{\text{union}}$  (at 133%) or, when the size of the union was  $\geq 1000$  cm<sup>3</sup>, smaller than  $CTV_{\text{smallest}}$  (at -33%). Finally, for both stages, plan selection volumes (PSVs) were constructed by adding a uniform margin of 3 mm to these contours. Assuming that half of the uncertainties would be removed by using a LoP, hence, this additional margin was added to preserve a 7-mm margin of the original 10-mm PTV margin to account for remaining uncertainties.

#### 4.2.4 Inter-observer study

Twelve observers were asked to perform plan selections: 6 expert radiation therapy technologists (eRTTs; experts in CBCT-guided ART), 2 RTTs, 3 radiation oncologists (in training) and 1 physicist. Since at our institutes RTTs clinically perform plan selections for bladder, cervix and rectal cancer, most observers were RTTs. All 12 observers participated in both the training and the assessment stage.

##### **Training stage**

The training stage included a lecture on target definition by an expert radiation oncologist, plan selections on the training set, and a consensus meeting for all observers. The aim of the training stage was to increase uniformity in plan selections and to evaluate the method used to create the LoP and observer instructions.

Plan selections were performed in random patient order by each observer individually on a training set, consisting of 23 CBCTs (3 CBCTs per patient, fractions 7, 15 and 23; 2 CBCTs for the patient with 24 fractions, fractions 7 and 15). Observers were asked to select the smallest PSV that encompassed the target. When observers selected the largest or the smallest plan, they were asked to specify whether the PSV was too small or too large, respectively. Furthermore,



an option was available for when the observers could not identify the stomach and, therefore, could not select a plan. Observers were not allowed to adjust the image registration and thereby shift the PSVs.

During the consensus meeting, plan selections for all 23 CBCTs were discussed. Every observer was able to compare their plan selections with the modal plans (i.e., the most frequently selected plan per fraction;  $PSV_{mod}$ ). Agreement in plan selections was pursued to increase plan selection uniformity.

### **Assessment stage**

Plan selections were performed in random patient order by each observer individually on the remaining 136 CBCTs (17 CBCTs per patient). The delineations, the LoP and the instructions were altered after the consensus meeting, to reduce interpretation errors (see section 4.2.3).

The observers were asked to select the smallest PSV that encompassed the target. Based on the training stage, the specification was added that stomach content was not allowed to be outside the selected PSV. Again, each observer was able to specify whether the selected PSV was too small, too large or whether they could not select a plan, and no adjustments in image registrations were allowed. For each plan selection, there was the possibility to supply comments.

For all patients, the PSVs were labeled A, B, C and D from smallest to largest plan. When the smallest plan was too large or when the largest plan was too small, this was denoted by plan <A and plan >D, respectively.

### **4.2.5 Analysis**

To assess target coverage of single-plan radiotherapy, we determined for the 40 delineated CBCTs the CTV coverage by the  $PTV_{pCT}$  (i.e., CTV on pCT + 10-mm margin). Hereby, potentially missed CTV during the first week of radiotherapy was identified and, subsequently, the adequacy of single plan radiotherapy was evaluated. For both training and assessment stage, agreement between observers was evaluated for each fraction, with agreement defined as the percentage of observers who selected  $PSV_{mod}$ .

## **4.3 Results**

CTV adjustments on the CBCT images were made for all 40 CBCTs. However, often no adjustments with respect to the CTV of the pCT were made in caudal direction, because of poor visibility of the anatomical CTV borders due to low image quality.

Thirty-six out of 40 delineated CTVs (90%) were partially outside the  $PTV_{pCT}$ , with on average 2.9% of the volume (range: 0.0%–12.5%; range in absolute volume: 0.0–103.4 cc). For the clinical registration, on average 2.9% of the volume was outside the  $PTV_{pCT}$  (range: 0.0%–14.4%).

In the training stage (23 plan selections per observer), all 3 PSVs were  $PSV_{mod}$  for at least one fraction (see Supplemental Materials S4A). Out of 276 plan selections, 9 times an observer indicated they could not select a PSV due to image quality. For 15 fractions (65.2%), agreement was  $\geq 66\%$ .

During the consensus meeting, the provided PSVs proved not to be adequate. Initially, the non-uniform spacing between the provided PSVs (Figure 4.2A) induced interpretation differences amongst observers. In addition, the target was initially delineated in the axial plane, often resulting in discontinuous contours in the sagittal and coronal planes. Although the initial delineations were clinically acceptable, their discontinuity, combined with the instructions that the PSV should encompass the target, could cause observers to dismiss otherwise suitable contours. Because of these challenges, a new LoP strategy was implemented in the assessment stage. The delineations were altered and smoothed to reduce contour discontinuity in the assessment stage. Moreover, many observers preferred an additional PSV, hence, there were 4 PSVs in the assessment stage.

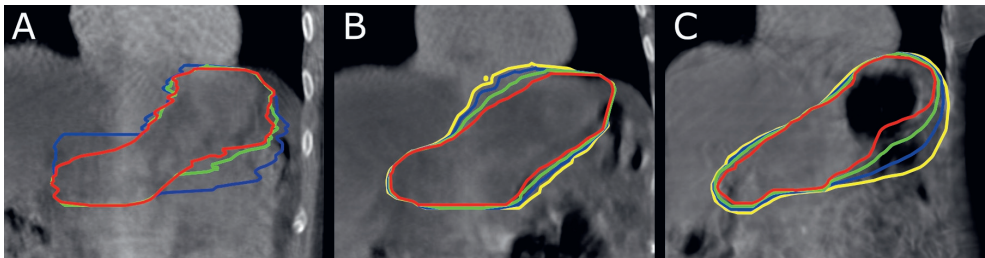


Figure 4.2: Examples of LoPs in coronal view on CBCT images, in training stage (A, patient 6) and assessment stage (B, patient 5 and C, patient 3), illustrating non-uniform spacing in the training stage and delineations being smoother in the assessment stage.

In the assessment stage (136 plan selections per observer, 1632 in total),  $PSV_{mod}$  varied considerably per patient and fraction (see Supplemental Materials S4B). Although observers did select the smallest PSV (i.e., PSV A), it was never  $PSV_{mod}$  for any fraction (Figure 4.3A). PSV A was never assessed as too large (i.e.,  $PSV < A$ ), whereas in 16 fractions (11.8%)  $PSV_{mod}$  was  $PSV > D$  (i.e., PSV D being too small). Mostly when  $PSV > D$  was selected, observers commented that this was only due to a small portion of the volume of the CTV being outside the PSV. Out of 1632 total plan selections, only 7 times (0.4%) an observer indicated they could not select a PSV due to image quality.

For every patient,  $PSV_{mod}$  varied over the fractions. There were 2 different  $PSV_{mod}$  for 1 patient, 3 different  $PSV_{mod}$  for 4 patients and 4 different  $PSV_{mod}$  for 3 patients (Figure 4.3B).

Looking at all fractions combined, and considering plan <A and >D as additional PSVs, for most fractions (51%) 3 different PSVs were selected by the observers. A single PSV (i.e., full agreement between observers) was selected for 8 fractions (6%) and 2 and 4 PSVs were selected for 32 (24%) and 27 (20%) fractions, respectively (Figure 4.3C).

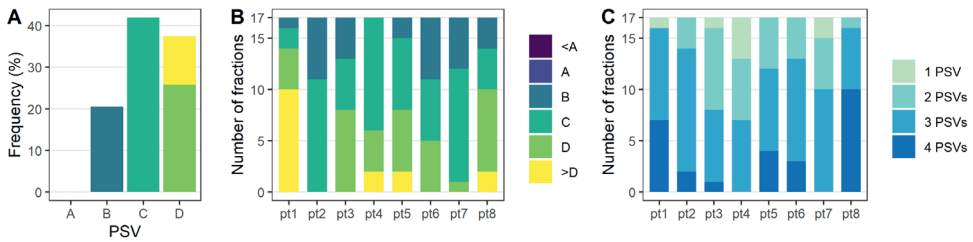


Figure 4.3: Results for assessment stage. A) The most frequently selected PSV ( $PSV_{mod}$ ) for all fractions. B)  $PSV_{mod}$  per patient. C) Number of different PSVs selected per patient per fraction.

Overall, the agreement between observers per fraction ranged from 33%–100% (median=75%) but varied between patients. In total, for 70% of fractions agreement was  $\geq 66\%$ . Furthermore, for only 5 fractions (4%), agreement was  $< 50\%$ .

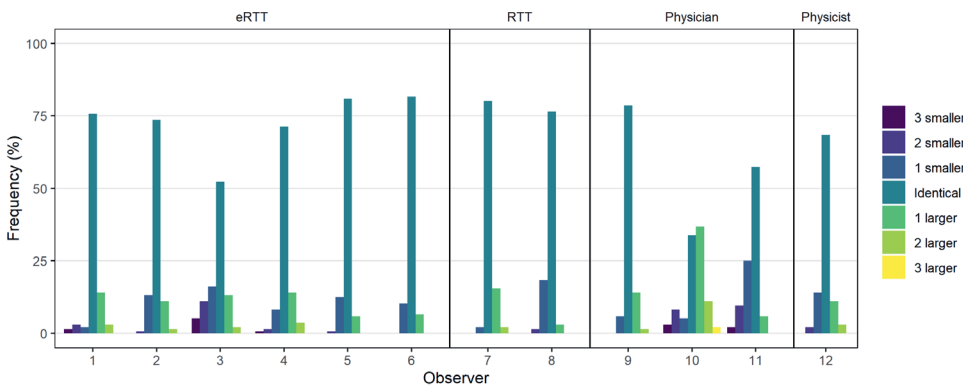


Figure 4.4: For each observer, difference between selected plan selection volumes (PSVs) and most frequently selected plan selection volume ( $PSV_{mod}$ ) per fraction.  $N=136$  per observer.

It can be noted that all observers most frequently selected  $PSV_{mod}$ , except observer 10 (Figure 4.4). None of the observers selected a PSV that was more than three PSVs smaller or larger than  $PSV_{mod}$ .

For every patient except patient 2, the average selected PTV volume in the assessment stage was larger than the  $PTV_{pCT}$  with the average difference in volume over 8 patients being 171.8  $cm^3$ .

## 4.4 Discussion

In this study, we evaluated the feasibility of CBCT-guided gastric ART by retrospectively creating a LoP and performing a plan selection study with multiple observers. Our results indicate acceptable visibility of the target on the first 5 CBCTs, as the physician was always able to adjust the original CTV to the anatomy on the CBCT. However, visibility was poor in the caudal regions of the CTV (e.g., peripancreatic lymph node area), also expressed by few alterations to delineations in these regions. Even though not all of the target could be clearly distinguished, we found that in 90% of the fractions part of the CTV would have been missed with single-plan radiotherapy. Consequently, delineations on the CBCT in the first week of treatment demonstrate the urgent need and potential for ART for gastric cancer patients.

As we used these delineations to create the LoP, PSVs were similar in anatomical regions where the physician was not able to clearly identify target boundaries. Similarly, the largest spacing between PSVs mostly occurred in anatomical regions where gas pockets in the stomach could be easily identified on CBCTs, i.e., the left lateral and ventral part of the stomach. In this inter-observer study, a selection could not be made in only 0.4% of the performed plan selections. Hence, visibility on CBCTs of the target was sufficient to perform plan selections. Heijkoop et al. (2014) suggested using a motion-robust backup plan in case no plan could be selected for cervical cancer ART<sup>94</sup>. This backup plan was based on the full motion range of the target, which is comparable to the largest PSV in this study. Hence, in case no plan can be selected, the largest PSV may be used as backup plan to optimize coverage. To increase target visibility, application of MR-guidance can be examined, as it offers superior soft tissue contrast<sup>96</sup>, or the use of fiducial markers with CBCT imaging may be explored. Fiducial markers in the upper abdomen have been used to increase visibility on CBCTs in, for instance, pancreatic cancer<sup>37</sup>. To further improve target visibility on CBCT, the benefit of fiducial markers in the less visible regions of the target will be investigated in a follow-up study.

Application of ART for gastric cancer may increase target coverage and/or normal tissue sparing. If the CTV is relatively small on the pCT, increased coverage can be expected when using a LoP rather than a single plan. Conversely, if the CTV on pCT is large, a LoP will mainly lead to more normal tissue sparing. In this study, the benefit of a LoP was primarily in target coverage since the average irradiated volume was larger with a LoP than with single-plan radiotherapy. The delineated CTVs on CBCT showed that single-plan radiotherapy with 10-mm PTV margins would have resulted in inadequate target coverage. However, the magnitude of

spacing between target volumes was patient dependent; small spacing differences between delineated CTVs translate to little spacing between different PSVs when using our LoP strategy (Figure 4.2B,C). Hence, the potential benefit of a LoP strategy for this patient group is patient dependent. To deal with this, a variable number of plans dependent upon the distance between the smallest delineation and the union may be used.

The importance of education and clear instructions for plan selections has already been stressed in studies for other targets, as it is likely to increase concordance amongst observers and, therefore, contribute to a treatment independent of the person who selects the plan<sup>42,100,101,103</sup>. The agreement in the training stage and the assessment stage were comparable. However, because we changed the LoP strategy and we did not use the same CBCTs before and after the consensus meeting, we were not able to look at the direct effect of the consensus meeting and the altered selection instructions, as has been done in other studies<sup>42,101</sup>. Nevertheless, we found that uniform spacing between contours, smooth delineations, and explicit instructions are crucial in reducing interpretation differences between observers.

For the bladder and cervix, several studies used a patient-specific LoP based on interpolation between a full and an empty bladder pre-treatment scan<sup>94,104,105</sup>. Stomach deformations, however, are less predictable than deformations of bladder or cervix. Pre-treatment scans with empty and full stomach are not expected to result in reliable stomach contours during the treatment course in this patient group, although this was not analyzed in this study. Therefore, we applied a method as described for deformable targets<sup>47</sup>. The first week of treatment is not necessarily predictive of the anatomical changes observed in the following weeks, which can be challenging. In addition, it should be noted that the union of all delineations does not represent the stomach as observed at any given time and therefore might be a suboptimal contour for a LoP. Furthermore, this LoP strategy did not consider the effect of respiratory motion on the target; how to include this in the LoP should be investigated. This study aimed to assess feasibility of CBCT-guided ART; consequently, what method of ART best to apply for gastric cancer was not evaluated. Even though the strategy of creating a LoP still needs improving, we already introduced this methodology in clinic.

Using this LoP strategy, the patient always receives at least one full week of single-plan radiotherapy, which may reduce coverage and/or increase dose to healthy tissue in the first week. Hence, to make full use of a LoP during the entire course of treatment, a patient-specific model-based LoP would be beneficial. A population analysis was performed in several studies to identify primary deformations and thereby predict the most likely anatomical deformations per patient<sup>48,106</sup>. From this, a LoP can be created, as has been done for cervical cancer<sup>48</sup>. Thus, to further improve gastric ART, the potential of a model-based LoP for this patient group will be investigated.

To conclude, this is the first study investigating ART for gastric cancer patients, in which feasibility of a CBCT-guided patient-specific LoP strategy was established. Although target visibility varied per anatomical region, the results indicate that target delineation and plan selections on CBCT are possible. The delineations on CBCT and the variation in modal plans showed inadequate target coverage using 10-mm PTV margin single-plan RT and the potential benefit of a LoP strategy. This demonstrates the urgent need for improvement of the current clinical practice of single-plan radiotherapy.

### ***Acknowledgements***

The authors like to thank Emina Ajanovic, Marije Frank, Lianne van Gurp, Arnout van den Hoek, Rianne de Jong, Sandy Loopeker, Eva Versteijne, Margriet Vriens, Kim Wortel and Jan Wiersma for performing the plan selections. The authors also thank Theo Driever for preparing and providing the patient data from the Netherlands Cancer Institute.



**Gastric deformation models for adaptive radiotherapy: Personalized vs population-based strategy**

5

Margot Bleeker  
Maarten C.C.M. Hulshof  
Arjan Bel  
Jan-Jakob Sonke  
Astrid van der Horst

Modified from:  
Radiotherapy and Oncology, 2022, 166, 126–132.  
DOI: [10.1016/j.radonc.2021.11.028](https://doi.org/10.1016/j.radonc.2021.11.028)



## Abstract

*Purpose:* To create a library of plans (LoP) for gastric cancer adaptive radiotherapy, accurate predictions of shape changes due to filling variations are essential. The ability of two strategies (personalized and population-based) to predict stomach shape based on filling was evaluated for volunteer and patient data to explore the potential for use in a LoP.

*Materials and methods:* For 19 healthy volunteers, stomachs were delineated on MRIs with empty (ES), half-full (HFS) and full stomach (FS). For the personalized strategy, a deformation vector field from HFS to corresponding ES was acquired and extrapolated to predict FS. For the population-based strategy, the average deformation vectors from HFS to FS of 18 volunteers were applied to the HFS of the remaining volunteer to predict FS (leave-one-out principle); thus, predictions were made for each volunteer. Reversed processes were performed to predict ES. To validate, for seven gastric cancer patients, the volunteer population-based model was applied to their pre-treatment CT to predict stomach shape on 2–3 repeat CTs. For all predictions, volume was made equal to true stomach volume.

*Results:* FS predictions were satisfactory, with median Dice similarity coefficient (mDSC) of 0.91 (population-based) and 0.89 (personalized). ES predictions were poorer: mDSC=0.82 for population-based; personalized strategy yielded unachievable volumes. Population-based shape predictions (both ES and FS) were comparable between patients (mDSC=0.87) and volunteers (0.88).

*Conclusion:* The population-based model outperformed the personalized model and demonstrated its ability in predicting filling-dependent stomach shape changes and, therefore, its potential for use in a gastric cancer LoP.

## 5.1 Introduction

Recently, research focus has shifted from post-operative to preoperative (chemo)radiation for gastric cancer, due to observed high toxicity and low patient compliance<sup>10</sup>. Currently in our institutes, preoperative radiotherapy is applied using a single plan to irradiate the entire stomach and regional lymph nodes. Large deformations due to filling can cause inadequate target coverage<sup>68</sup>, underlining the urgent need to adapt radiation treatment to the daily anatomy.

There are various adaptive radiotherapy strategies to account for daily anatomical deformations. A library of plans (LoP) consists of several plans from which daily the most fitting one can be chosen. However, its adequacy for the stomach depends on accurate prediction of stomach shape for different fillings. While creating multiple plans using a single pre-treatment scan and applying multiple PTV margins may be sufficient for rectal<sup>107</sup>, bladder<sup>108</sup> and cervical cancer<sup>109</sup>, due to the more complex deformations and volume changes of a stomach, gastric cancer likely requires a more sophisticated approach such as a personalized or population-based strategy.

A personalized strategy, in which multiple plans are created based on observed anatomical deformation within the patient, is frequently used for bladder and cervical cancer<sup>98,105,110</sup>. For these targets, a LoP is typically based on an empty and full bladder scan and inter- and extrapolations. For gastric cancer patients, acquiring two pre-treatment scans with different filling might be undesirable due to the commonly observed eating difficulties in this patient group. Alternatively, the LoP can be created based on the observed anatomy on the first few CBCTs<sup>47,111</sup>, as has been done for preoperative gastric radiotherapy<sup>68</sup>. However, using this method, there will be no adaptation to different gastric fillings for at least the first week of treatment.

Preferably, the LoP is based on a population-based deformation model and a single pre-treatment scan, such that the LoP is available from the start of treatment. Such a strategy was proposed for a cervical LoP using scans with different bladder fillings, yielding improved performance (i.e., target coverage and organ at risk sparing) compared to a personalized strategy (3-CT based library)<sup>48</sup>. For rectal cancer, using population statistics to create a LoP considerably reduced average PTV volume compared to conventional single-plan radiotherapy<sup>50</sup>. For abdominal organs including the stomach, a model has been developed to describe respiratory-induced deformation<sup>27</sup>; however, there has been no study proposing a filling-based gastric deformation model.

The aim of this study is to compare the performance between a personalized and a population-based model to predict stomach shape for different fillings. The comparison was performed

using magnetic resonance imaging scans (MRIs) of healthy volunteers. The best performing model was validated using patient data and its potential suitability for use in a LoP is discussed.

## 5.2 Materials and Methods

### 5.2.1 Imaging and stomach definition

MRIs (Ingenia 3T, Philips Healthcare, Best, The Netherlands) were acquired of 20 healthy volunteers (9 male, 11 female, age 21–75) with sequentially an empty (ES), half full (HFS) and full stomach (FS); all volunteers gave written informed consent within a medical ethics committee-approved trial (CCMO registration: NL65891.018.18). Volunteers abstained from food for 3 hours and drink for 1 hour prior to acquiring the ES scan. HFS and FS scans were acquired after eating half of a self-chosen meal (food and drink) and the remaining half meal, respectively. Total duration of an imaging session was approximately 2 hours. Due to a hiatal hernia observed in one volunteer, we continued with data of 19 volunteers.

MDixon scans (voxel pitch  $1.39 \times 1.39 \times 0.85 \text{ mm}^3$  in left-right, anterior-posterior and superior-inferior direction, respectively) in end-exhale breath-holding were acquired for all volunteers. One volunteer could not maintain breath-holding for the duration of the scan; they received a shorter survey scan ( $1.04 \times 2.00 \times 1.04 \text{ mm}^3$ , end-exhale).

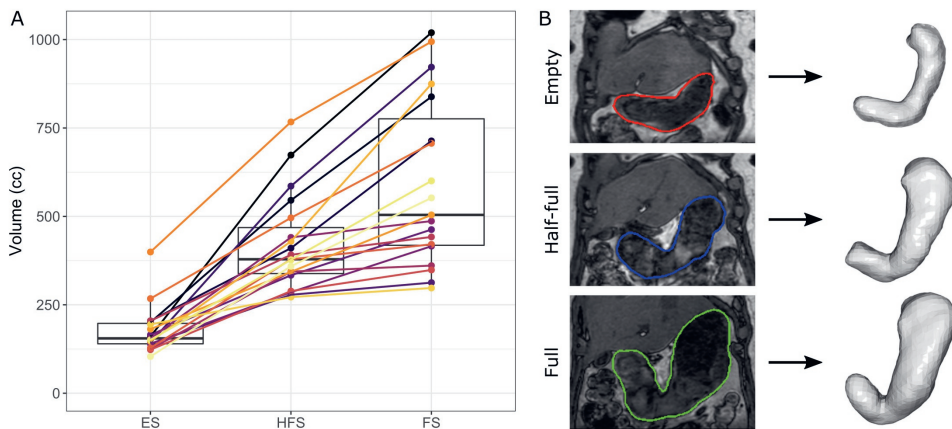


Figure 5.1: A) Stomach volumes for empty (ES), half-full (HFS) and full stomach (FS). Each line represents a volunteer. Median stomach volumes were 155 cc, 379 cc and 504 cc for ES, HFS and FS, respectively. B) Example of delineations on coronal slices and corresponding meshes (volunteer 3).

For each volunteer, the complete stomach was manually delineated on the ES, HFS and FS scans by a single observer (Velocity 4.0, Varian). Delineation was done on the mDixon signal out-of-phase scan (sOP); when needed, other contrast scans were used for guidance. Volumes were determined (Figure 5.1A). An automated grey value-based rigid bony anatomy registration was performed between the ES, HFS and FS scans and all delineations of a volunteer were aligned accordingly. The delineations were converted to point clouds, subsequently simplified (i.e., number of points reduced to approximately 1000) and finally converted to triangulated surface meshes with vertices and faces (Figure 5.1B, see Supplemental Materials S5A for all point clouds)<sup>112</sup>.

### 5.2.2 Personalized strategy

For the personalized strategy, a deformable mesh registration (DMR) from a HFS to its corresponding ES was performed, resulting in a set of deformation vectors (Figure 5.2). The rigid component of these deformation vectors (i.e., the average translation in each direction) was calculated and subtracted from the deformation vectors in order to eliminate displacements of the stomach relative to the bony anatomy between ES and HFS. The resulting deformation vectors were extrapolated with a scaling factor to create a FS of equal volume to the true FS. Often, locally small distances occurred between HFS and FS, which posed difficulties when extrapolating the vectors to obtain ES. Therefore, a personalized prediction of ES was not included in this study. All DMRs in our study were performed using a non-rigid iterative closest point algorithm (minimizing root mean square error)<sup>80</sup>.

### 5.2.3 Population-based strategy

To create a population-based FS for one volunteer, the average deformation from HFS to FS of the other 18 volunteers was used (leave-one-out principle; Figure 5.2-1). To create the model based on the 18 volunteers, DMRs were performed between all corresponding HFSs and FSs (Figure 5.2-1a). The rigid component (translations only) of the deformation vectors was calculated and subtracted from the deformation vectors. In addition, every HFS was rigidly aligned (translations and rotations) with a reference stomach (i.e., the HFS with median volume (volunteer 12), Figure 5.2-1b) followed by a DMR to acquire a point-to-point correspondence between all HFS and the reference stomach (Figure 5.2-1c). From this point-to-point correspondence, the vectors between HFS and FS of every volunteer were transferred to the reference stomach, such that every point on the reference stomach had 18 deformation vectors to a FS (Figure 5.2-1d; Supplemental Materials S5B). The model was finalized by averaging these 18 deformation vectors (Figure 5.2-1e).

The created model was subsequently applied to the HFS of the remaining one volunteer to obtain the predicted FS (Figure 5.2-2). First, the HFS of the volunteer was rigidly aligned with the reference stomach (Figure 5.2-2a) and a DMR was performed to achieve point-to-point correspondence between the HFS and the reference stomach (Figure 5.2-2b). Next, using this point-to-point correspondence, the scaled average deformation vector was applied to the HFS to create the predicted FS with equal volume to the true FS (Figure 5.2-2c). Finally, the inverse rigid alignment was applied to bring the predicted FS to the original location (Figure 5.2-2d). This strategy was repeated for all 19 volunteers. The same strategy, but based on the deformations between HFS and ES, was applied to predict ES.

#### 5.2.4 Evaluation

Performance of both strategies was evaluated using multiple post-alignment options to correct for position and orientation errors between predicted and true stomach: no alignment (No), translations (3 degrees of freedom (3DoF)) and translations and rotations (6DoF). Shape prediction was assessed using 6DoF alignment, shape and orientation prediction with 3DoF alignment, and shape, position and orientation prediction with no alignment. Alignments were performed using an iterative closest point algorithm.

Evaluation parameters were Hausdorff distance, 75<sup>th</sup> percentile nearest neighbor distance for every vertex on true FS to predicted stomach (i.e., largest distance of approximately 75% of the surface; nn75), Dice similarity coefficient (DSC) and volume of true stomach outside predicted stomach with a uniform 10-mm margin (i.e., missed volume if treatment plan is based on predicted stomach with 1 cm PTV-margin; missed volume). Statistical paired tests (i.e., t-test for parametric distributions and Wilcoxon signed-rank test for non-parametric distributions; normality tested with Shapiro-Wilk test) were performed between post-alignment options as well as between the personalized and population-based strategy using significance level  $\alpha=0.05$ .

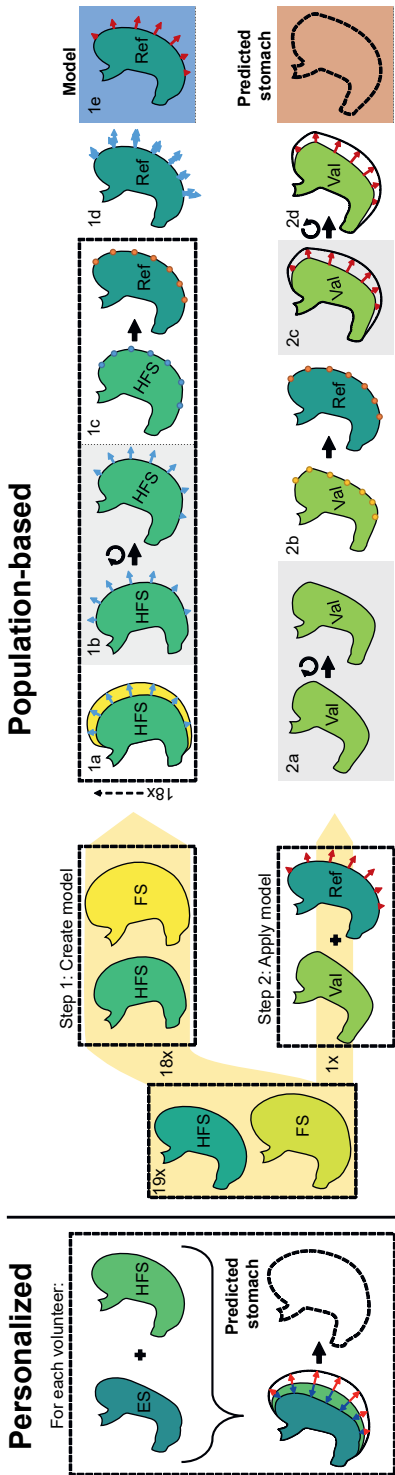


Figure 5.2: Schematic diagram of personalized and population-based strategy. For personalized strategy, the deformation vectors (blue arrows) between half-full stomach (HFS) and empty stomach (ES) were extrapolated (red arrows) to create the predicted full stomach (FS). For the population-based strategy, 19 HFSs and corresponding FSs were subdivided into 18 HFSs and FSs to create the model and 1 HFS (i.e., validation HFS (Val)) to apply the model on. To create the model (step 1): 1a) Perform a deformable mesh registration (DMR) between HFS and FS (light-blue arrows). 1b) Apply transformation matrix to HFS obtained from a rigid registration between the HFS and reference stomach (Ref). 1c) Next, find point-to-point correspondence between the HFS and Ref using DMR. 1d) Transfer all 18 deformation vectors to Ref. 1e) Average 18 deformation vectors (dark-red arrows). To apply the model to Val (step 2): 2a) first, perform a rigid registration of Val to match Ref. 2b) Find the point-to-point correspondence between Val and Ref using DMR. 2c) Apply average deformation vectors to Val to create predicted FS. 2d) Apply inverse rigid registration (from 2a) to Val and predicted FS.

### 5.2.5 Patient validation

Data of seven gastric cancer patients who received radiotherapy (CRITICS-II; NCT02931890<sup>10</sup>) and additional imaging (MaagART-01; Netherlands Trial Register NL7036) were used for validation of the population-based strategy (i.e., based on healthy volunteer data). For each patient, a pre-treatment computed tomography scan (CT) and 2-3 repeat CTs (19 repeat CTs total) were available. On treatment/imaging days, patients were allowed to eat a light breakfast and all scans were acquired prior to 1 pm. The stomach was delineated on all scans using the AI-enhanced image segmentation unit of the Varian Ethos Treatment Planning simulator (Varian Medical Systems, version 02.00.10). Delineations were visually checked, adjusted where necessary and subsequently converted to triangulated surface meshes.

For each of the 19 repeat CTs, stomach shape was predicted using stomach on pre-treatment CT and the population-based model based on all 19 volunteers (Supplemental Materials S5B). For each repeat CT, predicted stomach was of equal volume as true stomach by scaling of the average deformation vector. Performance was evaluated using the same parameters as mentioned in section 'Evaluation' and compared with the performance of the population-based strategy on volunteer data using statistical tests (i.e., t-test for parametric distributions and Wilcoxon signed-rank test for non-parametric distributions; normality tested with Shapiro-Wilk test; interpreting the patient data as independent observations).

## 5.3 Results

For personalized versus population-based predicted FSs, the population-based strategy performed significantly better than or comparable to the personalized strategy, for all post-alignments and all evaluation parameters (Figure 5.3; see Supplemental Materials S5C for all results). Regarding the post-alignment options, 6DoF post-alignment was often significantly better and never significantly worse than 3DoF post-alignment for all parameters. Also, both post-alignment options outperformed the 'No' post-alignment for all evaluation parameters and both strategies. Overall, the population-based strategy with 6DoF post-alignment resulted in full stomach shape prediction with a median nn75 of 3.9 mm, a median DSC of 0.91 and no missed volume in 16 out of 19 predicted volumes.

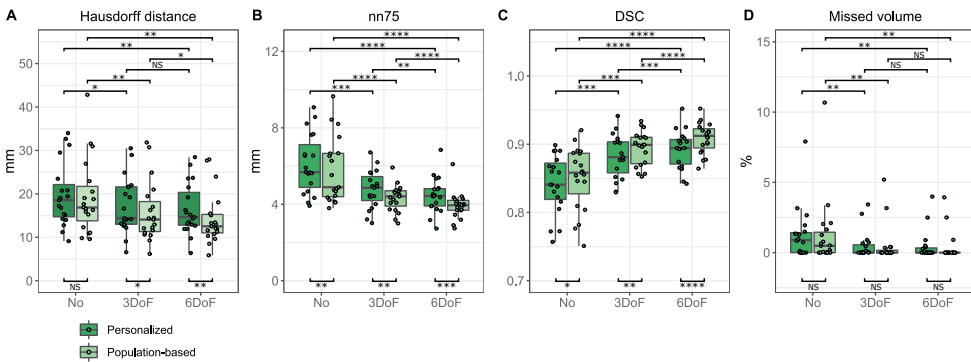


Figure 5.3: Performance of personalized and population-based strategies with no post-alignment (No), 3DoF post-alignment and 6DoF post-alignment between predicted full stomach and true full stomach for (A) Hausdorff distance, (B) 75th percentile nearest neighbor distance, (C) Dice similarity coefficient (DSC) and (D) percentage of missed volume with 10-mm margin. Boxplots: box=interquartile range (IQR), whiskers=lowest and highest data point within  $1.5 \times \text{IQR}$ . Paired tests (t-test or Wilcoxon signed-rank) were performed. NS  $p \geq 0.05$ , \*  $p < 0.05$ , \*\*  $p < 0.01$ , \*\*\*  $p < 0.001$ , \*\*\*\*  $p < 0.0001$ .

ES prediction (only with population-based strategy) was comparable to or significantly worse than FS prediction for all parameters (see Supplemental Materials S5D). Also, considering post-alignment options, ES prediction performance using 6DoF post-alignment was comparable to 3DoF post-alignment for all parameters but the DCS. Furthermore, both post-alignment options outperformed 'No' post-alignment, for all evaluation parameters but nn75.

In a visual assessment, we noted differences between stomachs generated by the population-based and personalized strategy. Typically, the personalized strategy resulted in more erratically shaped volumes, which made these volumes less comparable to true stomach (Figure 5.4). This was also reflected in the corresponding evaluation parameters, which were slightly worse for the personalized strategy compared with the population-based strategy.

Upon performing post-alignment (either 3DoF or 6DoF) between predicted and true stomach, the nearest neighbor distance decreased for most vertices on true FS, as shown for two typical volunteers in Figure 5.5. For some volunteers, however, this overall decrease in nearest neighbor distances was accompanied by a (large) local increase in distance, yielding an increase in Hausdorff distance (Figure 5.5, volunteer 19).



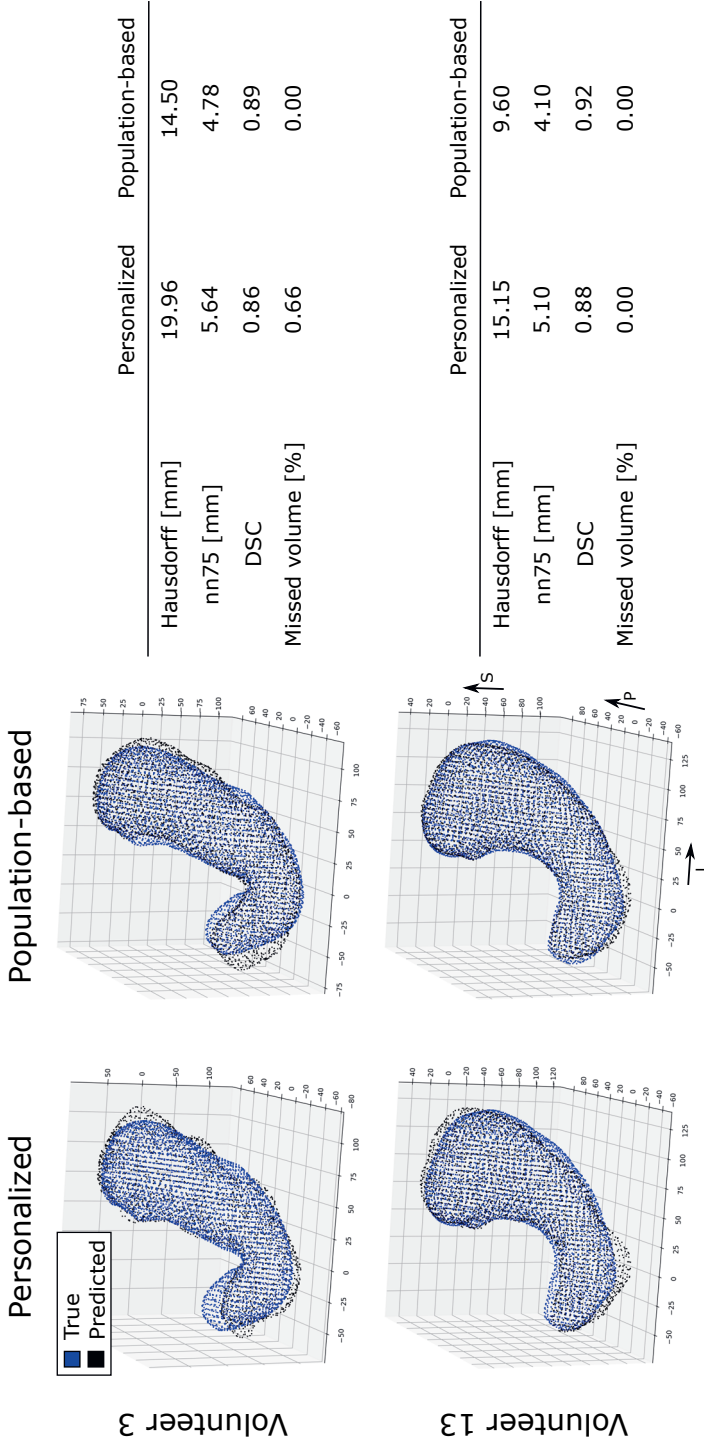


Figure 5.4: Vertices of true full stomach (blue) and predicted full stomach (black) with a 3DoF post-alignment for the personalized and population-based strategy for two volunteers. The corresponding evaluation parameters are listed in the tables. Superior (S), posterior (P) and left (L) direction are indicated in the figure.

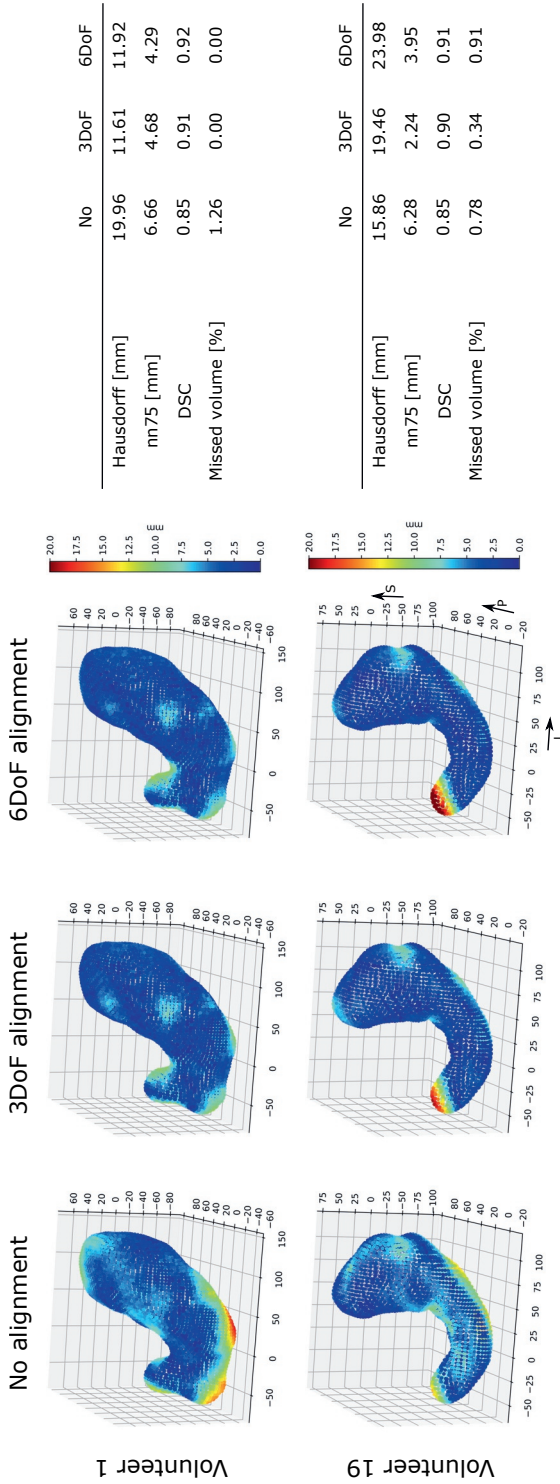


Figure 5.5: Nearest neighbor distance from every vertex on the true full stomach to population-based prediction of full stomach for two volunteers without post-alignment, with 3DoF post-alignment and with 6DoF post-alignment. The tables list the corresponding parameters for these volunteers. Superior (S), posterior (P) and left (L) direction are indicated in the figure.

For the patient data used for validation, stomach volume differences between pre-treatment CT and repeat CT ranged from -274 cc to +358 cc. Performance on patient data was comparable to or better than performance on volunteer data for all evaluation parameters and post-alignments, except when no post-alignment was performed for DSC and missed volume (Figure 5.6). For the patient data, 6DoF post-alignment was comparable to or significantly better than 3DoF and both significantly outperformed 'No' post-alignment, for all evaluation parameters. With a 6DoF post-alignment, median nn75 was 4.3 mm and 7.4 mm, and median DSC was 0.87 and 0.88 for patient and volunteer data (ES and FS prediction combined), respectively.

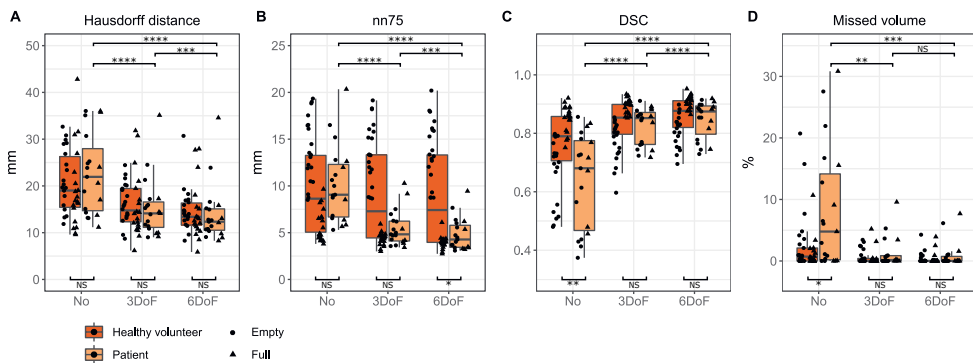


Figure 5.6: Performance of population-based model on healthy volunteer (red) and patient data (orange) for emptier (circles) and fuller stomach (triangles) predictions (i.e., emptier/fuller than stomach on pre-treatment CT (patients) or half-full stomach (volunteers)). (A) Hausdorff distance, (B) 75th percentile nearest neighbor distance (nn75), (C) Dice similarity coefficient (DSC) and (D) percentage of missed volume with 10-mm margin. Boxplots: box=interquartile range (IQR), whiskers=lowest and highest data point within  $1.5 \times IQR$ . Statistical tests (t-test or Wilcoxon signed-rank) were performed. NS  $p \geq 0.05$ , \*  $p < 0.05$ , \*\*  $p < 0.01$ , \*\*\*  $p < 0.001$ , \*\*\*\*  $p < 0.0001$ .

## 5.4 Discussion

This study compared performance of a personalized and a population-based model in predicting stomach shape for varying filling to eventually be used in a LoP that is available from the start of treatment. The best performing strategy, i.e., the population-based model, was subsequently used for validation on patient data.

Our results showed that in predicting FS shape the population-based strategy generally outperformed the personalized strategy, mainly expressed in better Hausdorff distance, nn75 and DSC. Population-based FS prediction with 6DoF post-alignment gave satisfactory results, with a median nn75 of 3.9 mm and median DSC of 0.91. Using the population-based strategy with post-alignment, the evaluation parameters demonstrated that stomach filling is a good predictor for shape.

When considering a population-based strategy for a LoP approach, performance should be evaluated in clinical perspective and using a combination of parameters<sup>13</sup>. To illustrate, a median Hausdorff distance of 12.5 mm (6DoF post-alignment) appears large with a 10-mm PTV margin; however, remarkably, median nn75 and DSC showed good results and there was no missed volume for 16 out of 19 volunteers. Although this appears inconsistent, it should be noted that when one volume is fully covered by another volume, missed volume is zero but the Hausdorff distance may be large. This underlines the importance of combining parameters in evaluating deformation models for clinical use.

The drawback of the personalized strategy is that it required two scans with different stomach fillings in order to predict stomach shape. The eating instructions required for the personalized strategy may be not feasible for gastric cancer patients. In addition, difficulties in extrapolation arose when the two stomach fillings used for prediction had small (local) differences or when locally the larger shape shifted to being the inner shape (see Supplemental Materials S5A for all volunteer stomach volumes). As a consequence, ES prediction using the personalized strategy was impossible, as it resulted in non-physical shapes. In contrast, using the population-based strategy, local unexpected anatomies were averaged out, which resulted in sensible/smooth surfaces and good overall performance.

The results for 6DoF post-alignment (i.e., rotations and translations) between predicted stomach and true stomach indicate good shape prediction performance. Most radiotherapy centers, though, only have the ability to perform translational couch corrections (i.e., 3DoF corrections). Also, daily manual 6DoF stomach registration may not be straightforward. Although slightly poorer than 6DoF, 3DoF post-alignment still yielded satisfactory prediction performance. However, with no correction for either position or orientation of the stomach, performance significantly decreases. Hence, when using the population-based model in a LoP, 3DoF or 6DoF post-alignment is strongly advised.

Within the patient data, some repeat scans showed stomachs of approximately equal volume as the stomach on pre-treatment CT and thus predicted stomachs were very similar to stomach on pre-treatment CT. Interestingly, for these predictions, performance was not improved compared to stomachs that underwent large deformations (see Supplemental Materials S5E). This indicates that, as expected, there are other factors aside from stomach filling that affect stomach shape (e.g., (filling in) surrounding organs). However, although stomach filling is not the only influencer of shape, our results do suggest that an adequate prediction of shape can be made using only filling as variable in the model.

Possibly, dietary restrictions would yield a more stable stomach volume over the course of radiotherapy. However, such restrictions might be undesirable for this patient group as they

already experience eating difficulties. More importantly, stomach volume does not only depend on intake of food or drinks; gas in the stomach can greatly affect volume and gastric cancer patients may have an obstruction that delays the passage of stomach content. Hence, with stomach volume not easily controlled, an adaptive radiotherapy strategy is desirable for this patient group.

Overall, even though model performance was similar between patient and volunteer data, patient data performance was significantly worse for DSC and missed volume when no post-alignment was performed. This could be caused by the difference in time between observations, as the timespan of the image acquisition was within hours and within weeks for volunteers and patients, respectively. This suggests that day-to-day positional variation of the stomach is larger than variations that occur within one day, which can be solved by and affirms the usefulness of post-alignment.

Stomach delineations were performed on MRI for volunteers and on CT for patients. As seen for other targets, delineations yield different volumes between MRI and CT<sup>114-116</sup>. However, the population-based model is based on relative deformations rather than absolute volumes. Therefore, we expect little to no effect of image modality on the prediction performance. And indeed, the MRI-based model performed well on the CT-based patient data.

Various other strategies, such as principle component analysis (PCA) and finite element modelling, have been reported that predict shape for other organs, such as cervix and bladder, with similar results to our study<sup>48,117</sup>. Although PCA has been used for bladder and cervix, it appears that the stomach undergoes too complex stomach shape variations to be applied for a LoP<sup>48</sup>. In addition, PCA was used to investigate geometrical variations in abdominal organs, including the stomach, during pancreatic cancer radiotherapy treatment<sup>106</sup>. The observed stomach volume differences were small compared with our study and their focus was thus not on volume-dependent stomach-shape predictions. Overall, considering the complex behavior of the stomach and large volume variations, the simple model presented in this study yields sufficient predicting performance of stomach shape.

Although the results indicate satisfactory performance, the population model is based on a limited number of 19 volunteers. By including more volunteers, the robustness of the model could potentially be improved. In addition, by using a larger population size, possibly a division between different types of stomach deformations amongst patients can be defined, as has been done for cervix LoP. For a cervix LoP, a distinction between patients with small deformations and large deformations is often made<sup>49,94,118</sup>. For the stomach, such a distinction might be made between the areas with largest and smallest stomach expansion.

The performance of the population-based strategy in predicting stomach shape, both for healthy volunteers and for gastric cancer patients, indicates its potential to be used in a LoP strategy. We found satisfactory results in both patients and volunteers; nonetheless, a validation in more patients would be valuable, also to assess the possible effect of tumor presence on deformation. Furthermore, this population-based model is created and validated in volunteers and patients from our region/institute. Whether the current population-based model is also applicable for patients from other institutes, could be evaluated. However, performance differences are likely limited since this population-based model is based on relative deformations rather than absolute volumes.

Several steps will have to be performed prior to clinical implementation of a LoP based on pre-treatment CT and the population-based model. The optimal number of treatment plans may still be investigated, as was done for cervix<sup>99</sup>; 3-4 plans are likely sufficient. These plans could, for example, cover a range of fixed stomach volumes or stomach volumes with equally spaced maximum distances, that are created based on the pre-treatment CT and the population-based model. From varying stomach volumes, a translation to CTV contours (i.e., stomach + lymph nodes) must be made. Also, the clinical implementation of the 3DoF or 6DoF alignment based on in-room imaging should be explored. Moreover, the existing uncertainties should be assessed to determine appropriate PTV margins for each plan in the LoP. Finally, a dosimetric study of clinical benefit of a LoP strategy should be performed.

To conclude, this study set out to investigate both a personalized and a population-based strategy in predicting stomach shape to eventually be used in a LoP for gastric cancer patients. The population based strategy has shown superior predicting performance over the personalized strategy and results suggest that stomach volume is a reasonable predictor of stomach shape. The patient validation has indicated that the population model based on healthy volunteers can be used on patient data with sufficient results for a LoP implementation. Using post-alignment, this population-based model demonstrated its ability in predicting shape in both healthy volunteers and gastric cancer patients, and therefore, its potential to be used in a LoP created prior to treatment.

### **Acknowledgements**

The authors like to thank Zdenko van Kesteren, Myrte Boon and Femke Beeksmas for their assistance with the MRI acquisitions.



**Dosimetric benefit of a library of plans versus single-plan strategy for preoperative gastric cancer radiotherapy**

6

Margot Bleeker  
Jorrit Visser  
Karin Goudschaal  
Arjan Bel  
Maarten C.C.M. Hulshof  
Jan-Jakob Sonke  
Astrid van der Horst

Modified from:  
Radiotherapy and Oncology, 2023, 182, 109582.  
DOI: 10.1016/j.radonc.2023.109582



## Abstract

*Purpose:* The stomach experiences large volume and shape changes during preoperative gastric radiotherapy. This study evaluates the dosimetric benefit for organs-at-risk (OARs) of a library of plans (LoP) compared to the traditional single-plan (SP) strategy.

*Materials and methods:* Twelve patients who received SP CBCT-guided preoperative gastric radiotherapy (45 Gy; 25 fractions) were included. Clinical target volume (CTV) consisted of CTV<sub>stomach</sub> (i.e., stomach + 10-mm uniform margin minus OARs) and CTV<sub>LN</sub> (i.e., regional lymph node stations). For LoP, five stomach volumes (approximately equidistant with fixed volumes) were created using a previously developed stomach deformation model (volume = 150–750 mL). Appropriate planning target volume (PTV) margins were calculated for CTV<sub>stomach</sub> (SP and LoP, separately) and CTV<sub>LN</sub>. Treatment plans were automatically generated/optimized and the best-fitting library plan was manually selected for each daily CBCT. OARs (i.e., liver, kidneys, heart, spleen, spinal canal) doses were accumulated and dose-volume histogram (DVH) parameters were evaluated.

*Results:* The non-isotropic PTV<sub>stomach</sub> margins were significantly ( $p < 0.05$ ) smaller for LoP than SP (median=13.1 vs 19.8 mm). For each patient, the average PTV was smaller using a LoP (difference range 134–1151 mL). For all OARs except the kidneys, DVH parameters were significantly reduced using a LoP. Differences in mean dose (Dmean) for liver, heart and spleen ranged between -1.8–5.7 Gy. For LoP, a benefit of heart Dmean > 4 Gy and spleen Dmean > 2 Gy was found in 4 and 5 patients, respectively.

*Conclusion:* A LoP strategy for preoperative gastric cancer reduced average PTV and reduced OAR dose compared to a SP strategy, thereby potentially reducing risks for radiation-induced toxicities.

## 6.1 Introduction

The stomach experiences large interfractional deformations, primarily due to filling changes. For preoperative gastric cancer radiotherapy with a single-plan (SP), these anatomical variations may compromise target coverage<sup>68</sup> and/or increase organ at risk (OAR) dose. This stresses the need for an adaptive radiotherapy strategy, such as a library of plans (LoP).

A LoP, consisting of multiple treatment plans from which each day the best fitting one can be chosen, has shown benefit for several other deformable targets, such as rectum, bladder and cervix<sup>43,49,98,100,101,110</sup>. Previously, we have demonstrated the feasibility of plan selections on CBCT for the stomach; for this, a sub-optimal LoP was used<sup>68</sup>. Furthermore, more recently, we presented a stomach deformation model that can predict stomach shape for variable stomach volumes using a single scan, with the potential to create an improved patient-specific LoP<sup>67</sup>. However, the strategy to create a clinically applicable LoP from the stomach deformation model is not straightforward and has not yet been proposed. Prior to clinical introduction of such a LoP, potential benefit can be evaluated by daily dose accumulation for SP and LoP<sup>118–120</sup>. Ensuring sufficient and equal target coverage between both strategies (by calculating appropriate PTV margins), allows for a comparison of OAR dose. Typical OARs in upper abdominal radiotherapy include liver and kidneys<sup>121</sup>; recently, more focus has been on spleen and heart as OARs<sup>16,122–124</sup>.

This study is the first to provide a dosimetric comparison between SP and a newly constructed model-based LoP for preoperative gastric cancer radiotherapy, focusing on OAR dose whilst ensuring sufficient target coverage for both strategies. For this, we 1) proposed a method to create clinical target volumes (CTV) for various stomach volumes, 2) calculated the necessary planning target volume (PTV) margins to ensure adequate and equal coverage between SP and LoP, and 3) simulated both strategies on daily acquired CBCT images prior to 4) voxel-wise dose accumulation for each OAR.

## 6.2 Materials and methods

### 6.2.1 Patient population and study setup

Retrospectively, 12 patients who received CBCT-guided preoperative gastric cancer radiotherapy (45Gy; 25 fractions) within the CRITICS-II trial (NCT02931890)<sup>10</sup> and additional imaging (MaagART-01; Netherlands Trial Register NL7036) were included in this study. For each patient, the total set of imaging data consisted of a pre-treatment CT (pCT; average 4DCT; voxel pitch 0.98×0.98×2.5 mm<sup>3</sup>), 2–3 repeat CTs (rCTs), and 20–25 CBCTs (1×1×1 or 0.91×0.91×1 mm<sup>3</sup>). pCTs were used to define CTVs, treatment planning and dose calculation, rCTs to calculate appropriate population-based PTV margins, and CBCTs to simulate both strategies.

Eating instructions were a light breakfast on pCT/treatment days (typically before 1pm).

Clinical target volume (CTV) was the entire stomach, lymph nodes surrounding the stomach and regional lymph node stations. OARs were liver, spleen, heart, both kidneys, and spinal canal. This study focused on possible benefits for OARs. Target dose evaluations would require accurate CTV delineations on CBCT, which proved challenging; therefore, we ensured target coverage by using homogeneous dose distributions and sufficiently large margins. Three degrees-of-freedom (3DoF; translation-only) OAR matches were performed between pCT and every daily CBCT for OAR dose accumulations. Target-based matches between pCT and CBCT/rCT and plan selections were based on stomach (not CTV), as the stomach is easier to distinguish on CBCT.

### 6.2.2 LoP-stomachs

For LoP, five 'virtual' stomachs (i.e., LoP-stomachs) with fixed and approximately equidistant volumes (150, 245, 373, 540, 750 mL) were created for every patient using their stomach on pCT and a population deformation model<sup>67</sup>. Stomach volume range was based on stomach volumes observed in 19 volunteers<sup>67</sup> and the included 12 patients (Supplemental Materials S6A).

### 6.2.3 CTV definition

For both SP and LoP, the CTV consisted of a highly deformable region ( $CTV_{stomach}$ ) and a region with assumed limited deformation ( $CTV_{LN}$ ).  $CTV_{stomach}$  was the entire stomach + 10-mm uniform margin for microscopic extension; OARs were subtracted from the margin (Figure 6.1A).  $CTV_{LN}$ , defined as duodenum and regional lymph node stations, was identical for SP and LoP.

For LoP, corresponding points were obtained between stomach on pCT and all LoP-stomachs, and between stomach and  $CTV_{stomach}$  on pCT, using a non-rigid ICP algorithm (NRICP)<sup>80</sup>. The stomach-to- $CTV_{stomach}$  expansion on pCT was propagated to the LoP-stomachs to create  $CTV_{stomach}$  (Figure 6.1B).

### 6.2.4 Delineations

The entire stomach was delineated on all pCTs and rCTs using the AI-enhanced image segmentation algorithm of the Varian Ethos Treatment Planning simulator (Varian Medical Systems, v02.00.10); delineations were visually checked and adjusted when necessary by one observer (MB). Delineations of duodenum and regional lymph node stations (i.e., hepatic hilum, hepatogastric ligament, splenic hilum, para-aortic nodes, peripancreatic nodes and,

dependent upon tumor location, the distal part of the esophagus) were performed by one observer (MB) on each pCT and subsequently checked and adjusted when necessary by two observers (AH, MH). For each pCT, the clinically used OAR delineations were visually checked and adjusted when necessary (MB) and the body (i.e., patient outer contour) was automatically delineated (RayStation 9A, RaySearch Laboratories). For each rCT, OARs were delineated (MB).

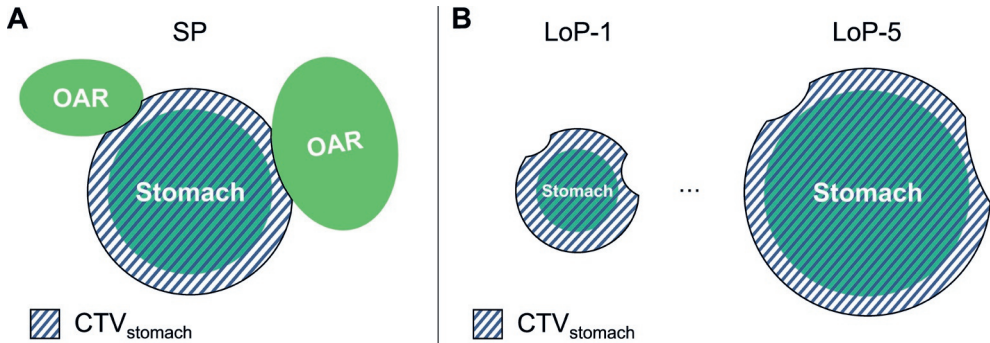


Figure 6.1: Schematic representation of  $CTV_{stomach}$  for single-plan (SP) and library of plans (LoP). A) For SP,  $CTV_{stomach}$  is created by expanding the stomach delineation with a 10-mm uniform margin and subtracting overlapping organs-at-risk (OAR) from this margin. B) For LoP, this SP stomach-to- $CTV_{stomach}$  expansion is propagated to all stomachs in the library.

## 6.2.4 Delineations

The entire stomach was delineated on all pCTs and rCTs using the AI-enhanced image segmentation algorithm of the Varian Ethos Treatment Planning simulator (Varian Medical Systems, v02.00.10); delineations were visually checked and adjusted when necessary by one observer (MB). Delineations of duodenum and regional lymph node stations (i.e., hepatic hilum, hepatogastric ligament, splenic hilum, para-aortic nodes, peripancreatic nodes and, dependent upon tumor location, the distal part of the esophagus) were performed by one observer (MB) on each pCT and subsequently checked and adjusted when necessary by two observers (AH, MH). For each pCT, the clinically used OAR delineations were visually checked and adjusted when necessary (MB) and the body (i.e., patient outer contour) was automatically delineated (RayStation 9A, RaySearch Laboratories). For each rCT, OARs were delineated (MB).

## 6.2.5 PTV margin

Population-based PTV margins were calculated separately for  $CTV_{stomach}$  and  $CTV_{LNr}$  using the non-linear van Herk formula, which ensures a minimum dose to the CTV of 95% for 90% of patients for rigid targets<sup>81</sup>:

$$M = \alpha \Sigma + 1.64 \sqrt{\sigma^2 + \sigma_p^2} - 1.64 \sigma_p \quad (\text{Eq. 6.1})$$

with standard deviation (SD) of systematic error  $\Sigma$ , SD of random errors  $\sigma$ , systematic error factor  $\alpha$ , and width of penumbra  $\sigma_p$  (details in Supplemental Materials S6B).

Local perpendicular  $CTV_{\text{stomach}}$ -to- $PTV_{\text{stomach}}$  margins, calculated for SP and LoP separately, included uncertainties due to delineations (2 mm), intrafractional motion (2.4 mm; in-house determined), respiratory motion ( $0.358 \times A^{87}$ , amplitude A is estimated as 8, 3, and 2 mm in superior-inferior (SI), anterior-posterior (AP), and left-right direction (LR), respectively) and interfractional shape variation. Since the stomach is not a rigid organ,  $\alpha \neq 2.5$ ; we determined  $\alpha = 2.8$  (Supplemental Materials S6B). Local interfractional shape variation differed between SP and LoP, as it was determined by the variation in  $CTV_{\text{stomach}}$  on rCTs with respect to the (selected) treatment plan<sup>50</sup>. Shape variations were calculated following a 3DoF match (iterative closest point algorithm) between each stomach on rCT and SP/LoP stomach (i.e., corresponding to a couch shift), and subsequent stomach-based plan selections (mean signed distance from stomach on rCT to LoP-stomach closest to zero) on each rCT. As we aimed for equal target coverage between SP and LoP, we evaluated for both strategies whether the (selected)  $PTV_{\text{stomach}}$  fully encompassed  $CTV_{\text{stomach}}$  (Supplemental Materials S6B). To equalize target coverage between SP and LoP, SP  $PTV_{\text{stomach}}$  margin was enlarged by 25%.

The  $PTV_{LN}$  margin (assumed equal between SP and LoP) was calculated using the van Herk formula with  $\alpha = 2.5$ . This margin included uncertainties due to delineations (2 mm), respiratory motion ( $0.358 \times A$ , A: SI=8; AP=3; LR=2 mm) and interfractional displacements. Regarding the latter,  $CTV_{LN}$  is not entirely fixed to either bony anatomy or  $CTV_{\text{stomach}}$  and thus experiences smaller displacements than used for  $PTV_{\text{stomach}}$  calculations (approximately 0.5 times the average couch shift of SP and LoP; Supplemental Materials S6B).

## 6.2.6 Treatment planning and dose accumulation

The final PTVs were the union of  $PTV_{\text{stomach}}$  and  $PTV_{LN}$ , resulting in 6 PTVs per patient (SP and 5 LoP). Dual-arc volumetric modulated arc therapy treatment plans were created for each PTV (Figure 6.2; RayStation 9A). For treatment planning, when the PTV was close to or passing body boundaries, a virtual bolus with water density was applied to the part of the PTV+5-mm uniform margin outside the body. When the PTV overlapped with lung, the overlap received a density override of water, as did the air in bowels and stomach. Optimized plans were automatically created using a priority list of goals. These goals are clinically used in our institute and also prescribed in the CRITICS-II trial except for mean spleen dose (<20 Gy (soft constraint) and < 24Gy (hard constraint)), see Table 6.1. In the final priority list, target coverage has the highest priority (Supplemental Materials S6C).

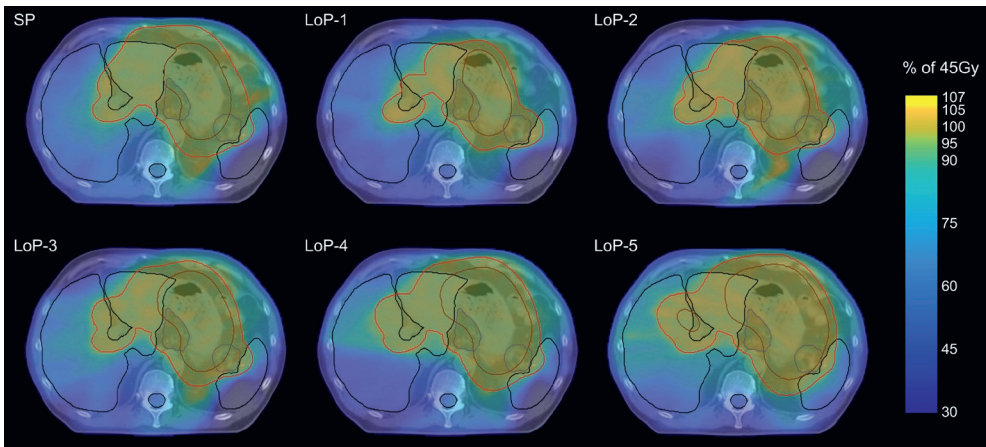


Figure 6.2: Typical example of dose distributions of optimized treatment plans on pCT for single-plan (SP) and the 5 plans in the library (LoP-1–LoP-5). Dose is depicted in percentage of the prescribed 45 Gy. Red lines: PTV; black lines: organs-at-risk visible in this slice (liver, spleen, and spinal canal); brown lines:  $CTV_{stomach}$ ; grey lines:  $CTV_{LN}$ .

SP and LoP treatments were simulated. First, a bony-anatomy match was performed between pCT and each daily CBCT. Subsequently, for each CBCT, manual stomach-based translations were performed for stomach on SP and each LoP-stomach to ensure optimal alignment of the treatment plan with daily CTV. For LoP, the best fitting LoP-stomach was selected with the smallest deviations to CBCT-stomach. Per patient, five random plan selections were checked by a second observer (AH).

Table 6.1: Clinical goals for preoperative gastric cancer radiotherapy at our institute, with 45 Gy prescription dose.  $D_{mean}$  = mean dose;  $VxGy$  = volume that received at least x Gy;  $Vx\%$  = volume that received at least x% of prescribed dose;  $D_{0.01cm^3}$  = maximum dose that  $0.01cm^3$  received.

Structure	Constraint
PTV	$V_{42.75Gy} (V_{95\%}) \geq 99\%$
Body	$D_{0.01cm^3} < 48.15 \text{ Gy} (V_{107\%})$
Kidneys (left and right)	$V_{18Gy} < 33\%$
Spinal canal	$D_{0.01cm^3} < 45 \text{ Gy}$
Heart	$V_{40Gy} < 30\%$
Liver	$D_{mean} > 30 \text{ Gy}$
Spleen	$D_{mean} < 24 \text{ Gy}$ ; but aim for $< 20 \text{ Gy}$

For dose calculations, a density override of water was applied to gas in bowels and stomach on pCT. Next, for each fraction, the treatment plan isocenter was shifted according to the stomach-based translations for SP and LoP in order to calculate daily dose distributions on pCT ( $2 \times 2 \times 2 \text{ mm}^3$ ; RayStation 9A). Per fraction, manual matches (3DoF) between each OAR on CBCT and pCT were performed (Supplemental Materials S6D). Daily dose distributions were resampled to a finer grid ( $0.5 \times 0.5 \times 0.5 \text{ mm}^3$ ) and, for each OAR, translated with the daily OAR match for SP and LoP separately (Matlab R2019b, The MathWorks Inc.). For spinal canal and body, translations were zero. Finally, dose was voxel-wise accumulated over the complete treatment course. For patients with  $<25$  fractions/CBCTs, accumulated dose was normalized to 25 fractions to ensure a fair comparison. Dose-volume histograms (DVHs) were calculated.

### 6.2.7 Evaluation

$PTV_{\text{stomach}}$  margin distributions were compared between SP and LoP. Furthermore, the variety of selected plans from the library and average PTV per patient were evaluated. Finally, DVH parameters from the clinical goals were compared between SP and LoP, as well as the maximum dose in the  $700 \text{ cm}^3$  volume of lowest liver dose, and mean heart and body dose. For comparisons, statistical paired tests were performed (i.e., t-test for parametric distributions and Mann-Whitney-Wilcoxon test for non-parametric distributions; normality tested with Shapiro-Wilk test; significance level  $\alpha=0.05$ ).

### 6.3 Results

$PTV_{\text{stomach}}$  margin distributions were  $19.8[14.8\text{--}26.6]$  mm (median[5–95 percentile]) for SP and  $13.1[8.5\text{--}19.2]$  mm for LoP (Figure 6.3). Local  $PTV_{\text{stomach}}$  margin was significantly smaller for LoP than SP (paired Mann-Whitney-Wilcoxon;  $p < 0.001$ ).  $PTV_{\text{LN}}$  margin was 7.5, 7.2, and 11.8 mm in LR, AP, and SI directions.

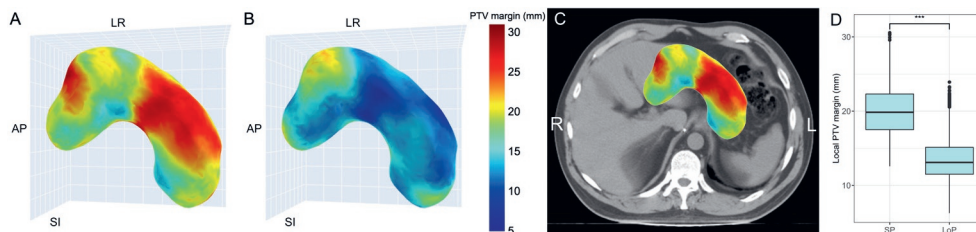


Figure 6.3: Local  $CTV_{\text{stomach}}$ -to- $PTV_{\text{stomach}}$  margin projected in color onto a  $CTV_{\text{stomach}}$  for (A) single-plan and (B) library of plans. (C) For anatomical reference, SP  $PTV_{\text{stomach}}$  margin superimposed on planning CT. (D) Boxplots of local  $PTV_{\text{stomach}}$  margin distribution for single-plan (SP) and library of plans (LoP). Margin distributions differed (paired Mann-Whitney-Wilcoxon test:  $***p < 0.001$ ). Boxplots: box = interquartile range (IQR), whiskers = lowest and highest data point within  $1.5 \times \text{IQR}$ .

Plan selections were performed on 293 CBCTs (Figure 6.4A). Plan 2 was mainly selected (56.0%), followed by plan 3 (27.6%) and 1 (13.3%). Plans 4 (2.7%) and 5 (0.3%) were barely selected. In 95.6% of CBCTs, LoP resulted in a smaller PTV than SP. For each patient, average PTV was smaller for LoP than for SP ( $p < 0.001$ ; Figure 6.4B). The difference in average PTV ranged from 134 mL to 1151 mL (median=336 mL).

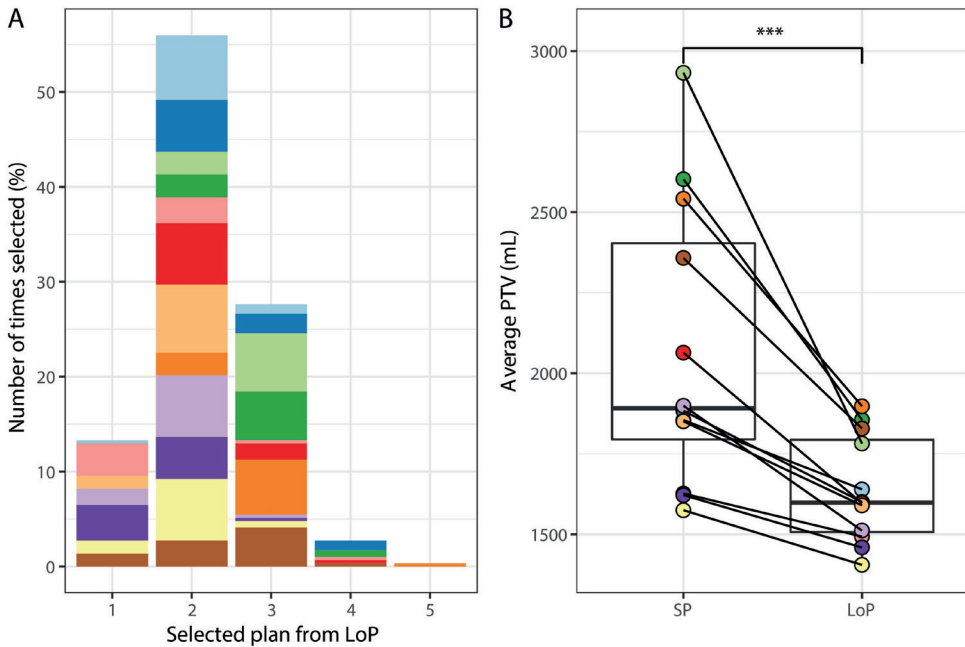


Figure 6.4: A) Percentage of selected plans from the library of plans (LoP) for 293 CBCTs. Each color represents a different patient (12 total). B) Boxplots of average PTV for SP and LoP. Each line represents a patient (colors corresponding to colors in A); paired t-test,  $p < 0.001$ . Boxplots: box = interquartile range (IQR), whiskers = lowest and highest data point within  $1.5 \times IQR$ .

Following dose accumulation for each OAR separately, the LoP performed significantly better on all evaluated dose parameters except for V18Gy for the kidneys, see Figure 6.5 and for absolute values Supplemental Materials S6E. Dmean differences for liver, heart, and spleen varied between -1.8–5.7 Gy. For LoP, a benefit for heart Dmean  $>4$  Gy was found in 4 patients, and for spleen Dmean  $>2$  Gy was found in 5 patients. For three patients, LoP performed better for all evaluated parameters. Larger average PTV differences correlated with worse performance for SP for liver Dmean (correlation coefficient  $r=0.62$ ,  $p=0.032$ ), heart V40Gy ( $r=0.76$ ,  $p=0.004$ ), heart Dmean ( $r=0.84$ ,  $p < 0.001$ ) and body Dmean ( $r=0.91$ ,  $p < 0.001$ ), see Supplemental Materials S6F.



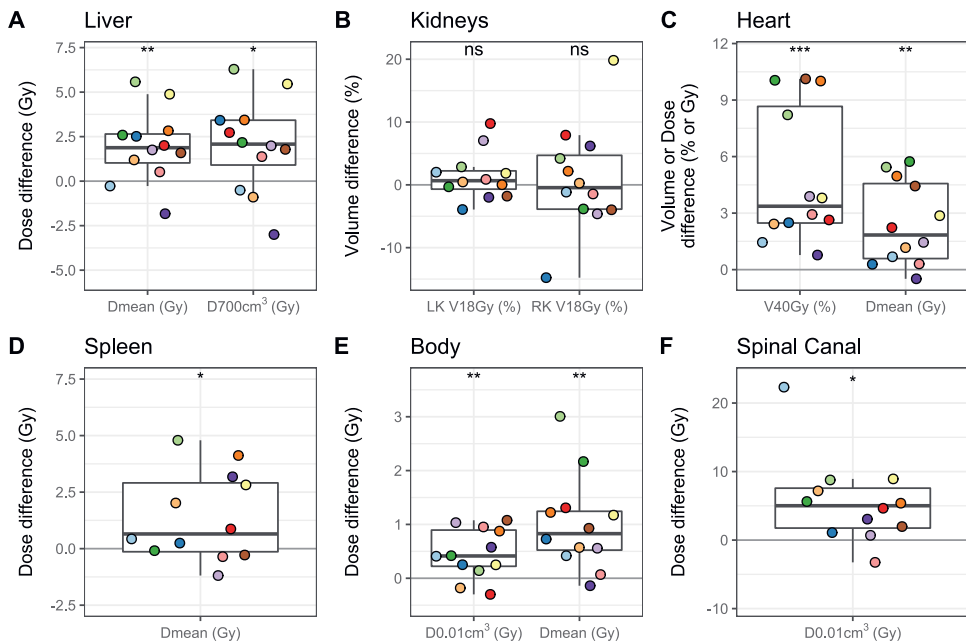


Figure 6.5: Dose-volume histogram parameter difference between single-plan (SP) and library of plans (LoP) for several dose parameters for liver (A), left (LK) and right kidney (RK; B), heart (C), spleen (D), body (E), and spinal canal (F). Positive difference: SP > LoP (i.e., LoP is beneficial). Dmean = mean dose, D700cm<sup>3</sup> = maximum dose in the 700cm<sup>3</sup> that received the lowest dose, D0.01cm<sup>3</sup> = maximum dose in 0.01cm<sup>3</sup>, VxGy = volume that received at least x Gy. Colors correspond to colors in Figure 6.4. Statistical tests (paired t-test or paired Mann–Whitney–Wilcoxon test): ns p ≥ 0.05, \*p < 0.05, \*\*p < 0.01, \*\*\*p < 0.001. Boxplots: box = interquartile range (IQR), whiskers = lowest and highest data point within 1.5 × IQR.

## 6.4 Discussion

This study is the first to perform a dosimetric comparison between SP and LoP for preoperative gastric cancer radiotherapy. We created CTVs from various stomach volumes, determined appropriate PTV margins, and simulated treatment for both strategies in order to accumulate daily dose for each OAR. Overall, this study demonstrated dosimetric benefit for a LoP by increased OAR sparing.

LoP resulted in reduced OAR dose compared to SP for liver, heart, spleen, and spinal canal, similar to studies for rectum and cervix<sup>46,118</sup>. For liver, heart and body DVH parameters, LoP benefit increased for larger differences between PTV on pCT and the average PTV during treatment. Recently, there has been more focus on the heart and spleen as OAR. For heart and spleen, studies reported that an increase in Dmean was associated with a decrease in

lymphocyte count nadir, introducing the risk for severe lymphopenia<sup>16,125,126</sup>. Additionally, for the heart, studies reported an increase in cumulative incidence of acute coronary events per Gy increase in Dmean<sup>123,124</sup>. Despite the relatively small median benefit in heart and spleen Dmean for LoP (1.8 Gy and 0.7 Gy, respectively), considerable individual benefits were observed (>4 Gy in heart, >2 Gy in spleen). For the kidneys, no significant dosimetric difference was found between both strategies, likely because for the majority of patients the PTV of all treatment plans (SP and LoP) were approximately identical near the kidneys. Overall, a significant dosimetric benefit for OARs was observed with a LoP, potentially reducing the risk for radiation-induced toxicities.

For each patient, a LoP reduced average PTV (median difference 336 mL), with reductions as large as 1151 mL, which was also reflected in a lower body Dmean. Potentially, there are more benefits related to this reduction in irradiated volumes than solely expressed in dose to the here evaluated OAR parameters. For instance, overlap of irradiated volumes with intestines might be relevant, as reviews suggest that dose to the gut microbiome affects radiotherapy efficacy and gastrointestinal toxicity<sup>127,128</sup>. Furthermore, larger PTV and body Dmean were associated with lower lymphocyte counts nadir in esophageal cancer and non-small cell lung cancer radiotherapy<sup>125,129,130</sup>. Consequently, as a LoP reduces average PTV and body Dmean, risks for these toxicities could also be reduced.

The benefit of LoP can be explained by the smaller PTV margins and the ability to select smaller plans when possible, similarly to rectal and bladder LoPs<sup>50,131</sup>. A LoP significantly reduced the necessary PTV<sub>stomach</sub> margins: median margins were 19.8 (SP) and 13.1 mm (LoP). Although these margins are large, they are smaller than PTV margins previously calculated for gastric irradiation (41.0, 50.8, and 30.3 mm in LR, AP, and SI, respectively)<sup>20</sup>. The currently clinically used 10-mm PTV margin is smaller than 100% and 88% of the local PTV<sub>stomach</sub> margin for SP and LoP, respectively. This accords with our earlier observation that generous margins are likely necessary to guarantee target coverage for SP<sup>68</sup>.

During plan selections on CBCT, mostly plans 1–3 were selected, representing stomach volumes of 150–373 mL. Plans 4 and 5, representing larger stomach volumes (540 mL and 750 mL), were only selected nine times (3%), consistent with stomach volumes observed on pCT and rCT (Supplemental Materials S6A). For cervix, a library of three plans was found to be optimal after considering OAR sparing and clinical workload<sup>99</sup>. Likely, also for a gastric LoP fewer plans (plans 1–3) will be sufficient. New PTV<sub>stomach</sub> margin calculations are probably not required when the library is reduced to three plans, because plan 4 or 5 was selected only once (i.e., one time plan 5; 3%) during plan selections on rCT for margin calculations. A reduction of five to three plans in the LoP could further reduce average PTV and reduce OAR dose. However, the optimal number of plans should be evaluated in a larger cohort. Furthermore, the current range of LoP

stomach volumes was based on observed stomach volumes in patients and volunteers from our center. However, as the created stomachs are based on a gastric deformation model and one pre-treatment CT, the LoP can easily be adapted to cover any desired range of stomach volumes, thereby potentially increasing its suitability for patients from other institutes.

Despite the limited number of 12 patients in this study, with 293 fractions/CBCTs the total amount of data is considered adequate. We expect these results can be extrapolated to larger cohorts, as this study demonstrated a reduction in average PTV for each individual patient and, for most patients, a dosimetric benefit for each OAR.

For  $CTV_{\text{stomach}}$ , we chose to propagate stomach-to- $CTV_{\text{stomach}}$  expansion to the LoP-stomachs, since we assumed OARs would move along with stomach volume increase/decrease when in close proximity. Simply adding a 10mm CTV margin, and thus neglecting stomach-induced OAR movement would have increased overlap between CTV and OAR. More elegantly,  $CTV_{\text{stomach}}$  could be created with an upper-abdominal multi-organ deformation model, as done for pancreatic cancer<sup>106</sup>. However, such a model with large stomach volume variations does not exist.  $CTV_{\text{LN}}$  was assumed to be approximately rigid for this study as it is not directly fixed to the stomach. However, as  $CTV_{\text{LN}}$  mainly included regional lymph nodes with no distinct boundaries, it is not possible to accurately and consistently delineate on rCT or CBCT and, thus, validate the assumption. When these regional lymph nodes would not be irradiated, OAR dose benefit for LoP would be even larger ( Supplemental Materials S6G).

For this study, several methodological choices were made. First, this study did not evaluate target dose, as this required CTV delineations on CBCTs. Manual delineations on CBCT or transfer of CTV delineations using deformable image registration (DIR) would lead to large uncertainties caused by the absence of clear CTV boundaries and inadequate DIRs (confirmed but not shown). Hence, in this study, benefit for OARs was evaluated while ensuring target coverage was maintained equal and sufficient for both SP and LoP (Supplemental Materials S6B). Second, the population-based PTV margins were based on limited data (12 patients, 2–3 rCTs), thereby introducing uncertainty in the calculated margins. Hence, target coverage was evaluated for both strategies to validate the margins. For SP, target coverage was lower than intended<sup>81</sup>; consequently,  $PTV_{\text{stomach}}$  margin for SP was enlarged by 25%, resulting in equal target coverage for SP and LoP. Lack of correction would have yielded an unfair comparison. Third, creating treatment plans for LoP with a single pCT is not straightforward, as there is substantial overlap between PTVs (LoP and SP) and OARs, and between PTVs and air in lungs or outside the body during treatment planning. Despite these (sometimes large) overlaps, treatment plans (SP and LoP) fulfilled most planning objectives, except for spleen (Dmean <24 Gy). However, for accumulated spleen dose, this objective was fulfilled for most patients. Fourth, for daily dose calculations, the original pCT was used with identical body contour

and overrides of gas in the body. Although this does not exactly represent the daily anatomy during treatment, it is a straightforward strategy with the ability to assess SP vs LoP exclusively. Fifth, we performed voxel-wise dose accumulation to evaluate OAR dose over the entire course of treatment. Many studies assess dose per fraction<sup>46,111,118</sup> which does not allow for such an evaluation. Generally, dose accumulation is performed using DIR as it has demonstrated better results than rigid registration<sup>132,133</sup>; however, this was not possible due to the absence of clear CTV boundaries and poor CBCT soft tissue contrast. Therefore, we performed rigid registration in this study. The rigid registration-based dose accumulation accuracy was improved by performing it separately for each OAR. Although rigid registration of the OAR does result in some uncertainty in the accumulated dose, since OAR deformation was limited, we expect our accumulated dose results to be sufficiently accurate to demonstrate benefit of LoP. Finally, an online adaptive strategy might be used as alternative to a LoP, as it may result in superior dosimetric benefits. However, respiratory motion, peristalsis, and gas in the stomach/bowels severely compromise image quality. Although quality was sufficient for plan selections, this might pose challenges for online adaptive radiotherapy.

Besides demonstrating dosimetric benefit of a LoP, this study presents a clear overview of all the necessary steps to create a LoP from a single pre-treatment CT and a gastric deformation model. This study specifically proposes a strategy to create CTVs from stomachs and provides the calculation of population-based PTV margins that allow adequate radiotherapy for both SP and LoP strategies, thus enabling other institutes to also create a gastric LoP using a gastric deformation model. As demonstrated, the necessary PTV margin for SP radiotherapy is considerably larger than the typically used 10 mm. Therefore, this work also facilitates adequate coverage for preoperative gastric cancer patients treated with a SP strategy.

In conclusion, this study has shown that a LoP for preoperative gastric cancer has a significant dosimetric benefit in OAR dose compared to a SP. Appropriate PTV margins were calculated and were significantly smaller for LoP than for SP. In addition, LoP resulted in a significantly decreased average PTV. Hence, we concluded that a LoP potentially reduces the risk for radiation-induced toxicity for gastric cancer patients compared to SP.



**General Discussion**

**7**

Preoperative gastric cancer radiotherapy is a novel treatment approach, and consequently, the difficulties encountered during radiotherapy are still largely unexplored. The stomach presents distinct challenges for radiotherapy due to its high mobility and deformability, proximity to various radiosensitive organs, and the typically large target volumes. Effective management of these geometric uncertainties is crucial to ensure accurate and precise delivery of radiotherapy for this target. Hence, this thesis aimed to explore a *cone-beam CT* (CBCT) guided adaptive strategy for preoperative gastric cancer radiotherapy.

The work was separated into three general objectives. First, the need for an adaptive strategy for this patient group was explored. For this purpose, fiducial markers were implanted in the stomach to enhance target visibility and could serve as landmarks to guide radiotherapy (**Chapter 2**). Using these fiducial markers, we identified and quantified interfractional and intrafractional stomach motions and deformations that may impact radiotherapy accuracy (**Chapter 3**). The second objective focused on exploring the feasibility of a *library of plans* (LoP) strategy. As the interfractional anatomical variations demonstrated that an adaptive strategy is likely beneficial for preoperative gastric cancer patients, we assessed whether the target's visibility on CBCT images was sufficient for plan selections from a LoP (**Chapter 4**). Knowing a LoP is a feasible strategy in terms of image quality, the third objective aimed to develop and evaluate the potential benefit of a LoP. For this, a personalized and population-based gastric deformation model was developed, and their ability to predict stomach shape for different stomach fillings was compared (**Chapter 5**). Using the population-based gastric deformation model, a LoP was created and demonstrated its potential dosimetric benefit compared to a single-plan approach (**Chapter 6**).

In this chapter, we will first explore the main findings of this thesis within a broader context, delving into the three objectives that guided this thesis. Subsequently, we will discuss this research in light of recent advancements in the field of radiotherapy and potential future directions for preoperative gastric cancer radiotherapy (Section 7.2).

## **7.1 Adaptive radiotherapy for preoperative gastric cancer**

### **7.1.1 The need for an adaptive strategy**

Accurate radiotherapy requires a comprehensive understanding of the anatomical variations during treatment. The need for an adaptive strategy for the stomach depends on the day-to-day (interfractional) anatomical variations the stomach experiences. Within this thesis, interfractional stomach motion and deformations were quantified using the implanted fiducial markers (**Chapters 2** and **Chapter 3**). Our findings revealed substantial day-to-day displacements of these markers, exhibiting varying magnitudes across the different anatomical

regions within the stomach.

The observed substantial daily variations in stomach shape and size are most likely attributed to changes in filling and gas pockets in the stomach and bowels (**Chapter 3**). However, we found that not every part of the stomach experiences the same deformations, as the deformations varied in magnitude between directions and across different stomach regions. Specifically, the systematic and random errors associated with these deformations were relatively small in the cardia, ranging from 1.6 to 4.8 mm and 2.2 to 2.8 mm, respectively. However, the deformations in the distal large curvature were much more pronounced, ranging from 6.6 to 8.8 mm and 6.6 to 8.2 mm, respectively. The substantial stomach shape changes that occur during the course of radiotherapy give rise to substantial geometric uncertainties during treatment. This can result in geometric misses or increased radiation dose to nearby *organs at risk* (OARs) when relying on a single treatment plan, despite the application of image-guidance techniques.

The obvious solution to mitigate the impact of daily variations in stomach shape and size is to impose dietary restrictions to minimize changes in stomach filling. However, previous studies have shown that such restrictions are not necessarily effective in practice<sup>19,20</sup>, possibly because the stomach shape and size are affected not only by food and drink intake but also by the presence of gas in the stomach. Moreover, imposing additional dietary restrictions beyond the current instructions, which entail a light breakfast and treatment before 1 pm, may be undesirable for this patient group as they often already face difficulties achieving sufficient food intake. Alternatively, another approach to mitigate the effect of these large shape and size changes is using large non-uniform safety margins to ensure adequate treatment during single-plan radiotherapy. However, such margins will inevitably increase the irradiated volume, consequently raising the dose to the OARs. Given that the typical treatment for these patients is already highly toxic and associated with low patient compliance<sup>8-10</sup>, increasing these margins and thus the OAR dose is not viable. Therefore, adaptive radiotherapy for preoperative gastric cancer becomes essential. By adapting the treatment to the observed daily anatomical variations, the substantial shape and size changes of the target can be partially or mostly accounted for. As such, adaptive radiotherapy will reduce the geometric uncertainties during radiotherapy and, therefore, the necessary safety margins. Consequently, adaptive radiotherapy offers a promising approach to enhance the accuracy of preoperative gastric cancer radiotherapy and can potentially improve treatment outcomes.

Some challenges posed by the daily anatomical variations and the need for adaptive strategies are not unique to preoperative gastric cancer. Other radiotherapy targets, including the bladder, cervix, and rectum, also experience similar issues. For example, the bladder and cervix undergo considerable changes in shape (and size for the bladder) due to variations in bladder filling<sup>134,135</sup>. Interfractional systematic errors for the bladder have been reported to range from



1 to 12 mm<sup>134</sup>, and for the cervix, values have been documented between 8 and 13 mm<sup>135</sup>, depending on the direction. Likewise, the rectum exhibits substantial positional and shape variations, with systematic errors ranging from 2 to 7 mm, dependent on the location<sup>136</sup>. While research on stomach motion and adaptive strategies for the stomach is still in its early stages, the bladder, cervix, and rectum have been extensively studied, leading to the implementation of daily adaptation for these targets and patients benefiting from the reduction of the *planning target volume* (PTV) and dose to OARs<sup>137</sup>. Although the stomach experiences its own specific motion characteristics, the benefits from adaptive radiotherapy observed in these other organs suggest that a similar approach may prove beneficial for preoperative gastric cancer radiotherapy.

### 7.1.2 Feasibility of a library of plans

Having established the importance of adaptive radiotherapy for preoperative gastric cancer, it is essential to assess the feasibility and potential benefits of an adaptive strategy. One such approach is the LoP, which has been proven effective for various organs, including the bladder<sup>42</sup>, cervix<sup>110</sup>, and rectum<sup>98</sup>. However, it is important to recognize that feasibility for these organs does not automatically guarantee feasibility for the stomach. The feasibility of a LoP depends on the quality of daily acquired imaging, which must be sufficient for target localization and plan selections. In the upper abdomen and for the stomach specifically, CBCT image quality is compromised because of the stomach's high mobility (e.g., respiratory and peristaltic motion), and (moving) gas pockets in the stomach and bowels during image acquisition. In **Chapter 4**, we developed a rudimentary LoP and evaluated the feasibility of this LoP. Given that several observers with varying expertise were able to identify the target and select the best-fitting plan with good agreement among each other, CBCT image quality was considered sufficient for a LoP for gastric cancer radiotherapy. Since preoperative gastric cancer radiotherapy is a new and relatively unexplored treatment approach, there has been no previous research on the gastric LoP. Therefore, this was the first study investigating a gastric LoP and deeming it feasible.

Even though CBCT image quality was generally assessed as sufficient for plan selections, image quality varied among patients and from day to day. Hence, stomach localization and plan selections can be more challenging on some CBCTs than others. To improve stomach localization, we implanted fiducial markers at various sites within the stomach wall (**Chapter 2**), similarly as done for other targets, including the esophagus<sup>40</sup>, bladder<sup>38</sup>, prostate<sup>36</sup>, and pancreas<sup>54</sup>. We demonstrated that fiducial marker implantations in the stomach were safe and feasible. Furthermore, most markers exhibited good visibility on both average reconstructed 4DCBCTs and individual phase 4DCBCTs, resulting in improved daily stomach localization, as confirmed by the radiation therapists (RTTs) responsible for treating these patients. Although

not included in this study, the implantation of fiducial markers in the tumor may also aid localization when more targeted radiotherapy is applied exclusively to the tumor. While experienced observers may rely less on these fiducial markers, they may be indispensable for accurate localization for observers with limited experience in stomach localization on CBCT. Importantly, CBCT image quality was sufficient for plan selections by experienced observers both without (**Chapter 4**) and with fiducial markers (**Chapter 6**). However, unfortunately, we did not evaluate whether the presence of fiducial markers leads to more consistent plan selections among observers with varying expertise. Overall, I consider fiducial markers to be a valuable aid in target localization, regardless of whether a single-plan or a LoP is employed, particularly in situations involving extremely poor CBCT quality or when dealing with less experienced observers.

For a LoP, which typically has lower image quality demands than for instance daily online replanning, we demonstrated that the current CBCT image protocols are sufficient for clinical use. However, when it comes to more demanding procedures, such as deformable image registrations between CT and CBCT, the current image quality of CBCT may prove insufficient, which has been experienced firsthand. The registration accuracy is compromised by the poor soft-tissue contrast, noise, and artifacts associated with CBCT imaging<sup>138</sup>. Ongoing efforts towards improving CBCT image quality have been made, including reducing image acquisition time from the traditional 2 to 4 minutes to <60 seconds, and implementing iterative reconstruction algorithms<sup>139,140</sup>. Although iterative reconstructions show promise in reducing noise and increasing image uniformity and overall image quality<sup>140,141</sup>, they are known to be sensitive to patient or organ motion during acquisition. This is especially concerning in the upper abdomen due to respiratory and peristaltic motion. Therefore, these iterative reconstructions are primarily used for scans of stationary anatomies, such as the pelvic and head-and-neck region<sup>142</sup>. In the case of more demanding radiotherapy approaches for preoperative gastric cancer, exploring additional strategies to improve CBCT image quality may still be necessary, and the feasibility of such approaches in the upper abdomen should be demonstrated. Alternatively, *magnetic resonance* (MR) guided radiotherapy emerges as a preferred approach, offering superior soft-tissue contrast and potentially eliminating the need for fiducial markers. However, practical limitations such as high cost, limited availability, the typically prolonged workflow, and the need for additional training exist for MR-guided *linear accelerators* (linacs). It is worth noting that the current CBCT image quality, preferably combined with implanted fiducial markers, enables sufficient target localization for the clinical use of a LoP. The feasibility of a CBCT-guided LoP, combined with the widespread availability of CBCT-linacs, renders a CBCT-guided LoP an adaptive strategy that can be readily implemented in numerous institutes for preoperative gastric cancer. However, before clinical implementation, developing an effective LoP and thoroughly exploring its potential benefits is essential.

### 7.1.3 Development and evaluation of a library of plans

A LoP should adequately cover the target's anatomical variations during treatment. For this, two strategies - a personalized and a population-based - were compared to predict stomach shape changes due to filling (**Chapter 5**). The population-based strategy, based on data from healthy volunteers, outperformed the personalized strategy in predicting shape changes in both healthy volunteers and patients. Therefore, this strategy was used to develop a LoP and evaluate its potential benefits compared to a single-plan approach (**Chapter 6**). The LoP demonstrated potential benefits over the single-plan approach, including a reduction of the required safety margins, a decreased average PTV volume over the course of treatment, and a lower accumulated dose to OARs, all while maintaining equal coverage.

#### ***Stomach shape prediction***

The effectiveness of a LoP for preoperative gastric cancer relies on the predictability of the shape changes experienced by the stomach. Our study showed that stomach shape can be reasonably predicted by stomach volume for patient data using population-derived deformations with a median Dice similarity coefficient of 0.87 (**Chapter 5**). Although this population-based strategy for shape prediction was used to create a LoP (**Chapter 6**), the LoP still required relatively large PTV margins (median 13.1 mm), suggesting potential room for further improvement in shape prediction.

The challenge in accurately predicting stomach shape lies in its complex anatomical deformations caused by various factors, such as ingested food or drinks, gas in the stomach or bowels, and bowel content. Additionally, the stomach is connected to the esophagus on one side and to the duodenum on the other, but neither is attached to bone, allowing the stomach to move. These elements affect stomach shape differently, making it difficult to model its variations accurately. While shape prediction models have been continuously explored and developed for use in a cervix<sup>48,49,143</sup> and bladder LoP<sup>117,144</sup>, these organs may exhibit more predictable motion patterns. For example, while the bladder does experience shape and size changes, these are typically more restricted to specific regions and directions of expansion as it primarily expands in the cranial-anterior direction and is more or less fixed at its base<sup>134</sup>. For a shape prediction model to address the complex anatomical variations of the stomach, more advanced strategies such as a (multi-organ) finite element model, developed for the bladder<sup>117</sup> and cervix<sup>49</sup>, or principal component analysis, developed for the bladder<sup>145</sup>, cervix<sup>48</sup>, and pancreas<sup>106</sup>, could be considered. However, implementing such models into a practical gastric LoP presents challenges as it requires many plans to cover the full range of anatomical variations, while typical libraries are limited to 3–6 plans for logistical and practical reasons. Therefore, including all potential anatomical variations of the stomach in a LoP may not be feasible. While the current shape prediction method demonstrates a reasonable level of

accuracy, other factors may also influence shape deformations, such as age, region, and tumor location. However, evaluating these factors requires a larger patient sample. Nevertheless, improvement of the shape prediction strategy for a LoP, while maintaining a limited number of plans, may not significantly reduce the calculated margins (see **Chapter 6**) due to the complexity of the stomach's shape changes. Alternatively, daily online segmentation and replanning can be a viable option when technically feasible as it eliminates the need for predicting anatomical changes (see section 7.2.3).

### ***Evaluation of margin calculations***

While necessary safety margins were calculated for both a LoP and single-plan approach (**Chapter 6**), these margins were not based on the measured intrafraction motion as quantified with fiducial markers in **Chapter 3**. This raises the question of whether the margin calculations should be retrospectively adjusted or whether the included uncertainties and selected values were sufficiently accurate. The calculated margins in **Chapter 6** included (residual) interfractional shape variation, delineation uncertainty, peristalsis-induced intrafractional motion, and respiratory motion. In the following, we delve into the calculated intrafraction motions as quantified with the fiducial markers (**Chapter 3**) and their implications for the margin calculations.

- **Respiratory amplitude value:** The selected population-based respiratory amplitudes were 8 mm, 3 mm, and 2 mm in the superior-inferior, anterior-posterior, and left-right directions, respectively. These values were based on previous studies on the pancreas<sup>78</sup> and the proximal part of the stomach<sup>41</sup>, and data from the first five patients<sup>146</sup>. These amplitudes appear to be reasonably accurate considering the median respiratory amplitudes observed in **Chapter 3**, which were 10.3 mm, 3.4 mm, and 0.7 mm, respectively. Adjusting the respiratory amplitudes in the margin calculation has a minimal effect, increasing the margins by approximately 0.05 mm for both the single-plan and LoP approach.
- **Inter- and intra-patient variability in respiratory amplitude:** The respiratory motion of patients can exhibit considerable variability, not only between individuals but also within individuals from one treatment day to another (**Chapter 3**). The inter-patient variability may suggest using patient-specific respiratory amplitudes in the safety margin. However, considering the minimal impact of adjustment of the population-based respiratory amplitudes on the resulting margin (as mentioned in the previous bullet point), incorporating patient-specific respiratory amplitudes in margin calculations would also have a negligible impact. Moreover, the intra-patient variability in respiratory amplitude indicates that the respiratory motion observed during the planning CT may not accurately represent the amplitude during treatment, as supported by other studies<sup>41,78</sup>. Although this uncertainty can be addressed by

incorporating it as an additional random error in the safety margin, with a median standard deviation of respiratory amplitude of 1.45 mm, the resulting margin increase is minimal, amounting to less than 0.4 mm.

- **Intrafractional drift:** Even though intrafractional stomach drifts were observed (**Chapter 3**), their impact on the margin is also small. Even in a worst-case scenario, where systematic and random errors were calculated with the full displacements, the margin increase remains below 10%.

Overall, the primary contributor to the margins remains the (residual) interfractional shape variations, regardless of whether the LoP or single-plan approach is employed. As the errors are combined through quadratic addition, larger errors have a greater impact on the total error (i.e., margin) compared to smaller errors. Consequently, the (minor) changes to existing uncertainties or the addition of relatively small uncertainties have minimal impact on the calculations. Therefore, I believe the calculated margins are sufficiently accurate. However, with potential future advancements in radiotherapy to minimize interfractional uncertainties, the uncertainties identified here may become more important and require further attention.

### ***Evaluation of library of plans versus single-plan radiotherapy***

Our results indicate that a LoP reduces the margins required for preoperative gastric cancer radiotherapy compared to a single-plan approach, which in turn reduces the irradiated volume and dose to neighboring OARs (**Chapter 6**). However, the current typical margin for single-plan radiotherapy of 10 mm is much smaller than the here calculated non-uniform margin for the stomach, which has a median margin almost twice as large (19.8 mm). Although the margin for the LoP was significantly smaller (13.1 mm), it still exceeds the currently clinically used margin. The aforementioned challenges in accurately predicting stomach shape primarily contribute to this relatively large margin. Nevertheless, we clearly demonstrated that the clinically used 10-mm PTV margin with a single-plan approach poses a risk for reduced target coverage, underscoring the need to improve the current clinical practice. Even though the LoP still requires relatively large margins, the LoP does yield dosimetric benefits in terms of average irradiated volume and accumulated OAR dose. Based on this, I believe a LoP should be preferred over a single-plan approach for this patient group. Strategies to further improve preoperative gastric cancer radiotherapy and potentially achieve greater benefits may be explored in the future, and such strategies will be discussed in the following section.

## **7.2 Outlook**

Throughout this thesis, we have explored an adaptive strategy for preoperative gastric cancer. We have demonstrated the need for an adaptive approach due to the challenges presented by the stomach's high mobility and deformability and its proximity to various radiosensitive

organs. We have also shown the feasibility of a LoP and its potential benefits in delivering more accurate radiotherapy. Despite these promising findings, the clinical application of preoperative gastric radiotherapy, being a novel treatment approach, is still limited. As a result, research into preoperative gastric cancer radiotherapy is scarce, leading to a lack of comparative studies to validate and compare our findings. This emphasizes the importance of further research into this treatment approach. The following sections will explore the potential clinical implications of this work. Furthermore, we will identify areas for future investigations and discuss potential avenues for further (technical and clinical) improvements, aiming to optimize radiotherapy for this patient group.

### 7.2.1 Clinical relevance

The primary objective of this thesis was to improve the accuracy and precision of preoperative radiotherapy for gastric cancer. However, the efficacy of preoperative radiotherapy for gastric cancer in general is still uncertain as ongoing clinical trials are still investigating its benefits. Radiotherapy was administered to the patients in this thesis as part of the CRITICS-II trial in which preoperative chemotherapy, preoperative chemotherapy and chemoradiotherapy, and preoperative chemoradiotherapy are compared<sup>10</sup>. Other trials are also conducted in search of the best treatment regimens<sup>11,12</sup>, such as the TOPGEAR trial in which perioperative chemotherapy alone or with preoperative chemoradiotherapy are compared<sup>51</sup>. But what if these trials do not definitively establish the benefits of preoperative radiotherapy for gastric cancer? In that case, what will be the clinical value and relevance of the work conducted in this thesis?

Before we abandon preoperative radiotherapy for gastric cancer based on the outcomes of these trials, it is crucial to consider the context of these trials. For example, in the CRITICS-II trial, all patients received a single plan with a 10-mm safety margin, which we demonstrated to be suboptimal as there is a substantial risk of compromised target coverage and OAR sparing. The decision on whether to abandon preoperative radiotherapy as part of the treatment will be driven by factors such as high toxicities and recurrences. However, as our research demonstrated the potential for improved radiotherapy accuracy using an adaptive strategy, there is an opportunity to reduce the toxicities associated with preoperative radiotherapy. Enhanced radiotherapy accuracy may prove beneficial in preventing recurrences at the edge of the target (i.e., marginal recurrences). For recurrences in locations consistently within the radiation field (i.e., infield recurrences), higher radiation doses may be necessary, and improved radiotherapy accuracy could limit the increased risk of toxicities resulting from this higher dose. Therefore, given the potential for improved radiotherapy accuracy as demonstrated in this research, implementation of adaptive radiotherapy as part of the treatment regimen may yield better outcomes. Regardless, gaining insights into the mobility of the stomach and its

implications for radiotherapy as well as enhancing the accuracy and precision of preoperative gastric cancer radiotherapy, remain important for the development of potential future studies on preoperative radiotherapy for gastric cancer.

### 7.2.2 Target definition

Preoperative radiotherapy for gastric cancer typically targets not only the tumor but also the entire stomach and the first draining lymph node stations. The regional lymph nodes are included in the *clinical target volume* (CTV) to address potential microscopic spread that may not be visible on the imaging. However, irradiating these nodes drastically increases the target volume for radiotherapy. Hence, whether the benefits of elective node irradiation outweigh the downsides of an increased target volume for radiotherapy could be questioned.

Given the poor overall survival for this patient group (see **Chapter 1**), it is important to consider the chances for curative treatment when there is microscopic spread toward the regional lymph node stations. This is especially relevant given that the prognostic prediction in gastric cancer following surgery heavily relies on the presence or absence of lymph node metastasis<sup>147</sup>. For esophageal cancer, studies are increasingly investigating the benefit of elective node irradiation compared to involved field irradiation (i.e., irradiation of only the affected areas)<sup>148</sup>. A systematic review and meta-analysis focused on esophageal cancer<sup>148</sup> revealed that involved field irradiation significantly improves 5-year overall survival rates while reducing treatment-related adverse events compared to elective node irradiation. Likewise, target volume reduction for preoperative gastric cancer may also be an interesting avenue for future investigations.

Furthermore, excluding regional lymph nodes from the CTV could also yield additional benefits for adaptive radiotherapy. The regional lymph node stations adjacent to the stomach, such as those surrounding the spleen, liver, aorta, and pancreas, are more rigid and positionally stable than the stomach itself. In **Chapter 6**, we incorporated these lymph nodes as a relatively fixed component of the clinical target volume (CTV<sub>rigid</sub>) and only predicted stomach deformations, following a similar approach as implemented for the bladder<sup>98</sup> and cervix<sup>149</sup>. As a result, given that CTV<sub>rigid</sub> constitutes a substantial portion of the total CTV, such adaptive strategies only account for shape changes in the part of the CTV that is not adjacent to the neighboring CTV<sub>rigid</sub>. Consequently, the potential dosimetric benefit of a LoP, or potentially adaptive radiotherapy in general, compared to a single-plan approach will increase when the target volume exclusively includes the stomach and its directly surrounding lymph nodes (i.e., within a 1 cm margin; **Chapter 6**). Thus, excluding regional lymph nodes from the target volume would amplify the benefit of an adaptive strategy compared to a single-plan approach.

### 7.2.3 Further advancements in adaptive radiotherapy

Throughout this thesis, we have occasionally touched upon one of the most promising advancements in the field of radiotherapy: the ability to generate new treatment plans on a daily basis. Recent technological advancements and dedicated research efforts over the past decade have led to the development of CBCT-guided and MR-guided linacs, enabling daily online segmentation and replanning. With the growing implementation of these techniques across different targets, it is foreseeable that in the near future the application of this emerging adaptive radiotherapy approach will be explored in the context of preoperative gastric cancer radiotherapy. The aforementioned inherent challenges posed by the stomach's high mobility and complex shape and size changes could make it a promising candidate for such a strategy. However, it is important to acknowledge that while daily online replanning may offer additional benefits compared to a LoP, it also presents distinct challenges and limitations.

Daily online segmentation and replanning of radiotherapy can potentially provide better dosimetric accuracy than a LoP, and allows for more precise adaptation to the daily anatomy observed on imaging than the predefined plans in a library. However, this approach involves multiple steps that need to be performed daily and each requires to be of sufficient quality. These steps include imaging acquisition, accurate segmentation of targets and OARs, plan optimization, plan quality verification, and plan delivery, making it a time-consuming approach. Artificial intelligence plays a crucial role in enhancing the quality and accelerating the workflow for tasks such as automated segmentation<sup>150</sup>, deformable registration<sup>151</sup>, and treatment planning<sup>152</sup>. Nevertheless, the longer process time associated with daily online segmentation and replanning introduces the possibility of an increase in intrafractional motion and associated uncertainties during treatment. Studies on the bladder<sup>153</sup> and cervix<sup>104</sup> have demonstrated that daily online MR-guided replanning offers advantages over a LoP, including improved target coverage and/or reduced irradiation of healthy tissue when treatment is delivered within a 15-minute timeframe. However, considering that treatment times are typically larger, further advancements in accelerating the workflow are still necessary. For gastric cancer patients, intrafraction anatomical variations such as gastric emptying, peristalsis, and patient movement may be more pronounced for longer treatment duration. Therefore, limiting treatment duration while ensuring the generation of high-quality treatment plans will be important when considering an online replanning strategy for preoperative gastric cancer radiotherapy.

Online replanning for the stomach can be particularly challenging due to the need for high-quality imaging (CBCT- or MR-guided) and automated segmentation of the CTV and OARs. While CBCT-guided online replanning has been successfully applied for various targets in the pelvis<sup>84,154,155</sup>, CBCT scans of the pelvis generally offer superior image quality compared



to those of the upper abdomen, thanks to the limited motion during image acquisition. Limited research has been conducted on applying CBCT-guided online replanning for upper abdominal sites. Although a case report demonstrated the potential of CBCT-guided online replanning with the Varian Ethos (i.e., a CBCT-guided linac capable of online replanning) for upper abdomen targets within a treatment duration of less than 30 minutes<sup>156</sup>, our personal experience was that the image quality obtained from conventional linacs was inadequate for the automatic identification and segmentation of the stomach using the same software as the case report. The CBCT quality of the upper abdomen acquired using the Varian Ethos yielded similar results, suggesting that the current limiting factor for applying CBCT-guided online replanning in preoperative gastric cancer is the quality of CBCT images and the accuracy of automatic segmentation. Ongoing efforts towards improving CBCT image quality<sup>139,140,157</sup> and advances in automatic segmentation<sup>150</sup> can potentially overcome these challenges in the future. On the other hand, MR-guided online replanning presents a promising alternative to CBCT-guided online replanning due to its superior soft-tissue contrast, which might enable accurate daily automatic segmentation. Even though MRI is also sensitive to motion<sup>29</sup>, the feasibility of automatic segmentations of the stomach on 4D MRI has been demonstrated<sup>22</sup>. Also, an ongoing clinical trial in the early phases of patient accrual is currently exploring the potential of MR-guided daily online replanning for preoperative gastric cancer patients<sup>158</sup>. Despite being in the early stages, preliminary results from the first three patients demonstrated the feasibility of this approach (personal communications, May 10, 2023)<sup>159</sup>.

When considering the best approach for adaptive radiotherapy in preoperative gastric cancer, factors such as cost and availability should also be taken into account. CBCT-linacs are more affordable than MR-linacs, making them the preferred option for online replanning when image quality is sufficient for the entire process. However, it is important to acknowledge that the availability of CBCT- and MR-linacs equipped for online replanning is still limited. Currently, conventional CBCT-linacs dominate the landscape of linacs used worldwide for image-guided radiotherapy. Therefore, the work conducted in this thesis, which focuses on exploring and developing a CBCT-guided LoP, remains highly valuable as it enables many institutes to perform adaptive radiotherapy and enhance treatment accuracy for preoperative gastric cancer patients, even with conventional CBCT-linacs.

### 7.3 Conclusions

In this thesis, the main focus was to explore a CBCT-guided adaptive strategy for preoperative gastric cancer radiotherapy. The stomach's highly mobile and deformable nature poses a substantial challenge during radiotherapy that needs to be addressed. We have uncovered that relying solely on a single treatment plan for this patient group is inadequate, given the substantial day-to-day changes in stomach shape, which introduces a high risk of missing the target and inadequate organ sparing. Based on these results, the next step towards improving radiotherapy for this patient group should be the implementation of adaptive radiotherapy to ensure accurate and effective treatment delivery.

By applying the CBCT-guided LoP approach, preferably with implanted fiducial markers to address poor CBCT quality, we can enhance treatment accuracy. While the LoP strategy we developed has proven viable, I also recognize the potential for further advancements in adaptive strategies. Exploring online replanning techniques holds great promise, as it allows for even more precise adaptations to accommodate the stomach shape changes. Accordingly, to move forward, I recommend further research and clinical validation to investigate and establish the technical feasibility, efficacy, and potential advantages of daily online segmentation and replanning strategies.

Overall, this thesis contributes to understanding the challenges associated with gastric cancer radiotherapy and offers a viable solution through the application of adaptive strategies, particularly the LoP approach. These insights are relevant for any chosen adaptive strategy, filling a crucial knowledge gap in the emerging field of preoperative radiotherapy for gastric cancer. As such, this work provides a foundation for further exploration, refinement, and implementation of adaptive strategies, with the ultimate goal of achieving greater treatment accuracy and better treatment outcomes for gastric cancer patients.



## Appendices



Bibliography  
Summary  
Samenvatting  
Supplemental Materials  
Dankwoord  
Curriculum Vitae

## Bibliography

1. O'Connor A, O'Moráin C. Digestive function of the stomach. *Dig Dis*. 2014;32(3):186-191. doi:10.1159/000357848
2. Sung H, Ferlay J, Siegel RL, et al. Global Cancer Statistics 2020: GLOBOCAN Estimates of Incidence and Mortality Worldwide for 36 Cancers in 185 Countries. *CA Cancer J Clin*. 2021;71(3):209-249. doi:10.3322/caac.21660
3. Plummer M, Franceschi S, Vignat J, Forman D, De Martel C. Global burden of gastric cancer attributable to pylori. *Int J Cancer*. 2015;136(2):487-490. doi:10.1002/ijc.28999
4. Yusefi AR, Lankarani KB, Bastani P, Radinmanesh M, Kavosi Z. Risk factors for gastric cancer: A systematic review. *Asian Pacific J Cancer Prev*. 2018;19(3):591. doi:10.22034/APJCP.2018.19.3.591
5. Dassen AE, Dikken JL, Bosscha K, et al. Gastric cancer: Decreasing incidence but stable survival in the Netherlands. *Acta Oncol (Madr)*. 2014;53(1):138-142. doi:10.3109/0284186X.2013.789139
6. Netherlands Cancer Registry (NCR). www.cijfersoverkanker.nl. Accessed March 22, 2023.
7. Smalley SR, Benedetti JK, Haller DG, et al. Updated analysis of SWOG-directed intergroup study 0116: A phase III trial of adjuvant radiochemotherapy versus observation after curative gastric cancer resection. *J Clin Oncol*. 2012;30(19):2327-2333. doi:10.1200/JCO.2011.36.7136
8. Cunningham D, Allum WH, Stenning SP, et al. Perioperative Chemotherapy versus Surgery Alone for Resectable Gastroesophageal Cancer. *N Engl J Med*. 2006;355(1):11-20. doi:10.1056/nejmoa055531
9. Cats A, Jansen EPM, van Grieken NCT, et al. Chemotherapy versus chemoradiotherapy after surgery and preoperative chemotherapy for resectable gastric cancer (CRITICS): an international, open-label, randomised phase 3 trial. *Lancet Oncol*. 2018;19(5):616-628. doi:10.1016/S1470-2045(18)30132-3
10. Slagter AE, Jansen EPM, van Laarhoven HWM, et al. CRITICS-II: A multicentre randomised phase II trial of neo-adjuvant chemotherapy followed by surgery versus neo-adjuvant chemotherapy and subsequent chemoradiotherapy followed by surgery versus neo-adjuvant chemoradiotherapy followed by surgery in resectable gastric cancer. *BMC Cancer*. 2018;18(1):877. doi:10.1186/s12885-018-4770-2
11. Yeh JH, Yeh YS, Tsai HL, et al. Neoadjuvant Chemoradiotherapy for Locally Advanced Gastric Cancer: Where Are We at? *Cancers (Basel)*. 2022;14(12):3026. doi:10.3390/cancers14123026
12. Mesci A, Wong RKS. Current and future strategies for radiation therapy in gastric cancer. *J Surg Oncol*. 2022;125(7):1161-1175. doi:10.1002/jso.26880
13. Van Herk M. Errors and Margins in Radiotherapy. *Semin Radiat Oncol*. 2004;14(1):52-64. doi:10.1053/j.semradonc.2003.10.003
14. Alicikus ZA, Aydin B. Toxicity Management for Upper Abdomen Tumors in Radiation Oncology. *Prev Manag Acute Late Toxicities Radiat Oncol Manag Toxicities Radiat Oncol*. 2020:171-229. doi:10.1007/978-3-030-37798-4\_5
15. Shadad AK, Sullivan FJ, Martin JD, Egan LJ. Gastrointestinal radiation injury: symptoms, risk factors and mechanisms. *World J Gastroenterol*. 2013;19(2):185. doi:10.3748/wjg.v19.i2.185
16. Alexandru M, Rodica A, Dragos-Eugen G, Mihai-Teodor G. Assessing the Spleen as an Organ at Risk in Radiation Therapy and Its Relationship With Radiation-Induced Lymphopenia: A Retrospective Study and Literature Review. *Adv Radiat Oncol*. 2021;6(6):100761. doi:10.1016/j.adro.2021.100761
17. Dawson LA, Kavanagh BD, Paulino AC, et al. Radiation-Associated Kidney Injury. *Int J Radiat Oncol Biol Phys*. 2010;76(3):S108-S115. doi:10.1016/j.ijrobp.2009.02.089
18. Bergom C, Bradley JA, Ng AK, et al. Past, Present, and Future of Radiation-Induced Cardiotoxicity: Refinements in Targeting, Surveillance, and Risk Stratification. *JACC CardioOncology*. 2021;3(3):343-359. doi:10.1016/j.jaccao.2021.06.007
19. Bouchard M, McAleer MF, Starkschall G. Impact of Gastric Filling on Radiation Dose Delivered to Gastroesophageal Junction Tumors. *Int J Radiat Oncol Biol Phys*. 2010;77(1):292-300. doi:10.1016/j.ijrobp.2009.08.026
20. Watanabe M, Isobe K, Takisima H, et al. Intrafractional gastric motion and interfractional stomach deformity during radiation therapy. *Radiother Oncol*. 2008;87(3):425-431. doi:10.1016/j.radonc.2007.12.018
21. Johansson A, Balter JM, Cao Y. Gastrointestinal 4D MRI with respiratory motion correction. *Med Phys*. 2021;48(5):2521-2527. doi:10.1002/mp.14786

22. Driever T, Hulshof MCCM, Bel A, Sonke JJ, van der Horst A. Quantifying intrafractional gastric motion using auto-segmentation on MRI: Deformation and respiratory-induced displacement compared. *J Appl Clin Med Phys*. 2022;24(4):e13864. doi:10.1002/acm2.13864
23. Wysocka B, Moseley J, Brock K, et al. Assessment of nonrespiratory stomach motion in healthy volunteers in fasting and postprandial states. *Pract Radiat Oncol*. 2014;4(5):288-293. doi:10.1016/j.prro.2013.10.001
24. Mostafaei F, Tai A, Omari E, et al. Variations of MRI-assessed peristaltic motions during radiation therapy. *PLoS One*. 2018;13(10):e0205917. doi:10.1371/journal.pone.0205917
25. Watanabe M, Isobe K, Uno T, et al. Intrafractional gastric motion and interfractional stomach deformity using CT images. *J Radiat Res*. 2011;52(5):660-665. doi:10.1269/jrr.11018
26. Wysocka B, Kassam Z, Lockwood G, et al. Interfraction and Respiratory Organ Motion During Conformal Radiotherapy in Gastric Cancer. *Int J Radiat Oncol Biol Phys*. 2010;77(1):53-59. doi:10.1016/j.ijrobp.2009.04.046
27. Nakao M, Nakamura M, Mizowaki T, Matsuda T. Statistical deformation reconstruction using multi-organ shape features for pancreatic cancer localization. *Med Image Anal*. 2021;67:101829. doi:10.1016/j.media.2020.101829
28. Sonke JJ, Zijp L, Remeijer P, Van Herk M. Respiratory correlated cone beam CT. *Med Phys*. 2005;32(4):176-1186. doi:10.1118/1.1869074
29. Zaitsev M, Maclaren J, Herbst M. Motion artifacts in MRI: A complex problem with many partial solutions. *J Magn Reson Imaging*. 2015;42(4):887-901. doi:10.1002/jmri.24850
30. Chen GTY, Kung JH, Beaudette KP. Artifacts in Computed Tomography Scanning of Moving Objects. *Semin Radiat Oncol*. 2004;14(1):19-26. doi:10.1053/j.semradonc.2003.10.004
31. Kupelian P, Sonke JJ. Magnetic Resonance-Guided Adaptive Radiotherapy: A Solution to the Future. *Semin Radiat Oncol*. 2014;24(3):227-232. doi:10.1016/j.semradonc.2014.02.013
32. Ng J, Gregucci F, Pennell RT, et al. MRI-LINAC: A transformative technology in radiation oncology. *Front Oncol*. 2023;13:1117874. doi:10.3389/fonc.2023.1117874
33. Machiels M, Jin P, van Hooft JE, et al. Reduced inter-observer and intra-observer delineation variation in esophageal cancer radiotherapy by use of fiducial markers. *Acta Oncol (Madr)*. 2019;58(6):943-950. doi:10.1080/0284186X.2019.1588991
34. Fernandez DC, Hoffe SE, Barthel JS, et al. Stability of endoscopic ultrasound-guided fiducial marker placement for esophageal cancer target delineation and image-guided radiation therapy. *Pract Radiat Oncol*. 2013;3(1):32-39. doi:10.1016/j.prro.2012.02.006
35. Jin P, van der Horst A, de Jong R, et al. Marker-based quantification of interfractional tumor position variation and the use of markers for setup verification in radiation therapy for esophageal cancer. *Radiother Oncol*. 2015;117(3):412-418. doi:10.1016/j.radonc.2015.10.005
36. van der Heide UA, Kotte ANTJ, Dehnad H, Hofman P, Lagenijk JJW, van Vulpen M. Analysis of fiducial marker-based position verification in the external beam radiotherapy of patients with prostate cancer. *Radiother Oncol*. 2007;82(1):38-45. doi:10.1016/j.radonc.2006.11.002
37. Van Der Horst A, Wognum S, Dávila Fajardo R, et al. Interfractional position variation of pancreatic tumors quantified using intratumoral fiducial markers and daily cone beam computed tomography. *Int J Radiat Oncol Biol Phys*. 2013;87(1):202-208. doi:10.1016/j.ijrobp.2013.05.001
38. Nolan CP, Forde EJ. A review of the use of fiducial markers for image-guided bladder radiotherapy. *Acta Oncol (Madr)*. 2016;55(5):533-538. doi:10.3109/0284186X.2015.1110250
39. De Blanck SR, Scherman-Rydhög J, Siemsen M, et al. Feasibility of a novel liquid fiducial marker for use in image guided radiotherapy of oesophageal cancer. *Br J Radiol*. 2018;91(1092):20180236. doi:10.1259/bjr.20180236
40. Machiels M, Van Hooft J, Jin P, et al. Endoscopy/EUS-guided fiducial marker placement in patients with esophageal cancer: A comparative analysis of 3 types of markers. *Gastrointest Endosc*. 2015;82(4):641-649. doi:10.1016/j.gie.2015.03.1972
41. Jin P, Hulshof MCCM, De Jong R, Van Hooft JE, Bel A, Alderliesten T. Quantification of respiration-induced esophageal tumor motion using fiducial markers and four-dimensional computed tomography. *Radiother Oncol*. 2016;118(3):492-497. doi:10.1016/j.radonc.2016.01.005
42. Collins SD, Leech MM. A review of plan library approaches in adaptive radiotherapy of bladder cancer. *Acta Oncol (Madr)*. 2018;57(5):566-573. doi:10.1080/0284186X.2017.1420908

43. McDonald F, Lalondrelle S, Taylor H, et al. Clinical implementation of adaptive hypofractionated bladder radiotherapy for improvement in normal tissue irradiation. *Clin Oncol.* 2013;25(9):549-556. doi:10.1016/j.clon.2013.06.001
44. Rigaud B, Simon A, Gobeli M, et al. CBCT-guided evolutive library for cervical adaptive IMRT. *Med Phys.* 2018;45(4):1379-1390. doi:10.1002/mp.12818
45. Buschmann M, Majercakova K, Sturdza A, et al. Image guided adaptive external beam radiation therapy for cervix cancer: Evaluation of a clinically implemented plan-of-the-day technique. *Z Med Phys.* 2018;28(3):184-195. doi:10.1016/j.zemedi.2017.09.004
46. de Jong R, Visser J, Crama KF, et al. Dosimetric benefit of an adaptive treatment by means of plan selection for rectal cancer patients in both short and long course radiation therapy. *Radiat Oncol.* 2020;15(1):1-11. doi:10.1186/s13014-020-1461-3
47. Wright P, Redpath AT, Høyer M, Muren LP. A method to individualize adaptive planning target volumes for deformable targets. *Phys Med Biol.* 2009;54(23):7121-7133. doi:10.1088/0031-9155/54/23/006
48. Rigaud B, Simon A, Gobeli M, et al. Statistical Shape Model to Generate a Planning Library for Cervical Adaptive Radiotherapy. *IEEE Trans Med Imaging.* 2019;38(2):406-416. doi:10.1109/TMI.2018.2865547
49. Beekman C, van Beek S, Stam J, Sonke JJ, Remeijer P. A biomechanical finite element model to generate a library of cervix CTVs. *Med Phys.* 2020;47(9):3852-3860. doi:10.1002/mp.14349
50. Beekman C, van Triest B, van Beek S, Sonke JJ, Remeijer P. Margin and PTV volume reduction using a population based library of plans strategy for rectal cancer radiotherapy. *Med Phys.* 2018;45(10):4345-4354. doi:10.1002/mp.13137
51. Leong T, Smithers BM, Haustermans K, et al. TOPGEAR: A Randomized, Phase III Trial of Perioperative ECF Chemotherapy with or Without Preoperative Chemoradiation for Resectable Gastric Cancer: Interim Results from an International, Intergroup Trial of the AGITG, TROG, EORTC and CCTG. *Ann Surg Oncol.* 2017;24(8):2252-2258. doi:10.1245/s10434-017-5830-6
52. De Ridder M, Gerbrandy LC, de Reijke TM, Hinnen KA, Hulshof MCCM. BioXmark® liquid fiducial markers for image-guided radiotherapy in muscle invasive bladder cancer: A safety and performance trial. *Br J Radiol.* 2020;93(1111):20200241. doi:10.1259/bjr.20200241
53. DiMaio CJ, Nagula S, Goodman KA, et al. EUS-guided fiducial placement for image-guided radiation therapy in GI malignancies by using a 22-gauge needle (with videos). *Gastrointest Endosc.* 2010;71(7):1204-1210. doi:10.1016/j.gie.2010.01.003
54. Dávila Fajardo R, Lekkerkerker SJ, Van Der Horst A, et al. EUS-guided fiducial markers placement with a 22-gauge needle for image-guided radiation therapy in pancreatic cancer. *Gastrointest Endosc.* 2014;79(5):851-855. doi:10.1016/j.gie.2013.12.027
55. Glissen Brown JR, Perumpail RB, Duran JF, et al. Preloaded 22-gauge fine-needle system facilitates placement of a higher number of fiducials for image-guided radiation therapy compared with traditional backloaded 19-gauge approach. *Gastrointest Endosc.* 2021;94(5):953-958. doi:10.1016/j.gie.2021.05.035
56. Dhadham G, Hoffe S, Harris C, Klapman J. Endoscopic ultrasound-guided fiducial marker placement for image-guided radiation therapy without fluoroscopy: safety and technical feasibility. *Endosc Int Open.* 2016;4(3):378-382. doi:10.1055/s-0042-100720
57. Rigter LS, Rijkmans EC, Inderson A, et al. EUS-guided fiducial marker placement for radiotherapy in rectal cancer: feasibility of two placement strategies and four fiducial types. *Endosc Int Open.* 2019;7(11):1357-1364. doi:10.1055/a-0958-2148
58. Machiels M, Voncken FEM, Jin P, et al. A Novel Liquid Fiducial Marker in Esophageal Cancer Image Guided Radiation Therapy: Technical Feasibility and Visibility on Imaging. *Pract Radiat Oncol.* 2019;9(6):506-515. doi:10.1016/j.pro.2019.06.018
59. Chandran S, Vaughan R, Efthymiou M, Sia J, Hamilton C. A pilot study of EUS-guided fiducial insertion for the multidisciplinary management of gastric cancer. *Endosc Int Open.* 2014;2(3):153-159. doi:10.1055/s-0034-1377523
60. Sia J, Glance S, Chandran S, Vaughan R, Hamilton C. The use of fiducial markers in image-guided radiotherapy for gastric cancer. *J Med Imaging Radiat Oncol.* 2013;57(5):626-628. doi:10.1111/1754-9485.12084
61. Abdelfatah MM, Gochanour EM. Fiducial placement for recurrent gastric cancer. *Arab J Gastroenterol.* 2019;20(1):56-58. doi:10.1016/j.ajg.2019.01.007

62. Phan VA, Dalfsen R, Le H, Nguyen NQ. Performance of a new preloaded fiducial needle to guide radiation therapy of upper gastrointestinal cancers. *Endoscopy*. 2019;51(5):463-467. doi:10.1055/a-0800-0033
63. Rit S, Wolthaus JWH, Van Herk M, Sonke JJ. On-the-fly motion-compensated cone-beam CT using an a priori model of the respiratory motion. *Med Phys*. 2009;36(6):2283-2296. doi:10.1118/1.3115691
64. Kim DW, Lee G, Hong TS, et al. Neoadjuvant versus Postoperative Chemoradiotherapy is Associated with Improved Survival for Patients with Resectable Gastric and Gastroesophageal Cancer. *Ann Surg Oncol*. 2022;29(1):242-252. doi:10.1245/s10434-021-10666-y
65. Wang T, Chen Y, Zhao L, et al. The effect of neoadjuvant therapies for patients with locally advanced gastric cancer: a propensity score matching study. *J Cancer*. 2020;12(2):379. doi:10.7150/jca.46847
66. Wong RKS, Jang R, Darling G. Postoperative chemoradiotherapy vs. preoperative chemoradiotherapy for locally advanced (operable) gastric cancer: Clarifying the role and technique of radiotherapy. *J Gastrointest Oncol*. 2015;6(1):89. doi:10.3978/j.issn.2078-6891.2014.089
67. Bleeker M, Hulshof MCCM, Bel A, Sonke JJ, van der Horst A. Gastric deformation models for adaptive radiotherapy: Personalized vs population-based strategy. *Radiother Oncol*. 2022;166:126-132. doi:10.1016/j.radonc.2021.11.028
68. Bleeker M, Goudschaal K, Bel A, Sonke JJ, Hulshof MCCM, van der Horst A. Feasibility of cone beam CT-guided library of plans strategy in pre-operative gastric cancer radiotherapy. *Radiother Oncol*. 2020;149:49-54. doi:10.1016/j.radonc.2020.04.057
69. Bleeker M, Visser J, Goudschaal K, et al. Dosimetric benefit of a library of plans versus single-plan strategy for pre-operative gastric cancer radiotherapy. *Radiother Oncol*. 2023;182:109582. doi:10.1016/j.radonc.2023.109582
70. Ajaj W, Goehde SC, Papanikolaou N, et al. Real time high resolution magnetic resonance imaging for the assessment of gastric motility disorders. *Gut*. 2004;53(9):1256-1261. doi:10.1136/gut.2003.038588
71. Liu L, Johansson A, Cao Y, Kashani R, Lawrence TS, Balter JM. Modeling intra-fractional abdominal configuration changes using breathing motion-corrected radial MRI. *Phys Med Biol*. 2021;66(8):085002. doi:10.1088/1361-6560/abef42
72. de Muinck Keizer DM, Kerkmeijer LGW, Willigenburg T, et al. Prostate intrafraction motion during the preparation and delivery of MR-guided radiotherapy sessions on a 1.5T MR-Linac. *Radiother Oncol*. 2020;151:88-94. doi:10.1016/j.radonc.2020.06.044
73. Boda-Heggemann J, Köhler FM, Wertz H, et al. Intrafraction motion of the prostate during an IMRT session: A fiducial-based 3D measurement with Cone-beam CT. *Radiat Oncol*. 2008;3(1):1-8. doi:10.1186/1748-717X-3-37
74. Case RB, Sonke JJ, Moseley DJ, Kim J, Brock KK, Dawson LA. Inter- and Intrafraction Variability in Liver Position in Non-Breath-Hold Stereotactic Body Radiotherapy. *Int J Radiat Oncol Biol Phys*. 2009;75(1):302-308. doi:10.1016/j.ijrobp.2009.03.058
75. van de Lindt TN, Nowee ME, Janssen T, et al. Technical feasibility and clinical evaluation of 4D-MRI guided liver SBRT on the MR-linac. *Radiother Oncol*. 2022;167:285-291. doi:10.1016/j.radonc.2022.01.009
76. Seppenwoolde Y, Shirato H, Kitamura K, et al. Precise and real-time measurement of 3D tumor motion in lung due to breathing and heartbeat, measured during radiotherapy. *Int J Radiat Oncol Biol Phys*. 2002;53(4):822-834. doi:10.1016/S0360-3016(02)02803-1
77. Takao S, Miyamoto N, Matsuura T, et al. Intrafractional baseline shift or drift of lung tumor motion during gated radiation therapy with a real-time tumor-tracking system. *Int J Radiat Oncol Biol Phys*. 2016;94(1):172-180. doi:10.1016/j.ijrobp.2015.09.024
78. Lens E, Van Der Horst A, Kroon PS, et al. Differences in respiratory-induced pancreatic tumor motion between 4D treatment planning CT and daily cone beam CT, measured using intratumoral fiducials. *Acta Oncol (Madr)*. 2014;53(9):1257-1264. doi:10.3109/0284186X.2014.905699
79. Balter JM, Lam KL, McGinn CJ, Lawrence TS, Ten Haken RK. Improvement of CT-based treatment-planning models of abdominal targets using static exhale imaging. *Int J Radiat Oncol Biol Phys*. 1998;41(4):939-943. doi:10.1016/S0360-3016(98)00130-8
80. Amberg B, Romdhani S, Vetter T. Optimal step nonrigid ICP algorithms for surface registration. *Proc IEEE Comput Soc Conf Comput Vis Pattern Recognit*. 2007:1-8. doi:10.1109/CVPR.2007.383165
81. Van Herk M, Remeijer P, Rasch C, Lebesque J V. The probability of correct target dosage: Dose-population histograms for deriving treatment margins in radiotherapy. *Int J Radiat Oncol Biol Phys*. 2000;47(4):1121-1135. doi:10.1016/S0360-3016(00)00518-6



82. Bleeker M, van der Horst A, Bel A, et al. Endoscopically placed fiducial markers for image-guided radiotherapy in preoperative gastric cancer: Technical feasibility and potential benefit. *Endosc Int Open*. 2023. doi:10.1055/a-2129-2840
83. Kibrom AZ, Knight KA. Adaptive radiation therapy for bladder cancer: A review of adaptive techniques used in clinical practice. *J Med Radiat Sci*. 2015;62:277-285. doi:10.1002/jmrs.129
84. Yock AD, Ahmed M, Ayala-Peacock D, Chakravarthy AB, Price M. Initial analysis of the dosimetric benefit and clinical resource cost of CBCT-based online adaptive radiotherapy for patients with cancers of the cervix or rectum. *J Appl Clin Med Phys*. 2021;22(10):210-221. doi:10.1002/acm2.13425
85. de Jong R, Visser J, van Wieringen N, Wiersma J, Geijssen D, Bel A. Feasibility of Conebeam CT-based online adaptive radiotherapy for neoadjuvant treatment of rectal cancer. *Radiat Oncol*. 2021;16(1):1-11. doi:10.1186/s13014-021-01866-7
86. Shelley CE, Barraclough LH, Nelder CL, Otter SJ, Stewart AJ. Adaptive Radiotherapy in the Management of Cervical Cancer: Review of Strategies and Clinical Implementation. *Clin Oncol*. 2021;33(9):579-590. doi:10.1016/j.clon.2021.06.007
87. Van Herk M, Witte M, Van Der Geer J, Schneider C, Lebesque J V. Biologic and physical fractionation effects of random geometric errors. *Int J Radiat Oncol Biol Phys*. 2003;57(5):1460-1471. doi:10.1016/j.ijrobp.2003.08.026
88. Ge J, Santanam L, Noel C, Parikh PJ. Planning 4-dimensional computed tomography (4DCT) cannot adequately represent daily intrafractional motion of abdominal tumors. *Int J Radiat Oncol Biol Phys*. 2013;85(4):999-1005. doi:10.1016/j.ijrobp.2012.09.014
89. Rankine L, Wan H, Parikh P, et al. Cone-beam computed tomography internal motion tracking should be used to validate 4-dimensional computed tomography for abdominal radiation therapy patients. *Int J Radiat Oncol Biol Phys*. 2016;95(2):818-826. doi:10.1016/j.ijrobp.2016.01.047
90. Abbas H, Chang B, Chen Z. Motion management in gastrointestinal cancers. *J Gastrointest Oncol*. 2014;5(3):223. doi:10.3978/j.issn.2078-6891.2014.028
91. van Kesteren Z, Veldman JK, Parkes MJ, et al. Quantifying the reduction of respiratory motion by mechanical ventilation with MRI for radiotherapy. *Radiat Oncol*. 2022;17(1):1-11. doi:10.1186/s13014-022-02068-5
92. Patel AA, Wolfgang JA, Niemierko A, Hong TS, Yock T, Choi NC. Implications of Respiratory Motion as Measured by Four-Dimensional Computed Tomography for Radiation Treatment Planning of Esophageal Cancer. *Int J Radiat Oncol Biol Phys*. 2009;74(1):290-296. doi:10.1016/j.ijrobp.2008.12.060
93. Yaremko BP, Guerrero TM, McAleer MF, et al. Determination of Respiratory Motion for Distal Esophagus Cancer Using Four-Dimensional Computed Tomography. *Int J Radiat Oncol Biol Phys*. 2008;70(1):145-153. doi:10.1016/j.ijrobp.2007.05.031
94. Heijkoop ST, Langerak TR, Quint S, et al. Clinical implementation of an online adaptive plan-of-the-day protocol for nonrigid motion management in locally advanced cervical cancer IMRT. *Int J Radiat Oncol Biol Phys*. 2014;90(3):673-679. doi:10.1016/j.ijrobp.2014.06.046
95. Orditura M, Galizia G, Sforza V, et al. Treatment of gastric cancer. *World J Gastroenterol*. 2014;20(7):1635-1649. doi:10.3748/wjg.v20.i7.1635
96. Mittauer K, Paliwal B, Hill P, et al. A New Era of Image Guidance with Magnetic Resonance-guided Radiation Therapy for Abdominal and Thoracic Malignancies. *Cureus*. 2018;10(4). doi:10.7759/cureus.2422
97. Vestergaard A, Muren LP, Lindberg H, et al. Normal tissue sparing in a phase II trial on daily adaptive plan selection in radiotherapy for urinary bladder cancer. *Acta Oncol (Madr)*. 2014;53(8):997-1004. doi:10.3109/0284186X.2014.928419
98. Lutkenhaus LJ, Visser J, De Jong R, Hulshof MCCM, Bel A. Evaluation of delivered dose for a clinical daily adaptive plan selection strategy for bladder cancer radiotherapy. *Radiother Oncol*. 2015;116:51-56. doi:10.1016/j.radonc.2015.06.003
99. Nováková E, Heijkoop ST, Quint S, et al. What is the optimal number of library plans in ART for locally advanced cervical cancer? *Radiother Oncol*. 2017;125:470-477. doi:10.1016/j.radonc.2017.08.033
100. de Jong R, Lutkenhaus L, van Wieringen N, et al. Plan selection strategy for rectum cancer patients: An interobserver study to assess clinical feasibility. *Radiother Oncol*. 2016;120(2):207-211. doi:10.1016/j.radonc.2016.07.027

101. van Beek S, Betgen A, Buijs M, et al. Pre-clinical experience of an adaptive plan library strategy in radiotherapy of rectal cancer: An inter-observer study. *Phys Imaging Radiat Oncol*. 2018;6:89-93. doi:10.1016/j.phro.2018.06.003
102. Canlas R, McVicar N, Nakano S, Sahota H, Mahajan P, Tyldesley S. Assessment of Adaptive Margins Using a Single Planning Computed Tomography Scan for Bladder Radiotherapy. *J Med Imaging Radiat Sci*. 2016;47(3):227-234. doi:10.1016/j.jmir.2016.05.001
103. Boejen A, Vestergaard A, Hoffmann L, et al. A learning programme qualifying radiation therapists to manage daily online adaptive radiotherapy. *Acta Oncol (Madr)*. 2015;54(9):1697-1701. doi:10.3109/0284186X.2015.1062914
104. Visser J, De Boer P, Crama KF, et al. Dosimetric comparison of library of plans and online MRI-guided radiotherapy of cervical cancer in the presence of intrafraction anatomical changes. *Radiat Oncol*. 2019;14(1):126. doi:10.1186/s13014-019-1322-0
105. Meijer GJ, Van Der Toorn PP, Bal M, Schuring D, Weterings J, De Wildt M. High precision bladder cancer irradiation by integrating a library planning procedure of 6 prospectively generated SIB IMRT plans with image guidance using lipiodol markers. *Radiother Oncol*. 2012;105(2):174-179. doi:10.1016/j.radonc.2012.08.011
106. Magallon-Baro A, Loi M, Milder MTW, et al. Modeling daily changes in organ-at-risk anatomy in a cohort of pancreatic cancer patients. *Radiother Oncol*. 2019;134:127-134. doi:10.1016/j.radonc.2019.01.030
107. Lutkenhaus LJ, de Jong R, Geijssen ED, Visser J, van Wieringen N, Bel A. Potential dosimetric benefit of an adaptive plan selection strategy for short-course radiotherapy in rectal cancer patients. *Radiother Oncol*. 2016;119(3):525-530. doi:10.1016/j.radonc.2016.04.018
108. Webster GJ, Stratford J, Rodgers J, Livsey JE, Macintosh D, Choudhury A. Comparison of adaptive radiotherapy techniques for the treatment of bladder cancer. *Br J Radiol*. 2013;86(1021):20120433-20120433. doi:10.1259/bjr.20120433
109. Ahmad R, Bondar L, Voet P, et al. A margin-of-the-day online adaptive intensity-modulated radiotherapy strategy for cervical cancer provides superior treatment accuracy compared to clinically recommended margins: A dosimetric evaluation. *Acta Oncol (Madr)*. 2013;52(7):1430-1436. doi:10.3109/0284186X.2013.813640
110. Bondar ML, Hoogeman MS, Mens JW, et al. Individualized nonadaptive and online-adaptive intensity-modulated radiotherapy treatment strategies for cervical cancer patients based on pretreatment acquired variable bladder filling computed tomography scans. *Int J Radiat Oncol Biol Phys*. 2012;83(5):1617-1623. doi:10.1016/j.ijrobp.2011.10.011
111. Foroudi F, Wong J, Kron T, et al. Online adaptive radiotherapy for muscle-invasive bladder cancer: Results of a pilot study. *Int J Radiat Oncol Biol Phys*. 2011;81(3):765-771. doi:10.1016/j.ijrobp.2010.06.061
112. Cignoni P, Callieri M, Corsini M, Dellepiane M, Ganovelli F, Ranzuglia G. MeshLab: An open-source mesh processing tool. *6th Eurographics Ital Chapter Conf 2008 - Proc*. 2008:129-136.
113. Sharp G, Fritscher KD, Pekar V, et al. Vision 20/20: Perspectives on automated image segmentation for radiotherapy. *Med Phys*. 2014;41(5):050902. doi:10.1118/1.4871620
114. Ramya R, Saravanan S, Vijayalakshmi J, Kumari K. Differences Between MRI- and CT-Based Delineation of Target Volume and Organs at Risk in High-Dose-Rate Brachytherapy of Cervix. *Indian J Gynecol Oncol*. 2019;17:1-7. doi:10.1007/s40944-019-0310-5
115. O'Neill BDP, Salerno G, Thomas K, Tait DM, Brown G. MR vs CT imaging: Low rectal cancer tumour delineation for three-dimensional conformal radiotherapy. *Br J Radiol*. 2009;82(978):509-513. doi:10.1259/bjr/60198873
116. Li J, Denniston KA, Hussain SM, Gan H, Lin C. Comparison of CT and MRI-Based Gross Tumor Volume and Organ at Risk Delineation for Pancreatic Cancer Patients Undergoing Neoadjuvant Stereotactic Body Radiation Therapy. *Int J Radiat Oncol*. 2014;90(1):S356. doi:10.1016/j.ijrobp.2014.05.1158
117. Chai X, Van Herk M, Van De Kamer JB, et al. Finite element based bladder modeling for image-guided radiotherapy of bladder cancer. *Med Phys*. 2011;38(1):142-150. doi:10.1118/1.3523624
118. van de Schoot AJAJ, de Boer P, Visser J, Stalpers LJA, Rasch CRN, Bel A. Dosimetric advantages of a clinical daily adaptive plan selection strategy compared with a non-adaptive strategy in cervical cancer radiation therapy. *Acta Oncol (Madr)*. 2017;56(5):667-674. doi:10.1080/0284186X.2017.1287949
119. Vestergaard A, Muren LP, Søndergaard J, Elstrøm UV, Høyer M, Petersen JB. Adaptive plan selection vs. re-optimisation in radiotherapy for bladder cancer: A dose accumulation comparison. *Radiother Oncol*. 2013;109:457-462. doi:10.1016/j.radonc.2013.08.045

120. Lowther NJ, Marsh SH, Louwe RJW. Dose accumulation to assess the validity of treatment plans with reduced margins in radiotherapy of head and neck cancer. *Phys Imaging Radiat Oncol.* 2020;14:53-60. doi:10.1016/j.phro.2020.05.004
121. Jabbour SK, Hashem SA, Bosch W, et al. Upper abdominal normal organ contouring guidelines and atlas: A Radiation Therapy Oncology Group consensus. *Pract Radiat Oncol.* 2014;4(2):82-89. doi:10.1016/j.prro.2013.06.004
122. Chadha AS, Liu G, Chen HC, et al. Does Unintentional Splenic Radiation Predict Outcomes After Pancreatic Cancer Radiation Therapy? *Int J Radiat Oncol Biol Phys.* 2017;97(2):323-332. doi:10.1016/j.ijrobp.2016.10.046
123. Van Den Bogaard VAB, Ta BDP, Van Der Schaaf A, et al. Validation and modification of a prediction model for acute cardiac events in patients with breast cancer treated with radiotherapy based on three-dimensional dose distributions to cardiac substructures. *J Clin Oncol.* 2017;35(11):1171. doi:10.1200/JCO.2016.69.8480
124. Darby SC, Ewertz M, McGale P, et al. Risk of Ischemic Heart Disease in Women after Radiotherapy for Breast Cancer. *N Engl J Med.* 2013;368(11):987-998. doi:10.1056/nejmoa1209825
125. So TH, Chan SK, Chan WL, et al. Lymphopenia and Radiation Dose to Circulating Lymphocytes With Neoadjuvant Chemoradiation in Esophageal Squamous Cell Carcinoma. *Adv Radiat Oncol.* 2020;5(5):880-888. doi:10.1016/j.adro.2020.03.021
126. Saito T, Toya R, Yoshida N, et al. Spleen dose-volume parameters as a predictor of treatment-related lymphopenia during definitive chemoradiotherapy for esophageal cancer. *In Vivo (Brooklyn).* 2018;32(6):1519-1525. doi:10.21873/invivo.11409
127. Liu J, Liu C, Yue J. Radiotherapy and the gut microbiome: facts and fiction. *Radiat Oncol.* 2021;16:1-15. doi:10.1186/s13014-020-01735-9
128. Tonneau M, Elkrief A, Pasquier D, et al. The role of the gut microbiome on radiation therapy efficacy and gastrointestinal complications: A systematic review. *Radiother Oncol.* 2021;156:1-9. doi:10.1016/j.radonc.2020.10.033
129. Wang X, Zhao Z, Wang P, Geng X, Zhu L, Li M. Low Lymphocyte Count Is Associated With Radiotherapy Parameters and Affects the Outcomes of Esophageal Squamous Cell Carcinoma Patients. *Front Oncol.* 2020;10:997. doi:10.3389/fonc.2020.00997
130. Tang C, Liao Z, Gomez D, et al. Lymphopenia association with gross tumor volume and lung V5 and its effects on non-small cell lung cancer patient outcomes. *Int J Radiat Oncol Biol Phys.* 2014;89(5):1084-1091. doi:10.1016/j.ijrobp.2014.04.025
131. Vestergaard A, Kallehauge JF, Petersen JBB, Høyer M, Søndergaard J, Muren LP. An adaptive radiotherapy planning strategy for bladder cancer using deformation vector fields. *Radiother Oncol.* 2014;112(3):371-375. doi:10.1016/j.radonc.2014.07.012
132. Ren J, Gong G, Yao X, Yin Y. Dosimetric comparison of dose accumulation between rigid registration and deformation registration in intensity-modulated radiation therapy for large volume non-small cell lung cancer. *Transl Cancer Res.* 2019;8(8):2878. doi:10.21037/tcr.2019.11.15
133. Nix M, Gregory S, Aldred M, et al. Dose summation and image registration strategies for radiobiologically and anatomically corrected dose accumulation in pelvic re-irradiation. *Acta Oncol (Madr).* 2022;61(1):64-72. doi:10.1080/0284186X.2021.1982145
134. Dees-Ribbers HM, Betgen A, Pos FJ, Witteveen T, Remeijer P, Van Herk M. Inter- and intra-fractional bladder motion during radiotherapy for bladder cancer: A comparison of full and empty bladders. *Radiother Oncol.* 2014;113(2):254-259. doi:10.1016/j.radonc.2014.08.019
135. Tan IZ, Tocco B, Court S, et al. PO-1287 Target Deformation and Intrafraction Motion Errors in LRCTV for MR-guided Cervix Cancer Radiotherapy. *Radiother Oncol.* 2021;161:S1061-S1062. doi:10.1016/s0167-8140(21)07738-0
136. Nijkamp J, Swellengrebel M, Hollmann B, et al. Repeat CT assessed CTV variation and PTV margins for short- and long-course pre-operative RT of rectal cancer. *Radiother Oncol.* 2012;102(3):399-405. doi:10.1016/j.radonc.2011.11.011
137. Thörnqvist S, Hysing LB, Tuomikoski L, et al. Adaptive radiotherapy strategies for pelvic tumors - a systematic review of clinical implementations. *Acta Oncol (Madr).* 2016;55(8):973-958. doi:10.3109/0284186X.2016.1156738
138. Barber J, Yuen J, Jameson M, et al. Deforming to Best Practice: Key considerations for deformable image registration in radiotherapy. *J Med Radiat Sci.* 2020;67(4):318-332. doi:10.1002/jmrs.417

139. Cai B, Laugeman E, Mazur TR, et al. Characterization of a prototype rapid kilovoltage x-ray image guidance system designed for a ring shape radiation therapy unit. *Med Phys.* 2019;46(3):1355-1370. doi:10.1002/mp.13396
140. Mao W, Liu C, Gardner SJ, et al. Evaluation and clinical application of a commercially available iterative reconstruction algorithm for CBCT-based IGRT. *Technol Cancer Res Treat.* 2019;18. doi:10.1177/1533033818823054
141. Lim R, Penoncello GP, Hobbis D, Harrington DP, Rong Y. Technical note: Characterization of novel iterative reconstructed cone beam CT images for dose tracking and adaptive radiotherapy on L-shape linacs. *Med Phys.* 2022;49(12):7715-7732. doi:10.1002/mp.15943
142. Varian's Iterative Cone-Beam Computed Tomography (iCBCT): Clear Soft Tissue Visualization for Precision Radiotherapy. <https://www.varian.com/varians-iterative-cone-beam-computed-tomography-icbct-clear>. Published 2020. Accessed May 24, 2023.
143. Bondar L, Hoogeman M, Mens JW, et al. Toward an individualized target motion management for IMRT of cervical cancer based on model-predicted cervix-uterus shape and position. *Radiother Oncol.* 2011;99(2):240-245. doi:10.1016/j.radonc.2011.03.013
144. Lotz HT, Remeijer P, Van Herk M, et al. A model to predict bladder shapes from changes in bladder and rectal filling. *Med Phys.* 2004;31(6):1415-1423. doi:10.1118/1.1738961
145. Chai X, Van Herk M, Betgen A, Hulshof M, Bel A. Automatic bladder segmentation on CBCT for multiple plan ART of bladder cancer using a patient-specific bladder model. *Phys Med Biol.* 2012;57(12):3945. doi:10.1088/0031-9155/57/12/3945
146. Bleeker M, Lie S, Bel A, Sonke J-J, Hulshof M, van der Horst A. Quantification of Intra- and Interfractional Target Motion and Deformation in Gastric Cancer Radiotherapy [abstract]. *Med Phys.* 2020;47(6).
147. Deng JY, Liang H. Clinical significance of lymph node metastasis in gastric cancer. *World J Gastroenterol.* 2014;20(14):3967. doi:10.3748/wjg.v20.i14.3967
148. Wang H, Song C, Zhao X, Deng W, Shen W. The role of involved field irradiation versus elective nodal irradiation in definitive radiotherapy or chemoradiotherapy for esophageal cancer- a systematic review and meta-analysis. *Front Oncol.* 2022;12:1034656. doi:10.3389/fonc.2022.1034656
149. Seppenwoolde Y, Stock M, Buschmann M, et al. Impact of organ shape variations on margin concepts for cervix cancer ART. *Radiother Oncol.* 2016;120(3):525-531. doi:10.1016/j.radonc.2016.08.004
150. Cardenas CE, Yang J, Anderson BM, Court LE, Brock KB. Advances in Auto-Segmentation. *Semin Radiat Oncol.* 2019;29(3):185-197. doi:10.1016/j.semradonc.2019.02.001
151. Zou J, Gao B, Song Y, Qin J. A review of deep learning-based deformable medical image registration. *Front Oncol.* 2022;12:1047215. doi:10.3389/fonc.2022.1047215
152. Wang C, Zhu X, Hong JC, Zheng D. Artificial Intelligence in Radiotherapy Treatment Planning: Present and Future. *Technol Cancer Res Treat.* 2019;18:1-11. doi:10.1177/1533033819873922
153. den Boer D, den Hartogh MD, Kotte ANTJ, et al. Comparison of Library of Plans with two daily adaptive strategies for whole bladder radiotherapy. *Phys Imaging Radiat Oncol.* 2021;20:82-87. doi:10.1016/j.phro.2021.11.002
154. Byrne M, Archibald-Heeren B, Hu Y, et al. Varian ethos online adaptive radiotherapy for prostate cancer: Early results of contouring accuracy, treatment plan quality, and treatment time. *J Appl Clin Med Phys.* 2022;23(1):e13479. doi:10.1002/acm2.13479
155. Sibolt P, Andersson LM, Calmels L, et al. Clinical implementation of artificial intelligence-driven cone-beam computed tomography-guided online adaptive radiotherapy in the pelvic region. *Phys Imaging Radiat Oncol.* 2021;17:1-7. doi:10.1016/j.phro.2020.12.004
156. Ward A, Martinou M, Kidane G, Graham S. Daily Adaptive Radiotherapy Using the Varian ETHOS System to Improve Dose Distribution During Treatment to the Upper Abdomen. *Clin Oncol.* 2022;34:e10. doi:10.1016/j.clon.2022.01.036
157. Rusanov B, Hassan GM, Reynolds M, et al. Deep learning methods for enhancing cone-beam CT image quality toward adaptive radiation therapy: A systematic review. *Med Phys.* 2022;49(9):6019-6054. doi:10.1002/mp.15840
158. Washington University School of Medicine. MR-guided Pre-operative RT in Gastric Cancer. ClinicalTrials.gov identifier: NCT04162665. <https://clinicaltrials.gov/ct2/show/NCT04162665>. Published 2020. Accessed June 1, 2023.
159. Kim H. Personal communications. Washington University School of medicine. May 10, 2023.

## Summary

Preoperative gastric cancer radiotherapy is a novel treatment approach, and many challenges that may be encountered during this treatment are still largely unexplored. Radiotherapy aims to precisely irradiate the target while sparing the surrounding healthy tissue as much as possible to limit potential adverse side effects.

Typically, a single treatment plan is created prior to radiotherapy delivery based on a CT scan that captures a static snapshot of the anatomy. According to this single treatment plan, the target is irradiated in daily fractions over several weeks. The target for preoperative gastric cancer radiotherapy comprises not only the tumor, but also the entire stomach and regional lymph nodes, and thus constitutes a substantial volume. Accurately irradiating the target proves challenging due to inherent motion and deformation of the stomach caused by respiration, peristalsis, and changes in filling. To ensure effective target coverage during radiotherapy, a safety margin is added to the target volume to account for (geometrical) uncertainties. However, an additional challenge during radiotherapy is induced by the proximity of the stomach to vital organs like the liver, pancreas, kidneys, spleen, and bowels. It is important to minimize radiation exposure of these organs (so-called organs at risk, OARs), while ensuring adequate irradiation of the target.

Prior to daily irradiations, daily image-guidance using cone-beam CT (CBCT) is typically employed for patient alignment. While daily alignment accounts for changes in target position, it does not account for variations in target shape and size. In the presence of substantial shape and size changes, such as experienced by the stomach, large safety margins are necessary to adequately irradiate the target, resulting in increased dose to surrounding healthy tissues. Accordingly, substantial day-to-day variations in stomach shape and size may render a single treatment plan suboptimal.

A promising alternative is to use an adaptive radiotherapy approach that accounts for day-to-day shape and size changes. With adaptive radiotherapy, imaging is used to adapt the treatment plan to better match the daily anatomy as visible on imaging. One straightforward adaptive strategy is a library of plans (LoP), where multiple treatment plans covering various anatomical variations are created, and each day the most appropriate plan is selected based on imaging.

The primary objective of this thesis was to explore a CBCT-guided adaptive strategy for preoperative gastric cancer radiotherapy to account for the stomach's mobile and deformable nature, thereby ensuring accurate and effective delivery of radiotherapy. To achieve this, we pursued the following objectives: 1) explore the need for an adaptive strategy by quantifying

stomach motions and deformations using fiducial markers, 2) assess the feasibility of a LoP strategy, and 3) develop and evaluate a LoP to determine its potential benefit.

### ***The need for an adaptive strategy***

The need for an adaptive strategy depends upon the day-to-day (i.e., interfractional) anatomical changes the stomach experiences. Fiducial markers were implanted in the stomach to improve target localization on CBCTs (**Chapter 2**). Our study demonstrated the technical feasibility of fiducial marker implantation in the stomach. Given that these markers were well visible on both CT and CBCT and positionally stable, they provide a potential benefit for image-guided radiotherapy.

The implanted fiducial markers also enabled the quantification of interfractional anatomical changes (**Chapter 3**). Substantial interfractional marker displacements were observed and quantified (up to >20 mm), demonstrating the deformable nature of the stomach and highlighting the need for an adaptive strategy.

### ***Feasibility of a library of plans***

The feasibility of a LoP depends upon the target's visibility on the acquired pre-treatment CBCTs. In **Chapter 4**, we successfully demonstrated the feasibility of utilizing a LoP based on these CBCTs. Through extensive observer evaluations, we confirmed that a range of observers were able to identify the target and consistently select the most appropriate treatment plan from the library. Moreover, as a variation of plans were selected for each patient, the potential benefit of a LoP was demonstrated.

### ***Development and evaluation of a library of plans***

With the necessity and feasibility of a LoP strategy established, the focus shifted towards developing an effective LoP. The performance of a LoP depends upon the accuracy of stomach shape predictions for various stomach volumes. A population-based and a personalized strategy to predict stomach shape were compared (**Chapter 5**). The personalized approach yielded multiple stomach shapes based on observed anatomical deformation within a subject (i.e., patient or healthy volunteer), whereas the population-based approach utilized general patterns in anatomical deformations in a group of healthy volunteers to predict shape changes. The population-based model outperformed the personalized model in shape predictions. Our study demonstrated that stomach shape could be reasonably predicted from stomach volume using the population-based deformation model, achieving a median Dice similarity coefficient of 0.87 for patient data.

In **Chapter 6**, a dosimetric comparison was conducted between the LoP created using the population-based gastric deformation model and a single-plan approach (comparable to the

current clinical practice). Appropriate safety margins were calculated for both approaches to ensure adequate target coverage, facilitating a fair comparison of the dose to OARs between both strategies. The LoP approach showcased its potential benefits by reducing the average irradiated volume throughout treatment and reducing the dose to OARs, while maintaining equal target coverage. These benefits underscore the significance of implementing a LoP strategy to adapt to the sizable and unavoidable interfractional anatomical changes experienced by gastric cancer patients during radiotherapy.

### **Conclusion**

This research has demonstrated the benefit of an adaptive strategy for preoperative gastric cancer radiotherapy. The stomach's highly mobile and deformable nature renders a single treatment plan inadequate. Through the successful development of a CBCT-guided LoP approach, we were able to highlight its potential benefits. Overall, this thesis significantly contributes to understanding the challenges associated with gastric cancer radiotherapy and offers a viable solution through the application of adaptive strategies, particularly the LoP approach. Moving forward, further research and clinical validation are crucial to establish the efficacy, feasibility, and potential advantages of daily online segmentation and replanning strategies, with the ultimate goal of improving treatment outcomes and quality of life for patients with gastric cancer.





## Samenvatting

Preoperatieve radiotherapie voor maagkanker is een nieuwe behandelplanpak, en veel van de uitdagingen die kunnen optreden tijdens deze behandeling zijn nog grotendeels onverkend. Radiotherapie heeft tot doel het doelgebied nauwkeurig te bestralen en tegelijkertijd het omringende gezonde weefsel zoveel mogelijk te vermijden om mogelijke nadelige bijwerkingen te beperken.

Normaal gesproken wordt voorafgaand aan de bestraling een enkel behandelplan opgesteld op basis van een CT-scan die een statisch beeld geeft van de anatomie. Het doelgebied wordt vervolgens in dagelijks fracties bestraald gedurende meerdere weken volgens dit ene vastgestelde behandelplan. Het doelgebied voor preoperatieve maagkanker bestraling omvat niet alleen de tumor, maar ook de hele maag en regionale lymfeklieren, en vormt dus een aanzienlijk volume. Het nauwkeurig bestralen van het doelgebied is een uitdaging vanwege de inherente beweging en vervorming van de maag, welke worden veroorzaakt door ademhaling, peristaltiek en veranderingen in vulling. Om tijdens de radiotherapie een effectieve dekking van het doelgebied te garanderen, wordt daarom een veiligheidsmarge toegevoegd aan het doelgebied om zo rekening te houden met (geometrische) onzekerheden. Daarnaast is er nog een extra uitdaging, welke wordt veroorzaakt door de nabijheid van de maag tot vitale organen zoals de lever, alvleesklier, nieren, milt en darmen. Het is belangrijk dat stralings-blootstelling van deze organen (zogenaamde risico-organen) geminimaliseerd wordt, terwijl een adequate bestraling van het doelgebied wordt gewaarborgd.

Voorafgaand aan de dagelijkse bestralingen wordt de patiënt doorgaans met behulp van cone-beam CT (CBCT) gepositioneerd. Hoewel dagelijkse positionering rekening houdt met veranderingen in de positie van het doelgebied, houdt het geen rekening met variaties in de vorm en grootte van het doelgebied. Bij aanzienlijke vorm- en grootteveranderingen, zoals bij de maag, zijn grote veiligheidsmarges nodig om te garanderen dat het doelgebied voldoende bestraald wordt. Dit resulteert echter in een verhoogde dosis voor het omliggende gezonde weefsel. Daarom is de huidige procedure op basis van een enkel behandelplan mogelijk minder geschikt.

Een veelbelovend alternatief is het gebruik van adaptieve radiotherapie, waarbij rekening wordt gehouden met dagelijkse vorm- en grootteveranderingen. Met adaptieve radiotherapie wordt beeldvorming gebruikt om het behandelplan aan te passen aan de dagelijkse anatomie zoals zichtbaar op die beeldvorming. Een eenvoudige adaptieve radiotherapie strategie is een bibliotheek van plannen (library of plans; LoP). Bij een LoP worden meerdere behandelplannen gemaakt die verschillende anatomische variaties omvatten, en elke dag wordt het meest geschikte behandelplan geselecteerd.

Het primaire doel van dit proefschrift was het onderzoeken van een CBCT-geleide adaptieve strategie voor preoperatieve radiotherapie voor maagkanker. Met deze methodiek kan rekening worden gehouden met de beweeglijke en vervormbare aard van de maag, en zo mogelijk een nauwkeurigere en effectievere bestraling worden gewaarborgd. Om dit te bereiken, hebben we de volgende doelstellingen nagestreefd: 1) het onderzoeken van de behoefte aan een adaptieve strategie door maagbewegingen en -vervormingen te kwantificeren met behulp van markers, 2) het beoordelen van de haalbaarheid van een LoP-strategie, en 3) het ontwikkelen van een LoP en het evalueren ervan om de potentiële voordelen ervan te bepalen.

### ***De behoefte aan een adaptieve strategie***

De behoefte aan een adaptieve strategie hangt af van de dagelijkse (d.w.z. interfractionele) anatomische veranderingen die de maag ondergaat. Markers werden geïmplanteed om het lokaliseren van het doelgebied op CBCT's te verbeteren (**Hoofdstuk 2**). Onze studie toonde de technische haalbaarheid aan van het implanteren van markers in de maag. Aangezien deze markers goed zichtbaar waren op zowel CT als CBCT en hun positie stabiel was, bieden ze een potentieel voordeel voor beeldgestuurde radiotherapie.

De geïmplanteerde markers maakten ook de kwantificering van interfractionele anatomische veranderingen mogelijk (**Hoofdstuk 3**). Er werden aanzienlijke verplaatsingen van de markers tussen bestralingsdagen waargenomen en gekwantificeerd (>20 mm), wat de vervormbare aard van de maag liet zien en de noodzaak van een adaptieve strategie benadrukte.

### ***Haalbaarheid van een 'library of plans'***

De haalbaarheid van een LoP hangt af van de zichtbaarheid van het doelgebied op de dagelijkse CBCT's, welke worden verkregen voorafgaand aan de dagelijkse bestraling. In **Hoofdstuk 4** hebben we succesvol de haalbaarheid aangetoond van het gebruik van een LoP op basis van deze CBCT's. Via uitgebreide beoordelingen door zowel artsen, laboranten en fysici hebben we bevestigd dat een breed scala aan zorgverleners in staat is het doelgebied te identificeren en consequent het meest geschikte behandelplan uit de bibliotheek te selecteren. Aangezien voor elke patiënt een variatie aan plannen (d.w.z., doelvolumes) werd geselecteerd voor de verschillende bestralingsdagen, werd het potentiële voordeel van een LoP aangetoond.

### ***Ontwikkeling en evaluatie van een 'library of plans'***

Met de vastgestelde behoefte aan en haalbaarheid van een LoP-strategie verschoof de focus naar de ontwikkeling van een effectieve LoP. De prestaties van een LoP hangen af van de nauwkeurigheid van voorspellingen van de maagvorm voor verschillende maagvolumes. Een populatie-gebaseerde en een gepersonaliseerde strategie voor het voorspellen van de maagvorm werden ontwikkeld en met elkaar vergeleken (**Hoofdstuk 5**). De gepersonaliseerde aanpak leverde meerdere maagvormen op die gebaseerd waren op waargenomen anatomische

vervormingen binnen een subject (d.w.z. patiënt of gezonde vrijwilliger), terwijl de populatie-gebaseerde aanpak algemene patronen in anatomische vervormingen in een groep gezonde vrijwilligers gebruikte om vormveranderingen te voorspellen. Het populatie-gebaseerde model presteerde beter in vormvoorspellingen. Onze studie toonde aan dat de maagvorm redelijk goed voorspeld kan worden aan de hand van het maagvolume met behulp van het op populatie-gebaseerde vervormingsmodel. Hierbij werd een gemiddelde Dice-coëfficiënt van 0.87 verkregen op basis van scans van patiënten, wat de mate van overeenkomst in vorm aangeeft (waarbij 0 geen overeenkomst betekent en 1 identieke vorm).

In **Hoofdstuk 6** werd vervolgens een dosimetrische vergelijking gemaakt tussen de LoP die werd gecreëerd met behulp van het populatie-gebaseerd model voor maagvervorming en één enkel behandelplan (vergelijkbaar met de huidige klinische praktijk). Voor beide benaderingen werden veiligheidsmarges berekend om een adequate dekking van het doelgebied te waarborgen. Dit zorgt voor een eerlijke vergelijking van de dosis aan risico-organen tussen beide strategieën. De LoP-aanpak toonde zijn potentiële voordelen omdat het gemiddelde bestraalde volume gedurende de behandeling verlaagd werd en daarmee de dosis aan risico-organen, terwijl een gelijke dekking van het doelgebied behouden werd. Deze voordelen benadrukken het belang van het implementeren van een LoP-strategie, omdat we met deze strategie in staat zijn om de bestraling aan te passen aan de aanzienlijke en onvermijdelijke interfractionele anatomische veranderingen die optreden bij patiënten met maagkanker tijdens radiotherapie.

### **Conclusie**

Dit onderzoek toont het voordeel van een adaptieve strategie voor preoperatieve radiotherapie voor maagkanker aan. De zeer beweeglijke en vervormbare aard van de maag maakt een enkel behandelplan ontoereikend. Door de succesvolle ontwikkeling van een CBCT-geleide LoP-aanpak hebben we de potentiële voordelen van een adaptieve strategie aangetoond. Dit proefschrift levert een belangrijke bijdrage aan het begrijpen van de uitdagingen die gepaard gaan met radiotherapie voor maagkanker en biedt een haalbare oplossing door het toepassen van adaptieve strategieën, met name de LoP-aanpak. Verder onderzoek en klinische validatie zijn echter essentieel om de werkzaamheid, haalbaarheid en mogelijke voordelen van dagelijkse online her-segmentatie en her-planning vast te stellen. Hierbij zou dagelijks een nieuw behandelplan gemaakt worden op basis van de anatomie van die dag, in tegenstelling tot de LoP-aanpak waar dagelijks gekozen kan worden uit meerdere plannen. Dit alles met als uiteindelijk doel het verbeteren van de behandeling en kwaliteit van leven van patiënten met maagkanker.



## Supplemental Materials

### Supplemental Materials to Chapter 2

#### ***Supplemental Materials S2A: Chemoradiotherapy course***

For all included patients, chemoradiotherapy (CRT) consisted of 45 Gy in 25 fractions, combined with weekly paclitaxel and carboplatin. Image-guided radiotherapy (IGRT) treatment planning was based on a reference computed tomography (CT) scan (resolution  $0.98 \times 0.98 \times 2.5 \text{ mm}^3$ ). For all patients except one, the reference scan was acquired after implantation (0–5 days, median 1 day); for the one patient, the reference scan was acquired two days before implantation. During IGRT delivery, daily cone-beam CTs (CBCT;  $1.00 \times 1.00 \times 1.00$  or  $0.91 \times 0.91 \times 1.00 \text{ mm}^3$ ) were acquired in the treatment position at the linear accelerator for position verification, as is typically done in our institute. Such CBCTs are low-quality 3D images that enable positioning on bony anatomy and, when visible, verification of target coverage using the fiducial markers. The CBCT acquisition time was approximately 4 minutes, thereby including multiple respiratory cycles and potential peristalsis. Furthermore, within this feasibility study, repeat CTs were acquired in the first, third and fifth week of radiotherapy.

For patients 1–5, CTs were acquired with the GE LightSpeed RT16 CT and CBCTs were acquired with the Elekta Infinity linear accelerator. For patients 6–14, CTs were acquired with the GE Discovery CT590 RT CT and CBCTs with the Varian TrueBeam linear accelerator.

### Supplemental Materials S2B: Marker visibility on respiratory phase scans

4DCTs and 4DCBCTs consist of a series of scans that each represent a different respiratory phase. Fiducial markers that are visible on respiratory phase scans can enable target respiratory motion assessments, which may aid in the accurate delivery of IGRT. Thus, marker visibility was also evaluated for such respiratory phase scans.

For CT and CBCT, 10 respiratory phase scans were reconstructed. As the same data is used to reconstruct the average scan and the 10 respiratory phase scans, image quality of the individual respiratory phase scans is lower than that of the average scans. For each marker, marker visibility was assessed on each end-inhale and end-exhale scan (Figure S2B.1). For respiratory phase scans, a marker was only regarded visible when it was visible on both end-exhale and end-inhale scans.

For CT scans, whereas all markers had good visibility on average scans, 5 gold markers were moderately visible on respiratory phase scans. Furthermore, for CBCT scans, there were 5 and 10 poorly visible markers on average and phase scans, respectively.

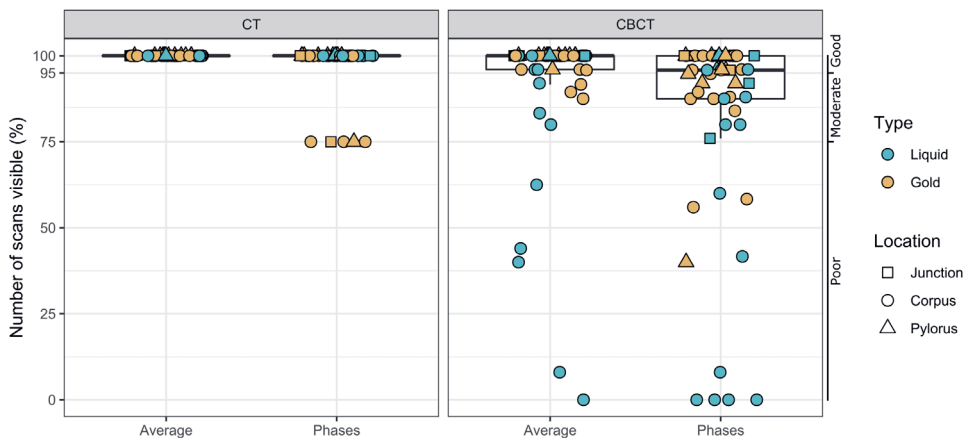


Figure S2B.1: Boxplots of the visibility of successfully placed markers ( $N=59$ ) on CT and CBCT average and phase scans, for liquid (blue) and gold markers (orange). A marker was regarded visible on a phase scan, when present on both end-inhale and end-exhale scans. Symbols indicate marker location: square = gastroesophageal junction (i.e., junction), circle = corpus, triangle = pylorus). Boxplots: box=interquartile range (IQR), whiskers=lowest and highest data point within  $1.5 \times \text{IQR}$ .

## Supplemental Materials to Chapter 3

### Supplemental Materials S3A: Patient and marker characteristics

Table S3A.1: Patient and marker characteristics

No.	Age (years)	Sex	Tumor location	Markers visible ≥8 EE CBCT scans
1	62	M	Cardia	4
2	38	M	Antrum	3
3	48	M	Corpus and pylorus	3
4	70	M	Corpus and antrum	4
5	65	M	Antrum	6
6	71	M	Antrum and pylorus	4*
7	58	F	Corpus	4
8	48	M	Cardia	4
9	45	M	Cardia	3
10	56	F	Antrum	4
11	64	M	Cardia and distal esophagus	5
12	69	M	Corpus	5
13	61	M	Cardia	2
14	60	M	Antrum and pylorus	3
Total	Median (range) 61 (38-71)			54 markers

\*For patient 6, only three of these four markers were visible on ≥8 CBCT EI scans

### Supplemental Materials S3B: Linear mixed-effect model

We aimed to investigate whether the 3D respiratory amplitude is different for different regions of the stomach. A linear mixed-effect analysis was performed of the relationship between 3D respiratory amplitude (*Amplitude*; the response variable; peak-to-peak vector length) and the marker coordinates on planning CT in superior-inferior (*SI*), anterior-posterior (*AP*) and left-right (*LR*) direction as fixed effects. To obtain a common coordinate system between patients, the origin was set at the top of the left diaphragm dome. Fractions nested within patients (*patients/Fx*) was selected as a random intercept to account for dependencies within this data. This means that respiratory amplitudes may differ between patients, but also within a patient between fractions. Analyses were performed in R with the *nlme* package.

In order to identify the model that best describes the data, multiple candidate models were created consisting of all possible additive combinations of fixed effects, ranging from the null model (without any fixed effects) to the full model (including all fixed effects; Supplemental Table S3B.1). All models were compared using the corrected Akaike Information Criterion (AICc). The best fitting model is the one with the lower AICc score, and thus explains the largest amount of variation using the fewest possible independent variables. As displayed in Table

S3B.1, the best fitting model was the model with all three marker coordinates as fixed effects (i.e., SI, AP and LR).

Following model selection, the best fitting model was evaluated. The marginal  $R^2$  was 0.081 (i.e., variance explained by the fixed effect) and conditional  $R^2$  was 0.74 (i.e., proportion of variance explained by both fixed and random effects). The model resulted in the following formula:  $3D \text{ amplitude} = 12.057 + 0.062 \times SI + 0.041 \times AP - 0.027 \times LR$ .

*Table S3B.1: Candidate models with all possible additive combinations of fixed effects, ranging from the null model to the full model. The corrected Akaike Information Criterion (AICc) for each model and the model rank based on the AICc are included. Fixed effects are the marker coordinates in superior-inferior (SI), anterior-posterior (AP) and left-right (LR) direction. Random effects are the fractions nested within patients (1|Patient/Fx).*

Model	Formula	AICc	Model rank
0	Amplitude $\sim 1 + (1 Patient/Fx)$	6035.52	8
1	Amplitude $\sim SI + (1 Patient/Fx)$	6023.03	6
2	Amplitude $\sim AP + (1 Patient/Fx)$	6031.22	7
3	Amplitude $\sim LR + (1 Patient/Fx)$	6021.30	5
4	Amplitude $\sim SI + AP + (1 Patient/Fx)$	5993.43	3
5	Amplitude $\sim SI + LR + (1 Patient/Fx)$	5974.76	2
6	Amplitude $\sim AP + LR + (1 Patient/Fx)$	6018.90	4
7	Amplitude $\sim SI + AP + LR + (1 Patient/Fx)$	5915.28	1

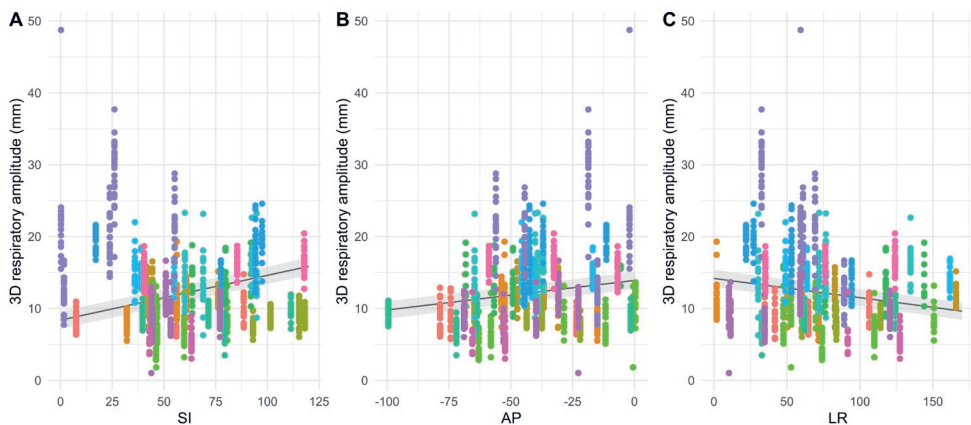


*Figure S3B.1: 3D respiratory amplitude (peak-to-peak vector length) for marker coordinates in superior-inferior (SI; A), anterior-posterior (AP; B) and left-right (LR; C) direction; the origin of the coordinate system was the left diaphragm dome, and S, A and R are positive. Data of each patient is reflected in a color. Each patient has multiple markers and is thus visible on multiple SI, AP and LR coordinates. Every marker has 20–25 respiratory amplitude measurements (i.e., CBCTs/fractions). The line represents the mixed-effect model with confidence interval represented by the grey area.*



**Supplemental Materials S3C: Time trends in marker interfraction displacement**

*Table S3C.1: Significant linear regression slopes in marker interfraction displacement with respect to its position on planning CT as function of fraction number. The slopes were assessed in superior-inferior (SI), anterior-posterior (AP), and left-right (LR) direction. For the analyses, the Bonferroni-Holm correction for multiple testing was applied with a significance level  $\alpha=0.05$ .*

Patient	Marker	Direction	Linear regression			
			Intercept (mm)	Slope (mm/Fx)	p-value slope	R <sup>2</sup>
1	1	AP	3.71	-0.31	0.00009	0.51
2	1	AP	-1.12	0.17	0.00000	0.63
4	1	AP	-1.27	0.23	0.00005	0.52
4	2	LR	-5.24	0.52	0.00007	0.51
4	3	AP	1.99	-1.46	0.00000	0.85
4	3	SI	3.69	-1.15	0.00000	0.65
4	4	AP	0.88	-0.65	0.00000	0.84
6	2	AP	5.84	-0.88	0.00014	0.56
6	3	AP	9.20	-1.10	0.00000	0.67
6	3	SI	13.96	-0.64	0.00013	0.48
6	4	AP	7.38	-1.07	0.00002	0.64
6	4	SI	14.82	-0.96	0.00019	0.55
7	1	SI	-3.21	-0.25	0.00000	0.67
7	3	SI	-0.04	-0.85	0.00000	0.77
7	3	LR	2.68	-0.52	0.00000	0.63
7	4	SI	2.07	-0.87	0.00000	0.77
7	4	AP	-2.95	-0.24	0.00024	0.45
7	5	SI	0.02	-0.88	0.00000	0.78
7	5	AP	-7.80	-0.32	0.00008	0.51
8	5	AP	3.05	-0.24	0.00009	0.51
10	1	SI	1.41	-0.28	0.00032	0.44
10	2	AP	-0.50	0.39	0.00012	0.50
10	2	SI	7.09	-0.56	0.00026	0.46
10	5	SI	10.91	-0.69	0.00008	0.50
11	1	LR	3.69	-0.33	0.00001	0.58
11	1	AP	2.32	-0.17	0.00006	0.51
11	2	SI	-1.19	0.38	0.00005	0.57
13	1	AP	5.34	-0.72	0.00001	0.79

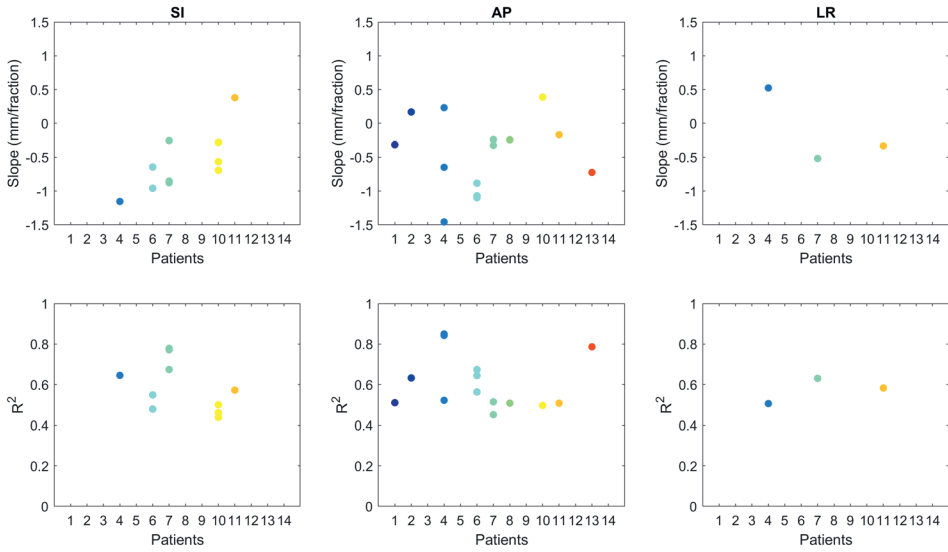


Figure S3C.1: Significant linear regression slopes (top row) and  $R^2$  (bottom row) of marker interfraction displacement with respect to its position on planning CT as a function of fraction number. The slopes were assessed in superior-inferior (SI), anterior-posterior (AP), and left-right (LR) direction.

**Supplemental Materials S3D: Time trends in marker-pair distance**

Table S3D.1: Significant linear regression slopes of the difference in marker-pair distance with respect to planning CT as function of fraction number. For the analyses, the Bonferroni-Holm correction for multiple testing was applied with a significance level  $\alpha=0.05$ .

Patient	Marker M1	Marker M2	Linear regression			
			Intercept (mm)	Slope (mm/Fx)	p-value slope	R <sup>2</sup>
4	1	2	-0.37	-0.73	0.00000	0.93
4	1	3	4.85	-1.42	0.00000	0.85
4	2	3	4.79	-1.18	0.00000	0.93
4	2	4	3.14	-0.41	0.00000	0.65
4	3	4	-0.41	-0.56	0.00000	0.63
6	2	4	0.30	-0.62	0.00008	0.61
6	3	4	-2.16	-0.33	0.00000	0.78
7	1	3	-1.83	-0.36	0.00000	0.76
7	1	4	1.28	-0.54	0.00000	0.86
7	1	5	3.01	-0.77	0.00000	0.76
7	3	4	-4.40	0.35	0.00008	0.50
9	1	4	-1.07	0.32	0.00052	0.41
11	1	3	-3.25	0.59	0.00006	0.51
11	1	4	-7.57	0.30	0.00000	0.64
11	2	4	-5.82	-0.35	0.00000	0.69
12	1	3	3.42	-0.19	0.00053	0.44
12	1	4	-0.24	-0.33	0.00034	0.48

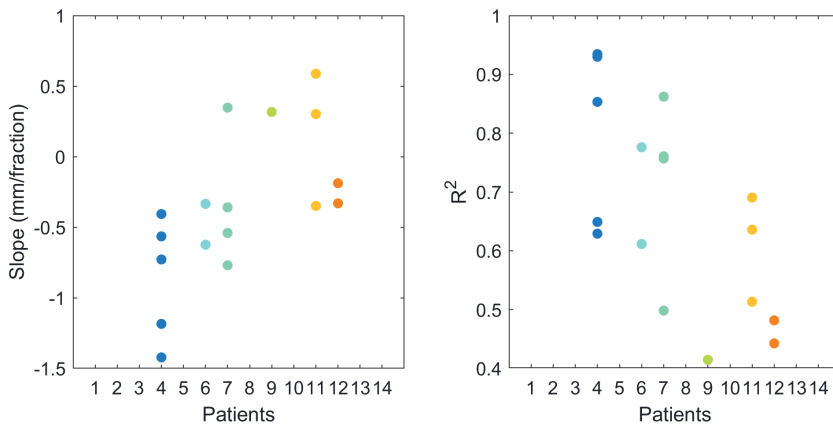


Figure S3D.1: Significant linear regressions in difference in marker-pair distance with respect to planning CT as a function of fraction number: slopes (left) and R<sup>2</sup> (right).

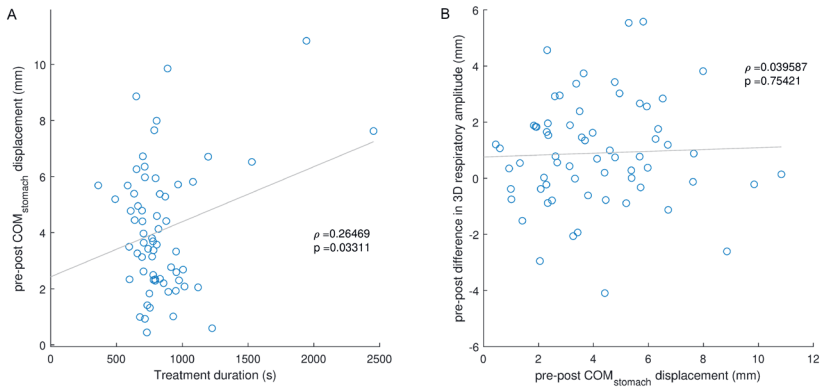
**Supplemental Materials S3E: Pearson correlation on pre-post displacements**

Figure S3E.1: A) Treatment duration (i.e., time between the acquisition of pre- and post-treatment CBCT) in seconds plotted against the pre-post 3D displacement of the center-of-mass of available markers ( $COM_{stomach}$ ). B) The 3D pre-post  $COM_{stomach}$  displacement plotted versus the pre-post difference in 3D respiratory amplitude. Both plots include the Pearson correlation line (grey), with Pearson correlation coefficient  $\rho$  and its corresponding p-value ( $p$ ).

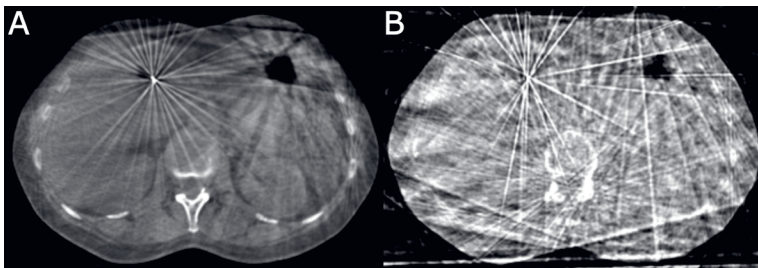
**Supplemental Materials S3F: Example of typical CBCT**

Figure S3F.1: A) Example of typical average reconstructed CBCT to demonstrate image quality and B) accompanying end-exhale phase CBCT image to demonstrate fiducial marker visibility. In both A and B, a gold fiducial marker is clearly visible.

&amp;

## Supplemental Materials to Chapter 4

### Supplemental Materials S4A: Results of plan selections in training stage

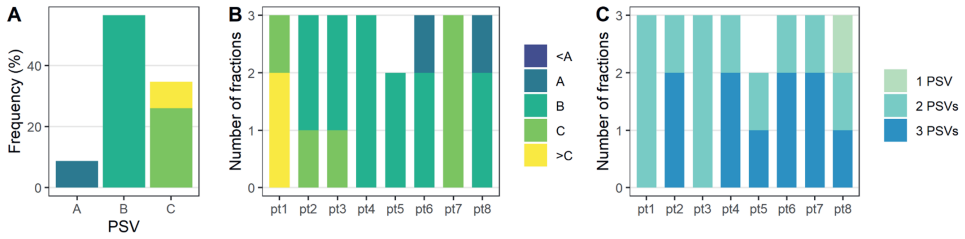


Figure S4A.1: Results of plan selections in training stage A) The most frequently selected PSV ( $PSV_{mod}$ ) for all fractions. B)  $PSV_{mod}$  per patient. C) Number of different PSVs selected per patient per fraction.

**Supplemental Materials S4B: Plan selections in assessment stage**

	Observer 1	Observer 2	Observer 3	Observer 4	Observer 5	Observer 6	Observer 7	Observer 8	Observer 9	Observer 10	Observer 11	Observer 12	Modal PSV
<b>Patient 1</b>	B	>D	C	>D	>D	>D	>D	>D	>D	B	D	NP	>D
	D	D	C	>D	>D	D	>D	D	D	B	D	C	D
	C	B	B	B	C	B	B	A	B	C	B	B	B
	>D	>D	C	>D	>D	>D	>D	>D	>D	B	B	NP	>D
	D	D	C	D	D	D	D	D	D	C	B	C	D
	>D	>D	C	>D	>D	>D	>D	>D	>D	C	B	>D	>D
	>D	>D	B	>D	>D	>D	>D	>D	>D	C	C	>D	>D
	>D	>D	B	>D	>D	>D	>D	>D	>D	C	C	>D	>D
	>D	D	B	>D	>D	>D	>D	>D	>D	C	C	>D	>D
	>D	D	B	>D	>D	>D	>D	>D	>D	C	C	>D	>D
	>D	D	C	>D	>D	>D	>D	D	>D	C	D	>D	>D
	D	C	C	C	C	C	C	D	C	C	C	C	C
	D	D	C	D	D	>D	D	D	C	C	C	D	D
	>D	D	C	>D	>D	>D	>D	>D	>D	C	C	>D	>D
	C	C	B	C	C	C	C	D	C	C	C	C	C
	>D	D	B	D	D	D	D	D	D	D	C	D	D
<b>Patient 2</b>	B	B	C	C	B	C	B	B	B	C	B	C	B
	C	C	C	C	C	C	C	C	B	C	C	D	C
	C	C	C	C	B	B	C	C	C	C	C	>D	C
	C	C	C	C	C	C	C	C	B	C	C	D	C
	C	C	C	C	C	C	C	C	C	C	B	D	C
	B	B	C	D	B	B	B	B	B	D	B	D	B
	C	C	C	D	C	C	D	B	C	C	B	D	C
	C	B	C	D	C	C	C	B	C	C	B	D	C
	C	C	C	D	C	C	C	C	C	C	C	D	C
	C	C	C	D	C	C	C	D	C	C	C	D	C
	C	B	C	D	B	B	B	B	B	C	C	C	B
	C	A	C	D	B	B	C	C	B	C	B	C	C
	C	D	C	D	B	B	B	A	B	C	B	C	B
	B	B	C	D	B	B	C	B	B	C	C	B	B
	B	B	C	D	B	B	B	B	B	C	B	D	B
	C	C	C	D	C	B	C	C	B	C	B	D	C
C	D	C	D	C	C	C	B	C	C	B	D	C	

Continues on next page



Patient 3	C	D	C	C	C	C	C	C	C	C	C	B	C
	C	C	C	C	B	C	C	C	C	D	C	C	C
	D	D	D	C	D	D	D	D	D	D	D	D	D
	C	D	D	C	C	C	C	C	C	D	C	C	C
	D	D	D	D	D	D	D	D	D	D	C	D	D
	B	B	B	B	B	B	B	B	B	C	B	B	B
	D	D	D	D	D	D	D	D	D	>D	D	D	D
	D	D	D	D	D	D	D	D	D	D	D	D	D
	D	D	C	NP	>D	NP	D	B	D	D	D	D	D
	C	C	C	B	B	NP	B	B	C	C	B	B	B
	B	D	C	B	B	B	B	NP	B	C	B	B	B
	C	C	C	B	C	C	C	B	C	D	C	C	C
	C	C	C	B	B	B	B	B	C	D	C	B	B
	D	D	C	C	C	C	D	B	D	D	C	D	D
	D	D	C	C	C	C	C	C	D	C	D	C	C
D	D	C	D	D	D	D	D	D	D	D	D	D	
D	D	C	D	D	D	D	D	D	D	D	D	D	
Patient 4	C	C	C	C	C	C	C	C	C	B	C	C	C
	D	C	D	D	C	D	D	C	D	B	C	D	D
	C	C	C	C	C	C	C	C	C	C	C	C	C
	C	C	C	D	C	D	C	C	D	D	C	>D	C
	D	D	D	D	C	C	D	C	D	D	C	C	D
	B	D	C	D	C	D	D	C	D	D	C	D	D
	NP	>D	>D	>D	>D	>D	>D	>D	>D	C	>D	>D	>D
	C	C	C	C	C	C	C	C	C	C	C	C	C
	A	C	C	C	C	C	D	C	D	D	C	C	C
	B	>D	D	D	>D	>D	>D	D	>D	>D	>D	>D	>D
	B	D	D	D	D	D	>D	D	>D	>D	>D	D	D
	C	C	C	C	C	C	C	C	C	C	C	C	C
	C	C	C	C	C	C	C	C	C	C	C	C	C
	C	C	C	C	C	C	C	C	C	D	C	C	C
	D	C	C	D	C	C	D	C	D	>D	C	C	C
Patient 5	C	D	C	D	C	C	D	C	D	D	C	D	C
	>D	D	B	>D	>D	>D	D	>D	>D	B	C	C	>D
	>D	>D	B	>D	>D	>D	D	>D	>D	B	C	C	>D
	C	C	B	C	C	C	C	C	C	B	C	C	C
	D	D	B	D	C	D	D	D	>D	>D	D	D	D
	D	D	B	D	D	D	D	D	D	D	D	D	D
	D	D	B	C	C	C	D	B	D	D	B	B	B
	D	D	B	D	C	D	D	D	>D	D	D	D	D
	C	C	B	C	B	C	C	C	C	C	C	C	C
	C	D	B	C	C	B	C	C	C	C	C	C	C
	A	A	B	B	B	B	B	A	B	C	A	B	B
	C	C	B	C	B	C	C	C	C	C	C	C	C
	C	D	B	B	D	C	C	D	D	C	C	C	C
	D	D	B	D	D	D	D	D	D	D	D	D	D
	D	D	B	D	D	D	D	D	D	D	D	D	D
D	D	B	C	D	C	D	C	D	D	C	C	D	

Continues on next page

Patient 6	C	C	B	C	B	B	C	B	B	C	B	B	B
	B	B	B	B	B	B	B	A	B	D	B	B	B
	D	D	C	C	C	C	D	D	D	D	D	D	D
	>D	C	C	C	D	D	D	D	>D	>D	D	D	D
	C	B	B	B	B	B	C	B	C	D	B	C	B
	D	C	C	B	D	C	D	D	D	D	C	C	D
	>D	C	C	C	C	C	D	C	C	D	C	C	C
	C	B	B	B	B	B	C	C	B	D	B	B	B
	C	B	C	C	C	B	C	B	C	>D	B	B	C
	C	B	D	C	C	B	C	B	C	>D	B	B	C
	B	B	B	B	B	B	B	B	B	D	B	B	B
	B	B	B	B	B	B	D	C	C	>D	B	B	B
	C	C	C	C	C	C	C	C	C	D	C	C	C
	B	C	C	C	C	B	C	C	C	D	B	B	C
B	B	B	B	B	B	B	B	B	D	C	B	B	
C	C	C	C	C	C	C	C	C	D	B	C	C	
B	D	B	D	D	>D	>D	D	C	>D	B	C	D	
Patient 7	A	A	B	B	B	A	B	A	B	B	B	A	B
	B	B	C	B	B	A	B	A	B	C	B	B	B
	C	B	B	B	B	B	A	A	A	B	B	B	B
	C	C	C	C	C	C	C	C	C	C	B	C	C
	>D	D	C	C	C	D	D	C	C	D	C	C	C
	C	C	C	B	B	B	B	B	B	D	B	B	B
	C	C	C	C	C	C	C	C	C	C	C	C	C
	B	B	C	B	C	B	B	B	A	C	B	B	B
	D	C	C	C	C	C	C	C	C	D	C	D	C
	C	C	C	C	C	C	C	C	C	D	C	C	C
	C	C	C	C	C	C	C	C	C	D	C	C	C
	C	B	C	C	C	C	C	C	C	D	B	C	C
	C	C	C	C	C	C	C	C	C	D	B	C	C
	D	D	D	D	D	D	D	D	D	D	D	D	D
C	C	C	C	C	C	C	C	C	D	B	C	C	
C	C	C	C	C	C	C	C	C	D	C	C	C	
Patient 8	>D	D	C	B	D	>D	>D	>D	>D	>D	C	>D	
	B	B	C	B	B	B	C	B	A	C	C	B	B
	B	B	C	B	B	B	B	B	B	C	B	A	B
	B	B	D	C	C	B	C	B	B	C	B	A	B
	C	B	C	B	A	A	C	A	C	D	B	A	C
	D	C	B	D	D	D	>D	D	>D	>D	C	C	D
	D	D	D	D	D	D	D	D	D	>D	C	D	D
	D	C	C	B	D	D	D	C	D	D	C	C	D
	>D	>D	>D	>D	>D	>D	>D	>D	>D	>D	D	>D	>D
	D	D	>D	D	C	D	D	C	D	>D	B	C	D
	D	C	C	C	C	D	D	C	C	>D	B	C	C
	C	C	C	C	B	C	C	B	C	>D	B	C	C
	>D	D	>D	D	D	>D	D	D	>D	>D	B	D	D
	D	D	C	D	C	C	D	C	D	>D	B	C	D
D	C	D	D	B	>D	D	D	>D	>D	B	C	D	
D	D	>D	D	D	D	D	D	D	>D	B	C	D	
D	C	C	C	C	D	C	C	C	>D	B	B	C	

NP = no plan selected





### Supplemental Materials to Chapter 5

#### Supplemental Materials S5A

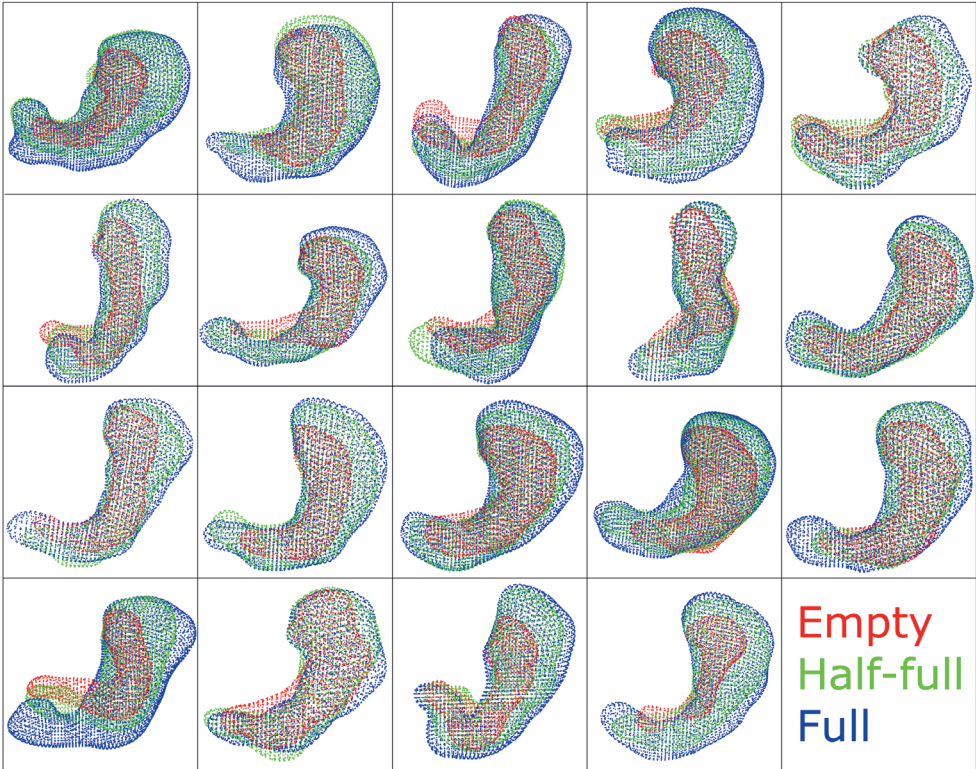


Figure S5A.1: Point cloud of the empty (red), half-full (green) and full stomach (blue) meshes of all 19 volunteers. (Note: scale and view angle differ between volunteers)

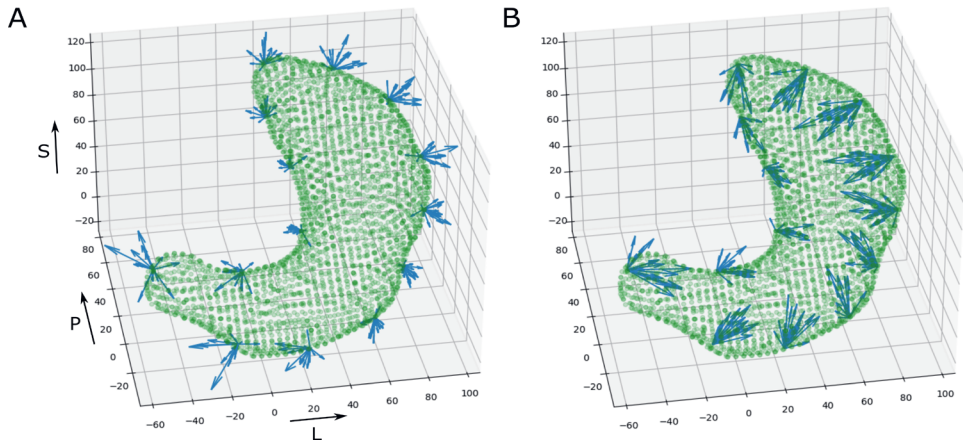
**Supplemental Materials S5B**

Figure S5B.1: Vertices of reference half-full stomach (green). For selected vertices, the 19 deformation vectors to the full (A) and empty stomach (B) are depicted in blue.

**Supplemental Materials S5C**

*Table S5C.1: Median and interquartile range of all evaluation parameters for the personalized strategy and population-based strategy for full and empty stomach prediction with no post-alignment (No), 3DoF or 6DoF post-alignment between predicted stomach and true stomach.*

Filling	Personalized				Population-based			
	Full				Full			
	No	3DoF	6DoF	No	No	3DoF	6DoF	6DoF
Post-Alignment	18.6 (14.7–22.1)	14.4 (13–21.6)	14.7 (12.8–20.3)	16.9 (13.8–21.7)	14.1 (11.3–18.2)	14.1 (11.3–18.2)	12.5 (11–15.3)	
Hausdorff distance [mm]	5.7 (4.9–7.1)	4.9 (4.2–5.5)	4.4 (3.9–4.8)	4.9 (4.4–6.7)	4.4 (3.9–4.7)	4.4 (3.9–4.7)	3.9 (3.7–4.2)	
nn75 [mm]	0.84 (0.82–0.87)	0.88 (0.86–0.9)	0.89 (0.87–0.91)	0.86 (0.83–0.89)	0.90 (0.87–0.91)	0.90 (0.87–0.91)	0.91 (0.89–0.92)	
Dice	0.9 (0.0–1.4)	0.0 (0.0–0.6)	0.0 (0.0–0.3)	0.5 (0.0–1.5)	0.0 (0.0–0.2)	0.0 (0.0–0.2)	0.0 (0.0–0.0)	
Missed volume [%]								
					Empty			
					3DoF			
					6DoF			
					20.3 (16.9–27.9)	16.1 (13.7–19.8)	14.1 (12.8–16.7)	
					13.3 (11.2–16.5)	13.3 (11.6–15.9)	13.4 (11.6–16.1)	
					0.7 (0.54–0.75)	0.79 (0.73–0.82)	0.82 (0.76–0.84)	
					0.7 (0.0–2.1)	0.0 (0.0–1.4)	0.0 (0.0–0.1)	
					Filling			
					Post-Alignment			
					No			
					20.3 (16.9–27.9)	16.1 (13.7–19.8)	14.1 (12.8–16.7)	
					13.3 (11.2–16.5)	13.3 (11.6–15.9)	13.4 (11.6–16.1)	
					0.7 (0.54–0.75)	0.79 (0.73–0.82)	0.82 (0.76–0.84)	
					0.7 (0.0–2.1)	0.0 (0.0–1.4)	0.0 (0.0–0.1)	

## Supplemental Materials S5D

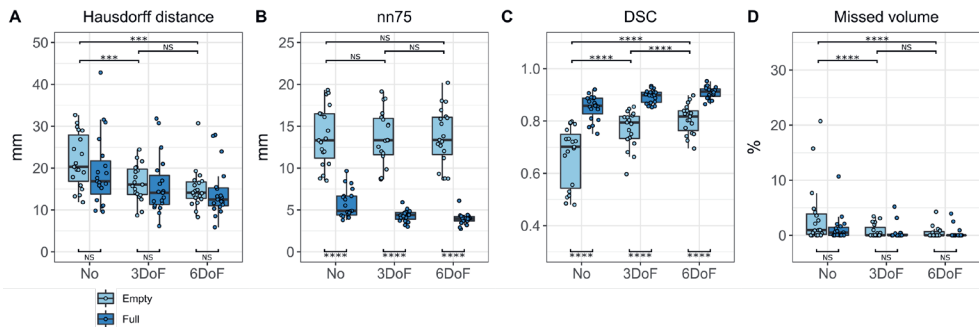


Figure S5D.1: Performance of population-based empty and full stomach predictions with no post-alignment (No), 3DoF post-alignment and 6DoF post-alignment between predicted stomach and true stomach for (A) Hausdorff distance, (B) 75th percentile nearest neighbor distance, (C) Dice similarity coefficient (DSC) and (D) percentage of missed volume with 10-mm margin. Note: these full stomach predictions are also depicted in Figure 3. Boxplots: box=interquartile range (IQR), whiskers=lowest and highest data point within  $1.5 \times \text{IQR}$ . Paired tests (t-test or Wilcoxon signed-rank) were performed. NS  $p \geq 0.05$ , \*  $p < 0.05$ , \*\*  $p < 0.01$ , \*\*\*  $p < 0.001$ , \*\*\*\*  $p < 0.0001$ .

## Supplemental Materials S5E

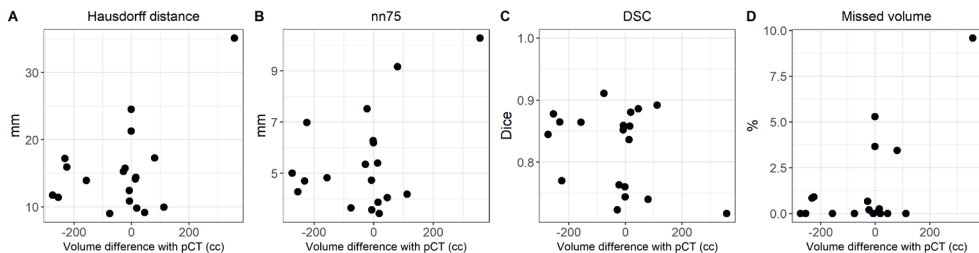


Figure S5E.1: Relation between volume difference of predicted stomach with stomach on pre-treatment CT (pCT) and performance of population-based model on patient data with a 3DoF post-alignment for (A) Hausdorff distance, (B) 75th percentile nearest neighbor distance, (C) Dice similarity coefficient (DSC) and (D) percentage of missed volume with 10-mm margin. Positive volume difference means predicted stomach is larger than original stomach, negative volume difference means predicted stomach is smaller than original stomach.

## Supplemental Materials to Chapter 6

### Supplemental Materials S6A: Observed stomach volumes

Stomach volumes observed in 19 healthy volunteers (basis for the gastric population deformation model) and the 12 patients from this study are depicted in Figure S6A.1. The stomach volumes of healthy volunteers were delineated on MRI's that were acquired with an empty stomach (i.e., no eating for 3 hours and no drinking for 1 hour), half-full stomach (i.e., after eating half a meal), and a full stomach (i.e., after eating the remaining meal). Patients were all allowed to eat a light breakfast and the imaging scans were all acquired prior to 1pm.

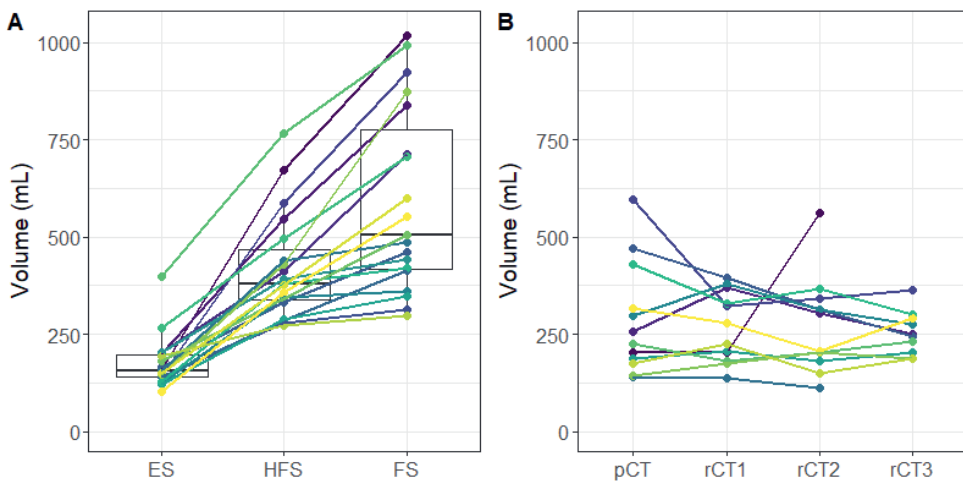


Figure S6A.1: Observed stomach volumes in (A) healthy volunteers and (B) patients. Healthy volunteer stomach volumes are depicted for empty (ES), half-full (HFS), and full stomach (FS). Patient stomach volumes were shown on pre-treatment CT (pCT) and the available repeat CTs (rCT). Each color represents a healthy volunteer/patient.

## Supplemental Materials S6B: PTV margins

PTV margins are used to cover uncertainties due to systematic and random error during radiotherapy and, when calculated with the van Herk formula, should ensure a minimum dose to the CTV of 95% for 90% of the patients<sup>1</sup>. Appropriate population-based PTV margins were separately calculated for CTV<sub>stomach</sub> and CTV<sub>LNr</sub> using the non-linear van Herk formula.

### S6B.1 CTV<sub>stomach</sub>

The CTV<sub>stomach</sub>-to-PTV<sub>stomach</sub> margin was calculated perpendicular to the surface, and the margin formula included uncertainties due to interfractional shape variation, delineation uncertainty, intrafractional shape variation, and respiration:

$$M = \alpha \sqrt{\Sigma_{shapevar}^2 - \left(\frac{\sigma_{shapevar}}{\sqrt{N}}\right)^2 + \Sigma_{del}^2 + \beta \sqrt{\sigma_{shapevar}^2 + \sigma_{intra}^2 + \sigma_p^2 + (0.358A)^2} - \beta \sigma_p + GM_{shapevar}} \quad Eq. S6B.1$$

In equation S6B.1, we used the typical values of a random error factor  $\beta = 1.64$  and the penumbra width of  $\sigma_p = 3.2$  mm. The commonly used value of  $\alpha = 2.5$  applies for rigid targets only. However, alpha can be determined for deformable targets, as shown by Nijkamp et al., who determined  $\alpha = 3.2$  for rectal cancer<sup>2</sup>. As the stomach is not a rigid organ, we empirically determined  $\alpha$  for the stomach in the SP scenario.

#### Alpha

Alpha should be chosen such that SP PTV<sub>stomach</sub> (consisting of only the systematic part of the margin including the group mean) completely encompasses the mean CTV<sub>stomach</sub> shape over all rCTs for 90% of the patients. As there are only 12 patients included in this study, at least for 11 patients the mean CTV<sub>stomach</sub> should be completely covered. Margins were calculated with  $\alpha$  varying from 2.5 to 3.2, with steps of 0.1. For every  $\alpha$ , we calculated the maximum signed nearest neighbor distance from PTV<sub>stomach</sub> on SP to mean CTV<sub>stomach</sub> ( $>0$ : mean CTV<sub>stomach</sub> outside PTV<sub>stomach</sub>) and fitted a linear regression line per patient (outlier rejection with Z-score  $> 2.5$ ; Figure S6B.1). At  $2.73 < \alpha < 3.75$ , PTV<sub>stomach</sub> encompassed mean CTV<sub>stomach</sub> for 11 patients, hence,  $\alpha = 2.8$ .

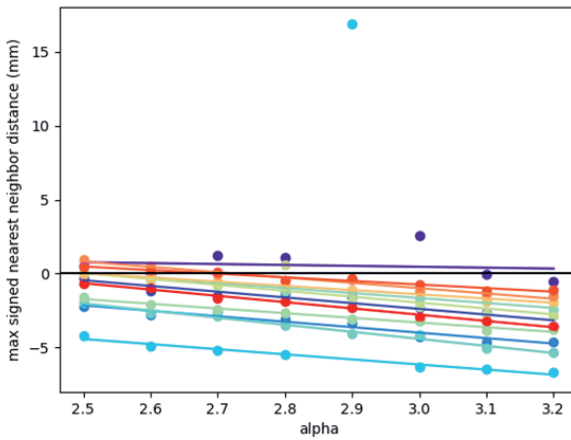


Figure S6B.1: Maximum nearest neighbor distance in mm for varying alpha. Colors represent different patients. Per patient, a linear regression line with outlier rejection ( $Z > 2.5$ ) was plotted.

### Interfractional shape variation

Interfractional shape variation is determined separately for SP and LoP, resulting in different PTV margin distributions between the two strategies. For SP, the interfractional shape variation of  $CTV_{stomach}$  on rCT is determined with respect to the fixed reference of  $CTV_{stomach}$  on pCT. For LoP, this is determined with respect to the variable reference of the best fitting plan for each rCT. Triangulated surface meshes of stomach and  $CTV_{stomach}$  were used to calculate these shape variations.

For SP, a stomach-based 3DoF (translations-only) match was performed between SP-stomach and each rCT-stomach using the iterative closest point algorithm (ICP). Subsequently, the remaining local shape difference was determined for each rCT by calculating the distance of every vertex of SP- $CTV_{stomach}$  to the closest point on each rCT- $CTV_{stomach}$ . These local distances were combined per patient into an average and standard deviation (SD) per vertex of SP- $CTV_{stomach}$ . Finally, using a point-to-point correspondence (acquired with a non-rigid ICP algorithm) between patient 9 (patient 9=median stomach volume on pCT) and all other patients, these average distances and SD were mapped to  $CTV_{stomach}$  on pCT of patient 9, such that the systematic ( $\Sigma_{shapevar}$ ), random error ( $\sigma_{shapevar}$ ) and the group mean of the population shape variation ( $GM_{shapevar}$ ) could be calculated.

For LoP, to determine shape difference with respect to the treatment plan, plan selections for each rCT were required. For each rCT, a 3DoF (translations-only) match was performed between every LoP-stomach and stomach on rCT using ICP. The LoP-stomach was selected for

which the mean signed distance from the true stomach on rCT to the LoP-stomach was closest to zero (i.e., smallest deviations between true stomach on rCT and LoP-stomach). These plan selections were in accordance with manually performed plan selections for 29 out of 34 rCTs. Next, local residual distances from every vertex on LoP-CTV<sub>stomach</sub> accompanying the selected LoP-stomach to closest point on rCT-CTV<sub>stomach</sub> were determined. Per patient, these local residual distances were mapped to CTV<sub>stomach</sub> on pCT using point-to-point correspondence and combined into an average and SD per vertex. The average and SD per point per patient were mapped to CTV<sub>stomach</sub> on pCT of patient 9. Subsequently, the systematic ( $\Sigma_{\text{shapevar}}$ ), random error ( $\sigma_{\text{shapevar}}$ ) and the group mean of the population shape variation ( $GM_{\text{shapevar}}$ ) were calculated.

#### *Limited data*

Due to the limited number of rCTs per patient (2–3 rCTs), an overestimation of the systematic error is expected. Therefore, a correction factor is included in the formula, with N the number of rCTs (N=3).

#### *Delineation*

Delineation uncertainty is included in the systematic error and was set at  $\Sigma_{\text{del}}=2$  mm, as typically done for clearly distinguishable targets. As the CTV in the current study has no clear boundaries, this delineation uncertainty is potentially underestimated.

#### *Intrafractional motion*

Intrafractional motion, e.g., peristalsis of the stomach, was  $\sigma_{\text{intra}}^2 = 2.4$ . The value was in-house determined in an ongoing study on intrafractional motion of the stomach.

#### *Respiratory motion*

In this population-based margin calculation, respiratory motion was included by 0.358 times amplitude  $A^3$ . The amplitude was set at 8 mm in superior-inferior (SI) direction, 3 mm in anterior-posterior (AP) direction, and 2 mm in left-right (LR) direction. We recognize that respiratory motion amplitude differs between patients and may depend on stomach volume. However, with no amplitude data available for different stomach volumes, and the fact that respiratory motion on pre-treatment CT may not be representative for motion during radiotherapy treatment<sup>4,5</sup>, we chose to use one respiratory value in each direction for all patients.

The selected respiratory amplitudes values were chosen similarly to respiratory amplitudes measured by fiducial markers in the pancreas (average 8.3, 2.9 and 2.4mm for SI, AP and LR, respectively) and cardia of the stomach (median 8.2, 5.3 and 3.7mm, respectively)<sup>5,6</sup>. Furthermore, for five included patients, the average respiratory amplitude was previously determined using fiducial markers implanted in the stomach to be 8.0, 3.2 and 1.4mm, respectively<sup>7</sup>. Since our own data reflected the previously determined amplitudes, we chose a respiratory amplitude for the current patient group of 8, 3 and 2 mm in SI, AP and LR direction,



respectively. The contribution of these directional amplitudes for every vertex on the CTV surface depended upon the normal vector angle at that vertex.

### Coverage

For both SP and LoP, we visually evaluated whether the (selected)  $PTV_{stomach}$  contour fully encompassed  $CTV_{stomach}$  for each CBCT (Figure S6B.2). For SP, for three patients, there was no complete coverage in 6 treatment days or more. Consequently, it is likely that accumulated dose would not result in adequate coverage for these three patients (25%), and the PTV margin principle (at least 95% of the prescribed dose to CTV in 90% of patients) was not satisfied. For LoP, only one patient had no complete coverage in 6 treatment days. For the other patients, a minimal number of scans, if any, with no complete coverage of the CTV was observed for LoP, suggesting that accumulated dose would probably only be insufficient in this single patient (8.3%). Therefore, PTV margin calculation for LoP appears adequate since sufficient coverage was obtained in approximately 10% of patients. However, for SP, the PTV margin appeared too small. In addition, as the starting point of this study was equal coverage in order to evaluate OAR dose, coverage between SP and LoP should be ensured equal.

As the calculated PTV margin for  $CTV_{stomach}$  appeared too small for SP, the PTV margin distribution was expanded by 10, 20, 25, and 30%, and coverage was again evaluated (Figure S6B.3). An expansion of 30% would result in better coverage for SP than LoP, and the expansion of 25% would result in slightly poorer coverage for SP than LoP. Consequently, local  $PTV_{stomach}$  margin was enlarged by 25% to ensure approximately equal coverage between SP and LoP.

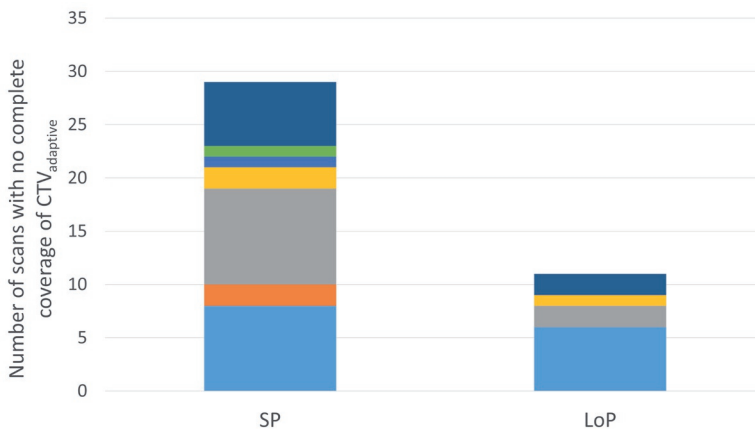


Figure S6B.2: Stacked barplot for single-plan (SP) and library of plans (LoP) with the number of scans with no complete coverage of  $CTV_{stomach}$  on CBCT with the (selected)  $PTV_{stomach}$ . Different colors represent different patients.

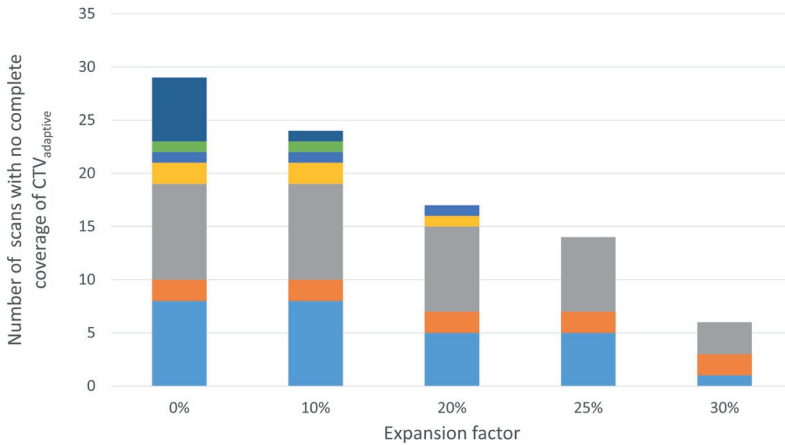


Figure S6B.3: Stacked barplot with the number of scans with no complete coverage of CTV<sub>stomach</sub> on CBCT with PTV<sub>stomach</sub> margin with various expansion factors for single-plan strategy. Different colors represent different patients.

### S6B.2 CTV<sub>LN</sub>

The CTV<sub>LN</sub>-to-PTV<sub>LN</sub> margin was assumed equal for SP and LoP and calculated using the van Herk formula (Eq. S6B.2).

$$M = \alpha \sqrt{\Sigma_{3DoF}^2 - \left(\frac{\sigma_{3DoF}}{\sqrt{3}}\right)^2} + \Sigma_{del}^2 + \beta \sqrt{\sigma_{3DoF}^2 + \sigma_p^2 + (0.358A)^2} - \beta \sigma_p \quad \text{Eq. S6B.2}$$

As we assume CTV<sub>LN</sub> to act rigid,  $\alpha = 2.5$  and  $\beta = 1.64$ . This margin calculation included uncertainties due to a 3DoF match, a delineation uncertainty of  $\Sigma_{del} = 2\text{mm}$ , and the respiratory motion similar to PTV<sub>stomach</sub> calculations ( $0.358 \times \text{Amplitude (A)}$ , A: SI=8, AP=3, LR=2mm).

For PTV<sub>stomach</sub> calculations (both SP and LoP) and daily alignment of the treatment plans with CTV, a stomach-based 3DoF match was performed. We expected CTV<sub>LN</sub> to not be entirely fixed to either bony anatomy or CTV<sub>stomachr</sub> causing an error in CTV<sub>LN</sub> location. In order to assess the interfractional CTV<sub>LN</sub> displacement, we also performed a manual CTV<sub>LN</sub> 3DoF match for some CBCT scans with large average (SP and LoP) CTV<sub>stomach</sub> matches (total of 9 scans from 9 different patients). With respect to the bony anatomy match, translations for CTV<sub>LN</sub> were approximately half the accompanying average translations for CTV<sub>stomachr</sub> with an  $R^2$  of 0.74 (Figure S6B.4). Consequently, the systematic and random error of this component was calculated by 0.5 times the averaged 3DoF match of SP and LoP per rCT. As there were only 2–3 rCTs per patient, the correction factor for limited data was again included.

&

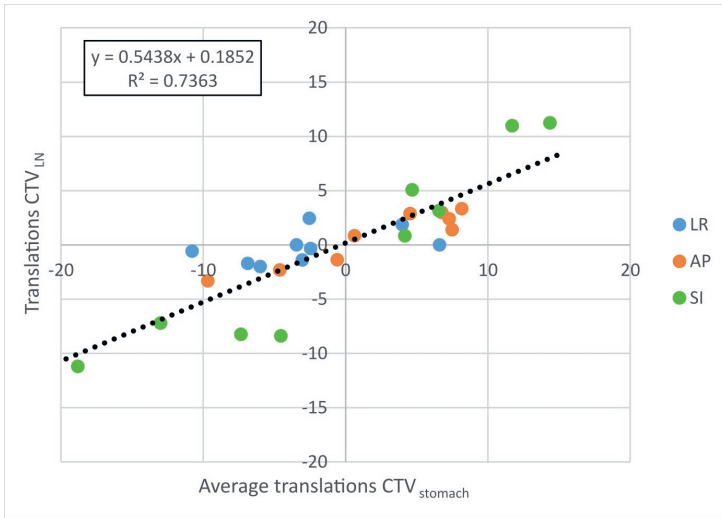


Figure S6B.4: Scatterplot of the average translations of  $CTV_{stomach}$  between single-plan and LoP versus the translations of  $CTV_{IN}$  in left-right (LR; blue), anterior-posterior (AP; orange) and superior-inferior (SI; grey). The reported translations are with respect to the bony anatomy match. A linear fit was plotted in dashed line of  $y=0.54x+0.19$  with  $R^2=0.73$ .

**References Supplemental Materials S6B**

1. Van Herk M, Remeijer P, Rasch C, Lebesque J V. The probability of correct target dosage: Dose-population histograms for deriving treatment margins in radiotherapy. *Int J Radiat Oncol Biol Phys.* 2000;47(4). doi:10.1016/S0360-3016(00)00518-6
2. Nijkamp J, Swellengrebel M, Hollmann B, et al. Repeat CT assessed CTV variation and PTV margins for short- and long-course pre-operative RT of rectal cancer. *Radiother Oncol.* 2012;102(3). doi:10.1016/j.radonc.2011.11.011
3. Van Herk M, Witte M, Van Der Geer J, Schneider C, Lebesque JV. Biologic and physical fractionation effects of random geometric errors. *Int J Radiat Oncol Biol Phys.* 2003;57(5). doi:10.1016/j.ijrobp.2003.08.026
4. Ge J, Santanam L, Noel C, Parikh PJ. Planning 4-dimensional computed tomography (4DCT) cannot adequately represent daily intrafractional motion of abdominal tumors. *Int J Radiat Oncol Biol Phys.* 2013;85(4). doi:10.1016/j.ijrobp.2012.09.014
5. Lens E, Van Der Horst A, Kroon PS, et al. Differences in respiratory-induced pancreatic tumor motion between 4D treatment planning CT and daily cone beam CT, measured using intratumoral fiducials. *Acta Oncol (Madr).* 2014;53(9). doi:10.3109/0284186X.2014.905699
6. Jin P, Hulshof M, De Jong R, Van Hooft JE, Bel A, Alderliesten T. Quantification of respiration-induced esophageal tumor motion using fiducial markers and four-dimensional computed tomography. *Radiother Oncol.* 2016;118(3). doi:10.1016/j.radonc.2016.01.005
7. Bleeker M, Lie S, Bel A, Sonke J-J, Hulshof M, van der Horst A. Quantification of Intra-and Interfractional Target Motion and Deformation in Gastric Cancer Radiotherapy [abstract]. *Med Phys.* 2020;47(6).



**Supplemental Materials S6C: Priority list automatic treatment plans***Table S6C.1: List of priorities used to create automatic treatment plans. Dmean = mean dose.*

Priority	Structure	Clinical goal*
1	Body	At most 48.15 Gy dose at 1 cm <sup>3</sup> volume
1	PTV	At least 99% volume at 42.75 Gy dose
2	Left kidney	At most 33% volume at 18 Gy
2	Right kidney	At most 33% volume at 18 Gy
3	Spleen	At most Dmean of 24 Gy
4	Body	Dose fall-off (45 Gy to 22.5 Gy in 1 cm)
5	Heart	At most 30% volume at 40 Gy dose
5	Left kidney – PTV	At most 20% volume at 18 Gy
5	Liver	At most Dmean of 30 Gy
5	Right kidney – PTV	At most 20% volume at 18 Gy
5	Spinal canal	At most 45 Gy at 0.01 cm <sup>3</sup> volume
5	Spleen – PTV	At most Dmean of 15 Gy
6	Heart	Reduce Dmean as much as possible
6	Left kidney – PTV	Reduce Dmean as much as possible
6	Liver	Reduce Dmean as much as possible
6	Right kidney – PTV	Reduce Dmean as much as possible
6	Spinal canal	Reduce Dmean as much as possible
6	Spleen – PTV	Reduce Dmean as much as possible

\*Clinical goals within the same priority are alphabetically ordered

**Supplemental Materials S6D: Organ at risk shifts with respect to stomach-based match for SP or selected LoP**

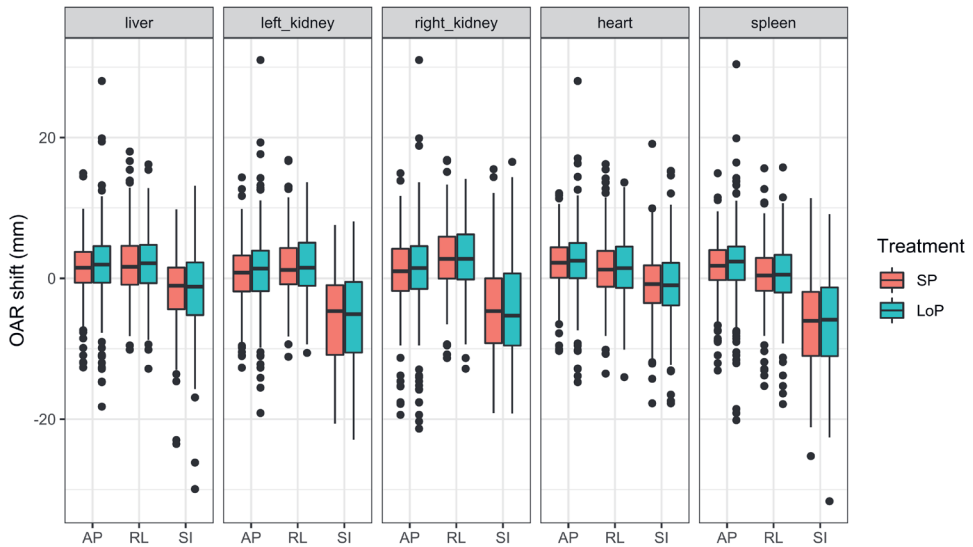


Figure S6D.1: Manual organ at risk (OAR) shifts with respect to the stomach-based match made for SP or the selected plan from LoP in anterior-posterior (AP), right-left (RL), or superior-inferior (SI) direction (A, R and S are positive). Each boxplot contains data from all patients and CBCTs (N=293).

**Supplemental Materials S6E: Absolute dose evaluation parameters for SP and LoP**

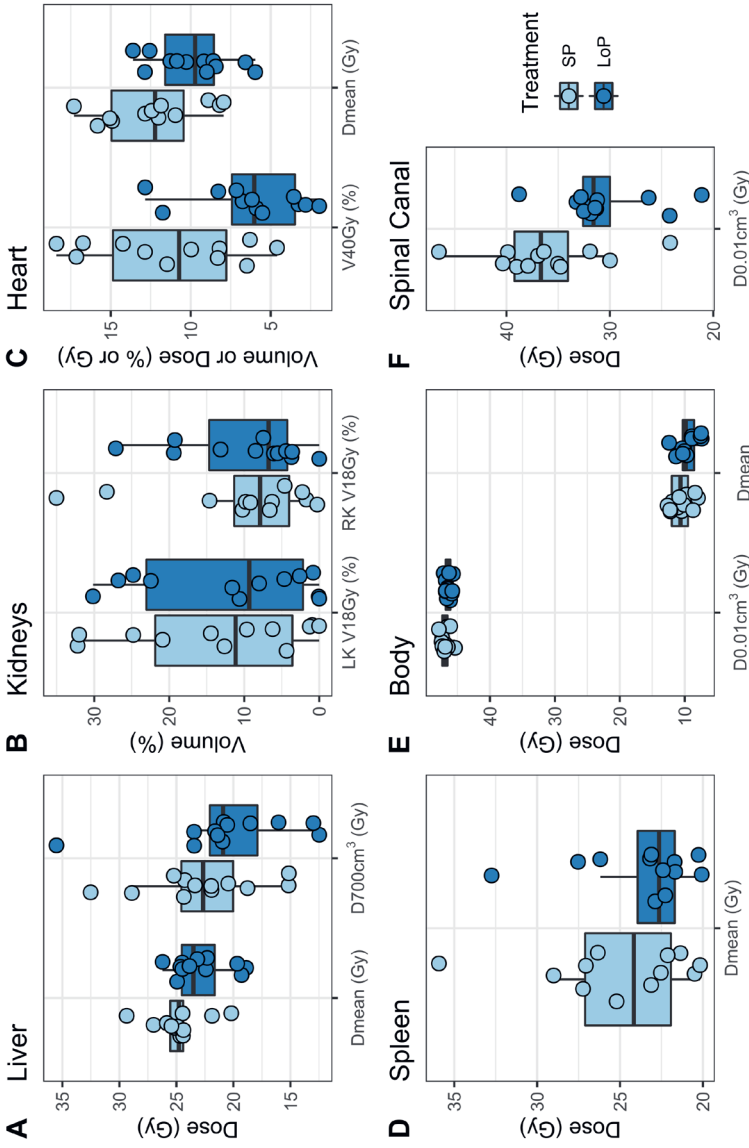
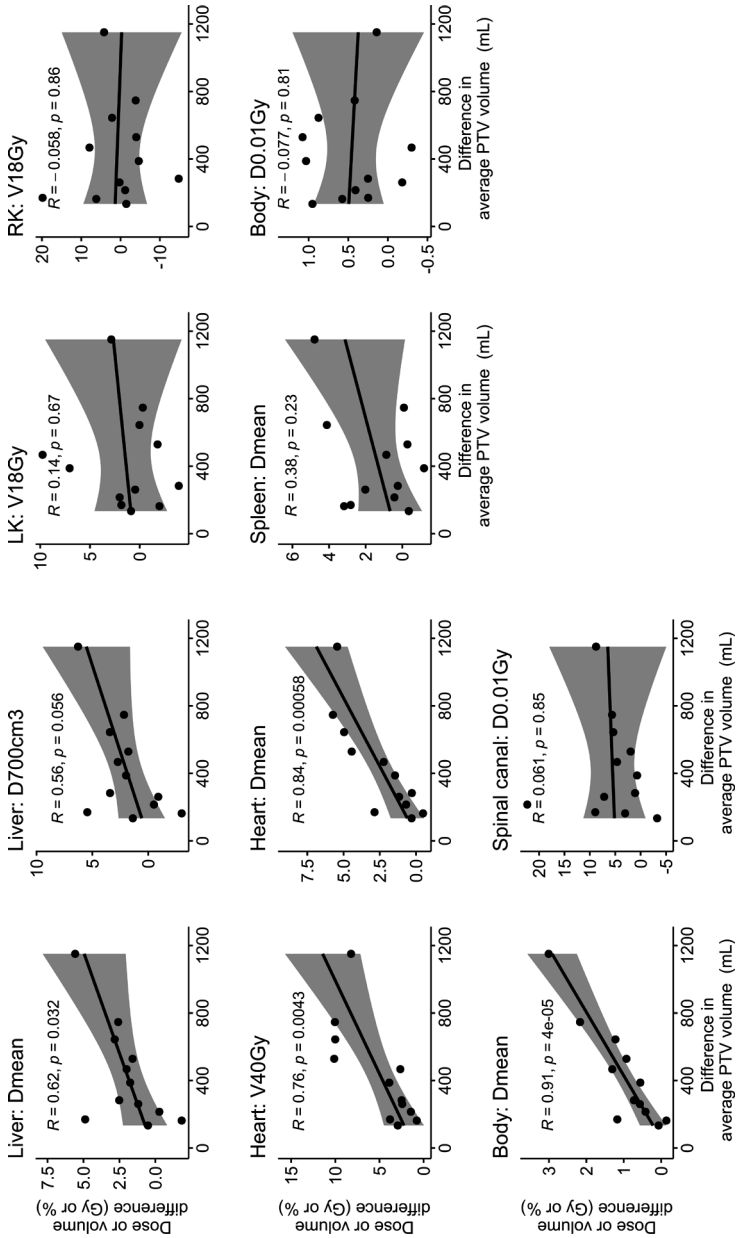


Figure S6E. 1: Evaluated parameters from dose-volume histograms for single-plan (SP; light blue) and library of plans (LoP; dark blue) of the organs-at-risk: liver (A), left (LK) and right kidney (RK; B), heart (C), spleen (D), body (E) and spinal canal (F). Dmean = mean dose, D700cm<sup>3</sup> = maximum dose in the 700cm<sup>3</sup> that received the lowest dose, D0.01cm<sup>3</sup> = maximum dose in 0.01cm<sup>3</sup>, VxGy = Volume that received at least x Gy. Boxplots: box = interquartile range (IQR), whiskers = lowest and highest data point within 1.5 × IQR.

**Supplemental Materials S6F: Correlation between difference in average PTV and difference in evaluating parameter**



*Figure S6F: i: Difference in average PTV (mL) between single-plan (SP) and library of plans (LoP) versus difference in dose (Gy) or volume (%) between SP and LoP of the evaluated parameter. The header contains the organ at risk and the evaluated parameter. Each plot contains the linear regression line and the 95% confidence interval (grey), with the Pearson correlation coefficient R and the p-value depicted. Dmean = mean dose, D700cm<sup>3</sup> = maximum dose in the 700cm<sup>3</sup> that received the lowest dose, D0.01cm<sup>3</sup> = maximum dose in 0.01cm<sup>3</sup>, VxGy = Volume that received at least x Gy.*





**Supplemental Materials S6G: Difference in evaluated parameters for PTV<sub>stomach</sub>**

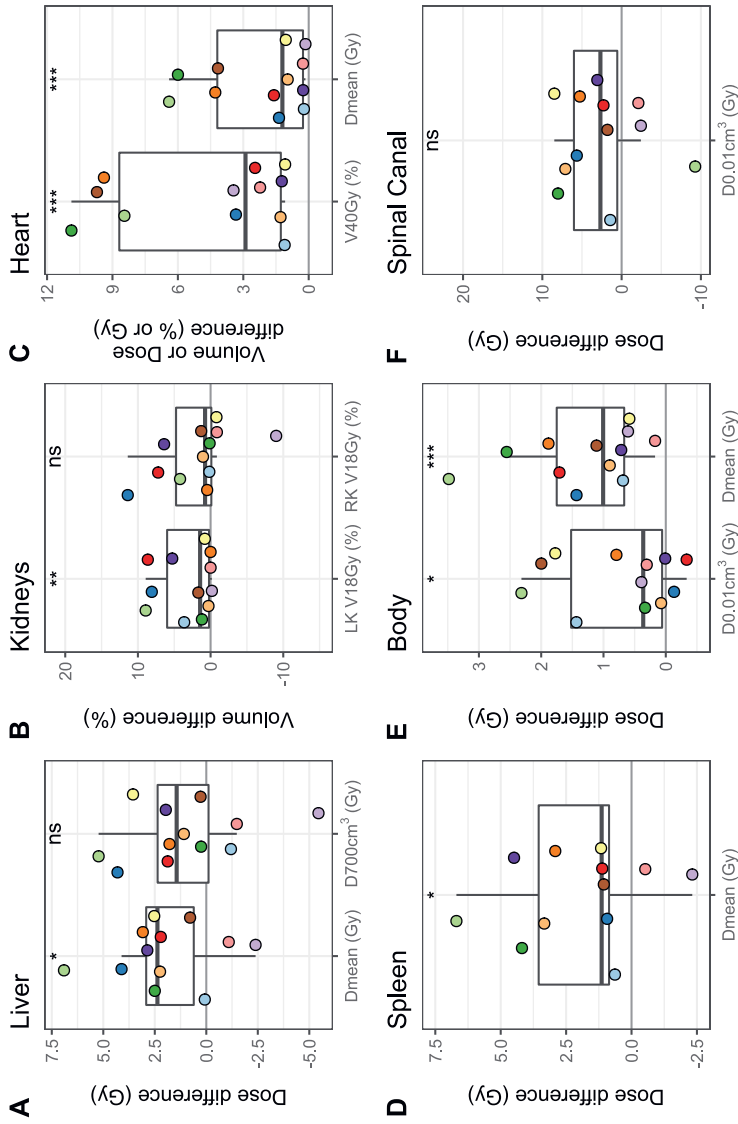


Figure S6G.1: Dose-volume histogram parameter difference between PTV<sub>stomach</sub> SP and LoP for several dose parameters for liver (A), left (LK) and right kidney (RK; B), heart (C), spleen (D), body (E) and spinal canal (F). Positive difference: SP > LoP (i.e., LoP is beneficial). Dmean = mean dose, D700cm³ = maximum dose in the 700cm³ that received the lowest dose, D0.01cm³ = maximum dose in 0.01cm³, VxGy = Volume that received at least x Gy. Colors correspond to colors in Figures 6.4 and 6.5. Statistical tests (t-test or Mann-Whitney-Wilcoxon test): NS p ≥ 0.05, \*p < 0.05, \*\*p < 0.01, \*\*\*p < 0.001. Boxplots: box = interquartile range (IQR), whiskers = lowest and highest data point within 1.5 × IQR.



## PhD Portfolio

### List of publications

**Bleeker M**, Goudschaal K, Bel A, Sonke JJ, Hulshof MCCM, van der Horst A. Feasibility of cone beam CT-guided library of plans strategy in pre-operative gastric cancer radiotherapy. *Radiotherapy and Oncology* 149 (2020): 49-54.

**Bleeker M**, Hulshof MCCM, Bel A, Sonke JJ, van der Horst A. Gastric deformation models for adaptive radiotherapy: Personalized vs population-based strategy. *Radiotherapy and Oncology* 166 (2022): 126-132.

**Bleeker M**, Visser J, Goudschaal K, Bel A, Hulshof MCCM, Sonke JJ, van der Horst A. Dosimetric benefit of a library of plans versus single-plan strategy for pre-operative gastric cancer radiotherapy. *Radiotherapy and Oncology* 182 (2023): 109582.

**Bleeker M**, van der Horst A, Bel A, Sonke JJ, van Hooft JE, Pouw RE, Hulshof MCCM. Endoscopically placed fiducial markers for image-guided radiotherapy in preoperative gastric cancer: Technical feasibility and potential benefit. *Endoscopy International Open* (2023): E866-E872.

**Bleeker M**, Hulshof MCCM, Bel A, Sonke JJ, van der Horst A. Stomach motion and deformation: implications for pre-operative gastric cancer radiotherapy. *International Journal of Radiation Oncology • Biology • Physics* (2023).

## International conferences

- ESTRO, Milan  
2019 CBCT-based library of plans approach in gastric cancer radiotherapy: proof of concept. **Bleeker, M., Goudschaal, K., Bel, A., Sonke, J.J., Hulshof, M.C.C.M., van der Horst, A.** (Poster)
- Joint AAPM|COMP, online  
2020 Cone Beam CT-Guided Adaptive Strategy in Pre-Operative Gastric Cancer Radiotherapy. **Bleeker, M., Goudschaal, K., Bel, A., Sonke, J.J., Hulshof, M.C.C.M., van der Horst, A.** (Poster)
- Quantification of Intra- and Interfractional Target Motion and Deformation in Gastric Cancer Radiotherapy. **Bleeker, M., Lie, S., Hulshof, M.C.C.M., Bel, A., Sonke, J.J., van der Horst, A.** (Poster)
- ESTRO, Madrid and online  
2021 Gastric deformation models for adaptive radiotherapy: Personalized vs Population-based strategy. **Bleeker, M., Hulshof, M.C.C.M., Bel, A., Sonke, J.J., van der Horst, A.** (Oral)
- ESTRO, Copenhagen  
2022 Feasibility of endoscopic fiducial marker implantation in the stomach for use in image-guided RT. **Bleeker, M., Pouw, R.E., Bel, A., Sonke, J.J., Hulshof, M.C.C.M., van der Horst, A.** (Poster)
- AAPM, Washington DC  
2022 Potential Benefit of a Library of Plans Strategy for Pre-Operative Gastric Cancer Radiotherapy. **Bleeker, M., Hulshof, M.C.C.M., Goudschaal, K., Bel, A., Sonke, J.J., van der Horst, A.** (Poster)

## Courses

- 2018 The AMC world of Science
- 2018 Practical Biostatistics
- 2019 Radiation Oncology (OOA)
- 2019 ESTRO pre-meeting course 'deep learning'
- 2020 ESTRO In-Room MRI guided-RT
- 2021 Indesign Thesis

## Supervision

- 2020 MSc student Medical Natural Sciences
- 2021 MSc student Technical medicine
- 2021 BSc student Medical Imaging and Radiotherapeutic Techniques (MBRT)

## Author Contributions

### Authors

MB	Margot Bleeker <sup>1,2</sup>
JS	Jan-Jakob Sonke <sup>3</sup>
AB	Arjan Bel <sup>1,2</sup>
AH	Astrid van der Horst <sup>1,3*</sup>
MH	Maarten C.C.M. Hulshof <sup>1</sup>
KG	Karin Goudschaal <sup>1</sup>
JH	Jeanin E. van Hoof <sup>4,5</sup>
RP	Roos E. Pouw <sup>2,6</sup>
JV	Jorrit Visser <sup>1</sup>

### Affiliations

<sup>1</sup>Department of Radiation Oncology, Amsterdam UMC, University of Amsterdam, Amsterdam, The Netherlands

<sup>2</sup>Cancer Center Amsterdam, Amsterdam, The Netherlands

<sup>3</sup>Department of Radiation Oncology, The Netherlands Cancer Institute, Amsterdam, The Netherlands

<sup>4</sup>Department of Gastroenterology and Hepatology, Amsterdam UMC, University of Amsterdam, Amsterdam, The Netherlands

<sup>5</sup>Department of Gastroenterology and Hepatology, Leiden University Medical Center, Leiden, The Netherlands

<sup>6</sup>Department of Gastroenterology and Hepatology, Amsterdam UMC, Vrije Universiteit Amsterdam, Amsterdam, The Netherlands

\*Affiliation <sup>1</sup> for Chapters 4 and 5; affiliations <sup>1,3</sup> for Chapters 2, 3 and 6.

Author contributions to Chapter 2 – 6 are as follows:

**Chapter 2: Endoscopically placed fiducial markers for image-guided radiotherapy in preoperative gastric cancer: Technical feasibility and potential benefit**

Study concept and design: MB, JS, AB, AH, MH, RP, JH

Experimental work and data collection: MB, AH, MH, RP, JH

Data analysis: MB

Interpretation: MB, AH, MH, JS, AB

Manuscript preparation: MB

Manuscript editing and reviewing: MB, JS, AB, AH, MH, RP, JH

**Chapter 3: Stomach motion and deformation: implications for preoperative gastric cancer radiotherapy**

Study concept and design: MB, JS, AB, AH, MH

Experimental work and data collection: MB, AH

Data analysis: MB

Interpretation: MB, AH, MH, JS, AB

Manuscript preparation: MB

Manuscript editing and reviewing: MB, JS, AB, AH, MH

**Chapter 4: Feasibility of cone beam CT-guided library of plans strategy in preoperative gastric cancer radiotherapy**

Study concept and design: MB, JS, AB, AH, MH, KG

Experimental work and data collection: MB, AH, KG

Data analysis: MB

Interpretation: MB, JS, AB, AH, MH, KG

Manuscript preparation: MB

Manuscript editing and reviewing: MB, JS, AB, AH, MH, KG



**Chapter 5: Gastric deformation models for adaptive radiotherapy: Personalized vs population-based strategy**

Study concept and design: MB, JS, AB, AH, MH  
Experimental work and data collection: MB, AH  
Data analysis: MB  
Interpretation: MB, JS, AB, AH, MH  
Manuscript preparation: MB  
Manuscript editing and reviewing: MB, JS, AB, AH, MH

**Chapter 6: Dosimetric benefit of a library of plans versus single-plan strategy for preoperative gastric cancer radiotherapy**

Study concept and design: MB, JS, AB, AH, MH, KG, JV  
Experimental work and data collection: MB, AH, JV  
Data analysis: MB  
Interpretation: MB, JS, AB, AH, MH  
Manuscript preparation: MB  
Manuscript editing and reviewing: MB, JS, AB, AH, MH, KG, JV





## Dankwoord

Dit promotietraject is een avontuur geweest die ik absoluut niet had willen missen. Het bracht uitdagingen met zich mee, maar het was een prachtige tijd vol waardevolle leermomenten. Mijn oprechte dank gaat uit naar een aantal mensen in het bijzonder die hierin een rol hebben gespeeld.

Ik wil beginnen met een bijzonder woord van dank aan Astrid, mijn dagelijks begeleider en co-promotor. Jouw aanstekelijke enthousiasme heeft mijn eigen passie voor dit werk echt aangewakkerd. Door jouw geduldige en uitvoerige begeleiding heb ik ontzettend veel geleerd en heb ik echt kunnen ervaren hoe het proces van 'goed onderzoek' er echt uit hoort te zien. Wat onze samenwerking extra speciaal maakte, was niet alleen de immense hoeveelheid kennis die ik heb opgedaan, maar ook de ontspannen en gezellige momenten die we deelden. Waar ik van nature nogal bescheiden ben, heb jij me geleerd trots te zijn op dit mooie werk en de mijlpalen te vieren (zelfs in COVID-tijd wanneer jij een speciaal-bier pakket bij mij thuis liet bezorgen). Wat ik vooral zal missen na het afronden van mijn promotietraject, is onze samenwerking. Alle toekomstige PhD-studenten die het voorrecht hebben om met jou samen te werken mogen zich gelukkig prijzen! Zonder jouw was dit prachtige proefschrift niet geworden wat het nu is. Dank je wel! Ik hoop oprecht dat we in de toekomst nog regelmatig contact zullen hebben.

Ik wil ook graag mijn oprechte dank uitspreken aan Jan-Jakob, Arjan en Maarten, mijn gewaardeerde (co)promotoren. Jan-Jakob, jouw begeleiding gedurende dit project, samen met je altijd kritische blik, hebben een onschatbare rol gespeeld. Ik heb veel van je geleerd en jouw inzichten hebben dit werk naar een hoger niveau getild. Ik heb geleerd dat wanneer jij iets zegt, dit vrijwel altijd de spijker op z'n kop slaat, of ik het nu op dat moment begrijp of niet. Daarnaast bedankt voor de vrijheid en kansen die je me hebt gegeven, waaronder de mogelijkheid om deel te nemen aan de Sonke group meetings. Arjan, bedankt voor je aanwezigheid en betrokkenheid gedurende dit traject. Dank ook voor jouw scherpe blik op consistentie, robuustheid en de figuren in de manuscripten. Dit heeft het werk mooier gemaakt. Maarten, bedankt voor je betrokkenheid en jouw onschatbare bijdrage van klinische kennis en context aan mijn onderzoek. Jouw inzicht heeft me geholpen om de relevantie van het onderzoek nooit uit het oog te verliezen. Bovendien wil ik je bedanken voor jouw verdraagzaamheid als 1) het weer erg technisch werd, 2) manuscripten wel erg bondig geschreven waren (helaas woordlimieten...), of 3) de manuscripten weer een bulk aan data en Supplemental Materials bevatte. Ook waardeer ik je altijd snelle reacties, waarbij je zelfs tijdens je pensioen razendsnel uit je 'andere wereld' kwam om je reacties op mijn stukken te geven.

Naast mijn (co)promotoren wil ik ook graag de andere co-auteurs van mijn artikelen bedanken:

Karin Goudschaal, Jorrit Visser, Roos Pouw en Jeanin Hooft. Bedankt voor jullie inzet en waardevolle bijdragen.

Leden van de commissie, dank voor de tijd en moeite die jullie hebben gestopt in het evalueren van mijn proefschrift.

Ik wil graag mijn kamergenoten en medestanders op het AMC bedanken, Karin M, Karin N, Daan, Jort, Pierre en Marjolein. Vanwege fusies en pandemieën hebben we helaas vooral aan het begin van mijn promotietraject veel contact gehad. Toch kijk ik met plezier terug op de gezellige momenten, de gedeelde lunches en het samen kunnen delen en doorstaan van alle uitdagingen tijdens onze trajecten. Karin Goudschaal, jij was niet enkel een co-auteur van enkele artikelen, maar ook een kamergenoot en fijne, gezellige collega. Dank je wel hiervoor! Ook mijn kamergenoten en collega's op het VUmc, bedankt voor het wegwijs maken op de nieuwe locatie en de gezelligheid. Mijn tijd op het VUmc werd een stuk leuker na het toetreden tot de 'Chamber of Darkness'. Ik wil tevens 'collega's' bij het NKI bedanken. Hoewel ik de afgelopen twee jaar van mijn promotietraject wekelijks deelnam aan de groepsbijeenkomsten, ben ik maar sporadisch op locatie geweest. Desondanks, bedankt voor de gezelligheid en de leuke herinneringen aan de ESTRO.

Daarnaast wil ik graag mijn dank uitspreken aan alle andere fysici, kfm-ers, ICT-ers, artsen en laboranten. De leuke gesprekken en hulp gedurende de afgelopen 5 jaar hebben van mijn promotietraject een leuke tijd gemaakt!

Ik wil ook graag Roni in het zonnetje zetten. Hoewel we vanaf de Master verschillende paden hebben bewandeld, hebben we het PhD-avontuur nu bijna gelijktijdig doorlopen. Ik genoot van de regelmatige koffiemomentjes, waarin we konden ventileren maar ook vooral veel konden kletsen.

En aan mijn dierbare familie en vrienden: jullie verzorgden de broodnodige gezelligheid en welkome afleiding tijdens mijn promotietraject. Dank jullie wel! Hard werken voelt pas echt waardevol wanneer er voldoende ontspanning en waardevolle sociale contacten tegen overstaan. Jullie aanwezigheid, steun en oprechte interesse hebben deze reis nog mooier gemaakt.

Ook spreek ik graag speciale dank uit aan mijn paranimfen, Karin en Karin. Ik wil graag deze periode afsluiten met de mensen naast me met wie ik altijd een hele fijne tijd heb gehad tijdens mijn PhD, dus bij deze ook nogmaals bedankt dat jullie mij op deze dag willen bijstaan!

En tot slot, Pim, wil ik jou graag bedanken. Voor al die momenten van steun, de keren dat

je meedenkt, de hulp als alles even tegenzit, en alle geweldige herinneringen die we samen hebben gemaakt. Vijf jaar geleden waren we slechts partners en beste maatjes, maar door al dat thuiswerken ben je ook uitgegroeid tot mijn allerliefste collega! Maar nu is het weer tijd voor ons samen, ik heb heel veel zin in onze toekomst!

## Curriculum Vitae

Margot Bleeker was born on the 8<sup>th</sup> of June in 1995 in Heemskerk, the Netherlands. After graduating with a VWO diploma from Bonhoeffer college in Castricum in 2013, she joined the Bachelor's program in Medical Natural Sciences at the VU University in Amsterdam. She conducted a Bachelor's internship project on the remote monitoring of heart rate and respiratory rate using polarized near infrared light under supervision of drs. John Klaessens at the VU Medical Center in Amsterdam. After graduating her Bachelor's programme *Cum Laude* in 2016, she started her Master's program in Medical Natural Sciences, in the Medical Physics track. During her Master's, Margot completed a literature review and two Master's internship projects. Her first Master's internship focused on ejection fraction extraction from [<sup>15</sup>O]H<sub>2</sub>O myocardial PET blood flow measurements under supervision of dr. Dennis Heijtel at the VU Medical Center in Amsterdam. In her literature review and second Master's internship, she evaluated a dual registration strategy using bony anatomy and surgical clips in breast cancer radiotherapy under supervision of dr. Anette Houweling at the University Medical Center Utrecht. After graduating her Master's program *Cum Laude*, Margot started her PhD project in 2018 at the Amsterdam University Medical Center Amsterdam under supervision of prof. dr. in. Jan-Jakob Sonke, prof. dr. Arjan Bel, dr. ing. Astrid van der Horst, and dr. Maarten C.C.M. Hulshof.



